AD-A164 561 DEFINITION STUDY OF A COORDINATED GROUP OF EXPERIMENTS TO MEASURE AND MON..(U) MASSACHUSETTS INST OF TECH CAMBRIDGE CENTER FOR SPACE RESEARC.. H S BRIDGE ET AL. 1/2

UNCLASSIFIED SEP 85 AFGL-TR-85-0238 F19628-83-K-0030 F/G 22/1 NL

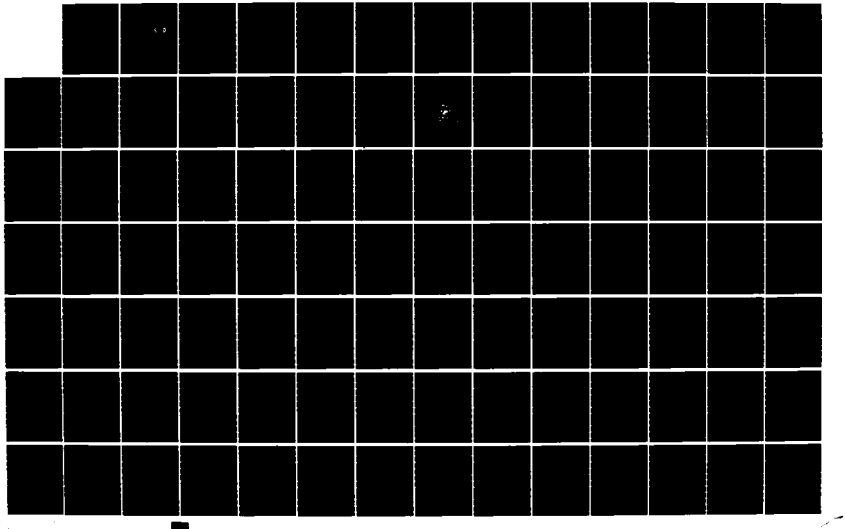

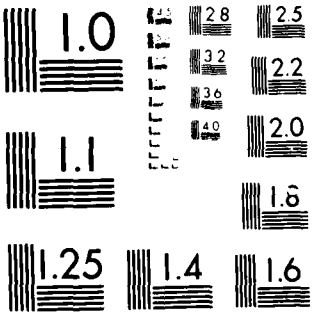

(2)

AFGL-TR-85-0238

DEFINITION STUDY OF A COORDINATED GROUP OF EXPERIMENTS TO MEASURE AND MONITOR THE IN SITU PLASMA AND ELECTROMAGNETIC ENVIRONMENT OF A POLAR ORBITING SPACE SHUTTLE

Herbert S. Bridge
Joseph H. Binsack

Massachusetts Institute of Technology
Center for Space Research
Cambridge, MA 02139

September 1985

Final Report
18 February 1983 - 18 September 1985

AIR FORCE GEOPHYSICS LABORATORY
AIR FORCE SYSTEMS COMMAND
UNITED STATES AIR FORCE
HANSCOM AIR FORCE BASE, MASSACHUSETTS 01731

This technical report has been reviewed and it is approved for publication

Michael J. Smiddy
MICHAEL SMIDDY
Contract Manager

William P. Sullivan
WILLIAM P. SULLIVAN
Acting Branch Chief

FOR THE COMMANDER

John A. Gaudet
JOHN A. GAUDET, Major, USAF
Deputy Director

This report has been reviewed by the ESD Public Affairs Office (PA) and is releasable to the National Technical Information Service (NTIS).

Qualified requestors may obtain additional copies from the Defense Technical Information Center. All others should apply to the National Technical Information Service.

If your address has changed, or if you wish to be removed from the mailing list, or if the addressee is no longer employed by your organization, please notify AFGL/DAA, Hanscom AFB, MA 01731. This will assist us in maintaining a current mailing list.

Unclassified

SECURITY CLASSIFICATION OF THIS PAGE

AD-A164 561

REPORT DOCUMENTATION PAGE

1a REPORT SECURITY CLASSIFICATION: Unclassified	1b RESTRICTIVE MARKINGS
2a SECURITY CLASSIFICATION AUTHORITY	3 DISTRIBUTION/AVAILABILITY OF REPORT: Approved for public release; Distribution unlimited.
2b DECLASSIFICATION/DOWNGRADING SCHEDULE	
4 PERFORMING ORGANIZATION REPORT NUMBER(S)	5 MONITORING ORGANIZATION REPORT NUMBER(S): AFGL-TR-85-0238
6a NAME OF PERFORMING ORGANIZATION: Massachusetts Institute of Technology; 6b OFFICE SYMBOL (If applicable)	7a NAME OF MONITORING ORGANIZATION: Air Force Geophysics Laboratory
6c ADDRESS (City, State and ZIP Code): Center for Space Research, Cambridge, MA 02139	7b ADDRESS (City, State and ZIP Code): Hanscom AFB, Massachusetts 01731
8a NAME OF FUNDING/SPONSORING ORGANIZATION; 8b OFFICE SYMBOL (If applicable)	9 PROCUREMENT INSTRUMENT IDENTIFICATION NUMBER: F19628-83-K-0030
8c ADDRESS (City, State and ZIP Code)	10 SOURCE OF FUNDING NOS: PROGRAM ELEMENT NO: 62101F; PROJECT NO: 7661; TASK NO: 10; WORK UNIT NO: AG
11 TITLE (Include Security Classification): Definition Study of a Coordinated Group of Experiments to (OVER)	
12 PERSONAL AUTHOR(S): Herbert S. Bridge, Joseph H. Binsack	
13a TYPE OF REPORT: Final; 13b TIME COVERED: FROM 2/18/83 TO 9/18/85	14 DATE OF REPORT (Yr., Mo., Day): 1985 September; 15 PAGE COUNT: 106
16 SUPPLEMENTARY NOTATION	

17 COSATI CODES		
FIELD	GROUP	SUB GR

18 SUBJECT TERMS (Continue on reverse if necessary and identify by block number):
Space plasmas; Cold plasma dispersion relations; Shuttle interactions in polar orbit; Electrodynamics of moving conductors

19 ABSTRACT (Continue on reverse if necessary and identify by block number):

This report describes a group of coordinated scientific experiments intended to provide basic information concerning the local plasma environment experienced by the STS in polar orbit. The information acquired should be adequate to evaluate the results of engineering experiments to be flown on the same mission. In addition, a systematic and complete treatment of the dispersion relations for a cold plasma is given and a novel treatment of the interaction between a magnetized plasma and a moving conductor is developed.

20 DISTRIBUTION/AVAILABILITY OF ABSTRACT: UNCLASSIFIED/UNLIMITED ☐ SAME AS RPT ☒ DTIC USERS ☐	21 ABSTRACT SECURITY CLASSIFICATION: Unclassified
22a NAME OF RESPONSIBLE INDIVIDUAL: Michael Smiddy	22b TELEPHONE NUMBER (Include Area Code); 22c OFFICE SYMBOL: AFGL/PHG

DD FORM 1473, 83 APR EDITION OF 1 JAN 73 IS OBSOLETE

Unclassified

SECURITY CLASSIFICATION OF THIS PAGE

Cont of Block 11:

Measure and Monitor the In Situ Plasma and Electromagnetic Environment of a Polar Orbiting Space Shuttle

I. Introduction

In November 1982 MIT proposed to conduct a definition study of a coordinated group of experiments to measure the electromagnetic and plasma environment of a space shuttle in polar orbit. This group of experiments was intended to provide scientific measurements and data sufficient to interpret the results of engineering experiments carried on the Interaction Measurement Payload for Shuttle (IMPS). The original objectives of the study were as follows:

1. Coordinate, with AFGL, the definition of the scientific and programmatic requirements of the investigation, including an understanding of any active plasma and particle experiments envisioned in the future.

2. Review current literature covering theory, observations and instrumentation, including visits to appropriate universities and other organizations.

3. Obtain a thorough understanding of the Space Transportation System, its operation, structure, materials and contaminants, with an emphasis on the effects the Shuttle will have on the environment and vice versa.

4. Develop preliminary psuedo-stationary models of the Shuttle's plasma and electromagnetic environment as it would be influenced by the environment of a typical polar orbit.

5. Explore the perturbations of the environment as it is affected by the dynamical interactions with external sources (solar and/or geomagnetic events) or internal sources (active plasma experiments, debris dumps, terminator crossings).

6. Recommend a package of coordinated experiments to be flown on an early polar orbiting Shuttle to investigate the Shuttle's local environment.

7. Present an implementation plan to procure these experiments, integrate them into the Shuttle, operate them in orbit, collect data, and finally analyze, interpret and publish the results in a timely fashion.

8. Provide a budgetary estimate of item No. 7. above based upon an expected flight of the Environmental Monitoring Package in FY1987.

The original proposal was funded for the period February 18, 1983 through November 30, 1983 and later extended through September 30, 1984. Program delays, reorientation and rescoping of the IMPS program and an inability on the part of MIT to find qualified personnel to work on the program resulted in some changes in emphasis and a reduction in scope of the original objectives. During the early phase of the project, theoretical work was started on a better understanding and general theoretical treatment of the dispersion relations for a cold plasma and on a general theoretical treatment of the interaction of a moving conductor with an ambient magnetized plasma (objectives 3, 4, and 5). A major effort was devoted to objective 6 (the definition of a coordinated set of scientific support experiments.

II. Recommended Scientific Monitoring Payload

A report and description of the recommended support experiments was completed and included in a progress report submitted to AFGL in April 1984. Obviously, the appropriate payload of scientific support experiments depends on the engineering experiments finally selected for IMPS and some modifications to the April report are included in the final report of work to evaluate the engineering experiments proposed by JPL which was carried out by MIT under AFGL contract F19628-83-K-0033.

A major point stressed in the MIT payload recommendations was that the scientific support experiments required measurements not just in the payload bay but as a function of distance from the STS. We suggested initially that the Spartan free flyer developed at GSFC be used for this purpose and this recommendation led directly to the idea of using the German SPASS vehicle to carry out the scientific support measurements. Note that in the JPL "Report on Final Recommendations for IMPS Engineering/Science Payload" and in the MIT

Final Report on the evaluation of the JPL recommendations, the ensemble of scientific support experiments is referred to as EIM, the Environmental and Interactions Monitor.

III. Theoretical Studies

One of the most important questions concerns the interaction of the STS and its payloads with the ambient magnetized plasma. In general a conducting body (even an insulated one) moving relative to a magnetized plasma generates a variety of plasma waves which not only are effects of scientific interest but may also result in practical engineering consequences and limitations. A related problem is the propagation of a given wave mode in the plasma as a function of physical parameters.

Obviously, radiation of electromagnetic signals by the STS or other conducting bodies in orbit is of direct interest for the IMPS program for many reasons, e.g., noise generation, satellite drag, charging effects, etc. For this reason Barnett and Olbert undertook a general study of the problem which they describe in Appendix II. This work has been supported first by AFGL under contract F19628-83-K-0030 and in its final stages by NASA/JPL under JPL contract 953733. A final paper describing this research has been completed and submitted to the Journal of Geophysical Research.

A complete analytic and numerical treatment of the phase and group velocities of waves in the cold plasma approximation was undertaken by Dr. Zdzislaw Musielak. This work was completed in October 1984 and is available as a Center for Space Research Technical Report, CSR-TR-84-3. This TR constitutes Appendix III of the present final report.

IV. Future Studies

To fully understand the interaction of the STS and other large structures with the ambient medium, the theoretical work described above must be expanded to include major modifications of the local STS plasma environment which result from large quantities of neutral gas emitted by the STS and cold plasma dispersion relations need to be modified to include warm and hot plasmas actually present during typical STS polar orbits. Eventually it should be possible to predict the near and far radiation fields expected and to design realistic experiments to measure the actual plasma waves generated by motion of the STS and other large structures through the ambient plasma.

Appendix I

The Environment Monitoring Payload

for use with the

Interaction Measurement Payload for Shuttle

Prepared by:

Herbert S. Bridge
Joseph H. Binsack
Massachusetts Institute
of Technology
April 4, 1984

THE ENVIRONMENT MONITORING PAYLOAD

I. INTRODUCTION

The purpose of the Environment Monitoring Payload (EMP) is to determine the in situ plasma and electromagnetic environment in and around the Shuttle in polar orbit and to measure the interaction of the Shuttle with that environment.

The near-Earth plasma and electromagnetic environment has been studied and monitored for well over two decades. The physics of the ionosphere and of the ionospheric-magnetospheric interaction are at present fairly well understood. For example, known mechanisms for production and loss of charged and neutral particles lead to models of the low and mid-latitude ionosphere which are in reasonable agreement with observations. At higher latitudes, extensiive spacecraft measurements have defined both the energy spectrum and the magnetospheric source regions for those precipitating particles which produce the visible aurora, and thus at least the qualitative physics of the auroral oval is in hand.

With the advent of the Space Transportation System (i.e., the Shuttle) a different aspect of the near-Earth's environment must be analyzed and monitored since, for the first time, the size of the space vehicle structure and its own atmosphere will substantially influence and possibly dominate the in situ plasma and electromagnetic environment. Some preliminary measurements have been and will be made on early STS flights from the Kennedy Space Center (KSC). However, a Shuttle in polar orbit will experience a far more varied environment due to the much wider range of geomagnetic latitudes (e.g., the STS will sample the high fluxes of energetic precipitating particles

associated with the auroral zone). The interaction of the STS with this environment is largely unknown.

II. BRIEF DESCRIPTION OF THE IN SITU ENVIRONMENT AND POSSIBLE SHUTTLE INTERACTIONS

The lowest practical altitude for a polar orbiting Shuttle is about 200 kilometers. At this altitude and at mid-latitudes, the Shuttle will be in the F1 region of the ionosphere. The various geophysical regions of interest that such a Shuttle will sample are: 1.) the polar cap; 2.) the auroral zone; and 3.) the low to middle geomagnetic latitudes below the auroral zone.

In the polar cap region, O^+ is probably the dominant ion, and the ambient thermal plasma has a density of 10^4 to 10^5 electrons/cc, with temperatures of a few tenths of an eV. There are soft precipitating electrons in this region (with energies from 10 eV to 100 eV) which are thought to be magnetosheath electrons which have gained entry into the mantle region and are subsequently precipitated. In addition, there is a plasma outflow (the polar wind) of O^+. In the nightside auroral zone, the ambient plasma densities are an order of magnitude higher than in the polar cap region. This increased density results from ionization of neutrals by the high fluxes of hard precipitating particles in the 1 to 10 keV range (predominately electrons but with proton fluxes at 10% of the electron levels). In the worst cases, auroral fluxes can reach 2×10^{10} electrons/cm^2 sec steradian. There is also an appreciable flux of electrons backscattered up the magnetic field lines, and copious numbers of secondary electrons are produced in the 10 eV to 100 eV range. On the dayside, photoionization produces electrons with 10 eV to 50 eV energies, with higher ambient densities compared to the nightside, and there is a softer spectrum of precipitating particles. Finally, in the low to mid-latitudes, there is no high energy electron component, and the electron densities (all due to photoionization) run from 10^5 to 10^6 electrons/cc in the dayside.

The interaction of the Shuttle with the plasma environment in a low Earth orbit is complicated. Theoretically, there is some understanding of steady-state satellite/plasma interactions at, for example, geostationary orbit. Here, the Debye length of the plasma, and the electron and proton gyroradii of the thermal particles, are large compared to the dimensions of a small satellite. In addition, orbital velocities are much less than typical ion thermal speeds. Such ambient plasma conditions at geostationary orbit allow one to make a number of approximations in modeling spacecraft charging, for example, that the plasma is unmagnetized, and that the satellite is at rest with respect to the plasma. In low-Earth orbit, in constrast, temperatures are much lower and magnetic field strengths and densities are much larger. As a consequence, the Debye length is only millimeters to centimeters, the gyroradii of the ambient electrons are centimeters, and gyroradii of typical ions are meters. In addition, the Shuttle orbital speed (~8 km/sec) greatly exceeds the ambient or ion thermal speeds (~1 km/sec). Thus, in modeling spacecraft charging, one cannot assume an unmagnetized plasma, and one cannot ignore wake effects. Because of these complications, there are major conceptual problems with any existing quasi-static charging code as applied to the Shuttle in low-Earth orbit. In addition the worst case in terms of the most severe charging environment for the Shuttle will undoubtedly be auroral currents, which have spatial scales down to tens of meters. At Shuttle orbital speeds, the Shuttle may sample such features so rapidly that quasi-static approximations to charging may not be valid. In this and other areas, there are major theoretical problems in modeling the STS plasma interaction, and such theoretical developments will undoubtedly have to be guided and verified by experimental results.

In addition to the question of the interaction of the Shuttle with the ambient plasma, there is the question of changes in ambient conditions introduced by the presence of the Shuttle, e.g., contamination due to venting, outgassing or thruster firings, or charging of the Shuttle due to "active" experiments such as electron beam experiments.

Recent flights of the Space Shuttle have shown that the local environment is dominated by contamination from the Orbiter itself. This contamination is in the form of gases, particulates, and glows that are either generated by the Shuttle-atmosphere interaction or a result of integration procedures and pre-launch conditions. These topics have been discussed in detail at a variety of meetings (AIAA meeting, 31 October 1983 to 2 November 1983, Washington, D.C.; AGU meeting, 5 December 1983, San Francisco; URSI meeting, 11 January 1984 to 13 January 1984, Boulder), in journal articles (e.g., see Geophys. Res. Lett., V10, #11, 1983 for Shuttle glow studies), and in technical reports (e.g., contamination reports in NASA-82-457 and NASA-82-524). The following limited summary highlights areas of concern for the Shuttle environment.

- local gas pressures vary from 10^{-4} to 10^{-7} Torr compared to the ambient 10^{-9} Torr,
- water vapor (H_2O) is the principal contaminant but high levels of helium (He) are also noted,
- high levels of electrostatic plasma waves, energetic ions, and suprathermal electrons have been measured--perhaps related to Shuttle glow,
- particulate levels are significant primarily during periods of ascent and descent and then only in the < 5 micron range.

Naturally, many of the above measurements are greatly influenced by and dependent on Shuttle attitude (e.g., bay-to-sun versus passive thermal control), orbital maneuvers (e.g., thruster firings), and operations (e.g.,

water dumps). The number of varying parameters complicates the analysis and the effects of the Shuttle-induced atmosphere on sensitive experimental measurements (e.g., infared radiation or ambient plasma measurements) are far from being understood.

All NASA Shuttle flights have been limited to the low and mid latitudes and have not traversed the auroral zones and polar caps. The auroral region is characterized by intense auroral electron precipitation. DMSP satellites within this region have shown that such fluxes of charged particles can lead to large electric potentials on the surface of the vehicle. Further, laboratory measurements of typical space-qualified materials, which have been irradiated with auroral-type electons, have shown that significant charge deposition can occur within exposed dielectrics. Both situations are hazardous since the possibility of arcing exists, and this arcing is known to upset on-board electronics. In the case of the Shuttle, charge effects are expected to be especially acute since the variety and nature of the surface materials are susceptible to differential and deep-dielectric charging.

III. RELATIONSHIP TO OTHER PROGRAMS

The thrust of the EMP is to measure the interaction of the Shuttle and its contaminants with the local plasma and electromagnetic environment in a polar orbit. Existing data sets and scheduled NASA projects do not specifically address the auroral environment. Specifically, the OSS-1 Pathfiinder Mission probed the near-Shuttle environment but at low latitudes. SPACELAB-II will have an increased measuring capability but is still limited in latitude. The instrumentation proposed for EMP is specifically geared towards measurements in the auroral zones.

The earliest possible flight opportunities are recommended for EMP in order to use the information gathered in the design and flight planning of sensitive Air Force Systems. Without knowledge of the contamination levels and effects of auroral particle precipitation, Air Force systems may be needlessly impacted. It is, therefore, strongly recommended that these experiments be conducted ASAP from a polar-orbiting Shuttle mission.

With the exception of EMP, no DoD payloads have been specifically defined to study the contamination levels and the Shuttle-auroral environment interaction on a polar-orbiting Shuttle mission. However, some other programs are complimentary and their results should be incorporated into the overall investigative program.

IMPS (AFGL)	is geared towards the engineering aspects or consequences of the environment. It is planned, however, that IMPS will use the EMP to accomplish its mission objectives by measuring the probable causes of those consequences.
SCIED (AFGL)	is concerned with large structures within the space environment. The auroral environment is not the principal concern here and the instrument compliment reflects this. The experimental techniques to be used by SCIED to measure the wake/ram effects of large bodies in space are different from EMP but will be useful in understanding the interaction.
SEPS (NRL)	is concerned with plasma irregularities and their effect on communication and surveillance systems. No provision is made for detailed auroral investigations.
PIE-II (ONR)	has provisions to study the effects of the auroral environment on spacecraft but is an active experiment attempting to determine the effects of man-induced plasma processes rather than those of natural processes.

IV. THE EMP PROGRAM

To fully explore the interaction of the Shuttle with the polar-magnetospheric environment will require a free-flying probe capable of maneuvering throughout the three-dimensional space in the vicinity of the

Shuttle. Other dimensions (time, orbital parameters, shuttle aspect angles, e.g., ram/wake, etc.) must be varied in order that a full characterization of the interaction be obtained.

It is recognized that many practical reasons will restrict the program from achieving all of these spatial and temporal measurements with a full compliment of experiments. It is equally important to realize that even with a full complement of measurements it is still a very difficult non-linear theoretical problem to fit a model to the results. The program must begin somewhere, and as long as we keep our sights on the ultimate payload and do not expect ultimate results from a lesser payload, then a somewhat less capable payload can be initiated to obtain some early results in the 1987 time frame.

A. The Early, Captive Program: SACS

A group of Shuttle Auroral and Contamination Sensors (SACS) can be assembled on a pallet-like structure to measure the gaseous, particulate, and plasma densities and the electromagnetic fields surrounding the Shuttle. While these sensors will not give a true and accurate measure of the interaction, even if deployed by the remote manipulating system (RMS), they will nevertheless give a fair indication of the in situ conditions in the Shuttle's cargo bay, particularly in regard to local contaminants. The Shuttle should present as many different aspect angles with respect to its orbital velocity as the time-line can accommodate so that ram/wake effects can be studied at various locations in the polar orbit.

The following complement of instruments should be included in the SACS package:

Mass Spectrometer - The ion/neutral quadrupole mass spectrometer obtains composition measurements of all incoming gases. Then by taking a second set

of measurements with a retarding voltage on a grid, one is able to discriminate against those gases that are being carried along with the Shuttle. The difference between the two measurements give an estimate of the Shuttle contamination. The preferred direction is into the RAM. The field-of-view is ± 20° and the mass range is 1 to 64 AMU.

Energetic Particle Detectors - This package includes an electrostatic analyzer and two solid-state detectors which will measure the energy spectra of electrons and ions in the ranges of 1 eV to 150 keV and 1 eV to 1 MeV, respectively. Such instrumentation is commonly used to detect auroral particle fluxes and to determine spacecraft charging. These particle detectors are optimized when viewing in the zenith direction although the nadir direction allows measurements of atmospherically-backscattered particles.

UV/Visible Spectrometer - This spectrometer consists of two telescopes (FL = 230 mm) and two 1/8-meter Ebert-Fastie scanning spectrometers mounted on a scan platform to change the look angle. A latching mechanism protects the gears during launch and landing and a retractable cover at the telescope entrance is used to protect the optics and provide an internal reflecting surface for the liveness lamp. To prevent detector damage by intense solar radiation, there is a sun sensor which, when activated, turns off the high voltage and closes the shutter. The wavelength range is determined by an optical grating and a photon counting photomultiplier tube.

Stereo Cameras - Two 16-mm Photo-Sonics IPI cameras are to be mounted in a stereo configuration along with an optional strobe light. Each camera has a self-contained 400-ft film magazine containing high-speed, high-contrast film. The cameras have internal heaters and are enclosed in a pressurized container. IRIG-B timing, generated by the Orbiter, is recorded on each film frame.

Pressure Gauge - This measurement technique is a gas-discharge manometer using a self-sustained, low-pressure discharge created by means of crossed magnetic and electric fields. The electric current extracted from the discharge region is proportional to the sensor internal pressure which, in turn, is established by ambient gas flow from the environment into the sensor volume. Laboratory calibrations and kinetic gas theory provide the basis for the interpretation of sensor output in terms of ambient gas flow or density.

Near-IR Photometer - A PbS detector assembly with mechanical chopper and circular variable filter between 2 and 3 microns observes near-IR emissions from contaminants. Laboratory calibrations establish the relation among voltage output, filter position, and the observed photon flux (watts/cm^2-ster). The photometer has a ± 20° field-of-view.

Plasma Probes - 1.) The Langmuir probe measures the local plasma density and temperature. As presently defined, it sweeps from -4V to +4V in 4 seconds and has pedestal offsets of 0, 4, 8, 12, and 16V. In the fixed-potential mode the probe measures variations in electron density.

2.) Either 2 or 3 orthogonal sets of dipole antennas will measure the local DC and AC electric fields within the Shuttle bay. Two swept-frequency receivers operating in the ranges 0 to 60 KHz and 0 to 5 MHz cover all expected plasma wave emissions excited by the Shuttle-atmospheric interactions.

Magnetic Fields - 1.) The fluxgate magnetometer measures the full DC and near-DC (<40 Hz) magnetic fields in the vicinity of the Orbiter. The sensitivity of this instrument is sufficient to detect auroral field-aligned currents but this measurement may be heavily impacted by Shuttle-generated noise.

2.) A 3-axis search coil is used to measure the AC magnetic field in the same frequency range as the AC electric system. It may be possible to use the same swept-frequency receiver as the electric field by appropriate switching of the input to the receiver.

Cameras - Within the aft flight deck conventional TV and still cameras are to be used to photograph the aurora during geomagnetically active periods. A wide-angle camera within the bay is to be used to photograph the aurora under a more controlled situation. Clearly, for this latter case the Orbiter bay should be nadir pointing. A simple grating may be used in front of the camera to yield spectral information.

SHUTTLE AURORAL AND CONTAMINATION SENSORS

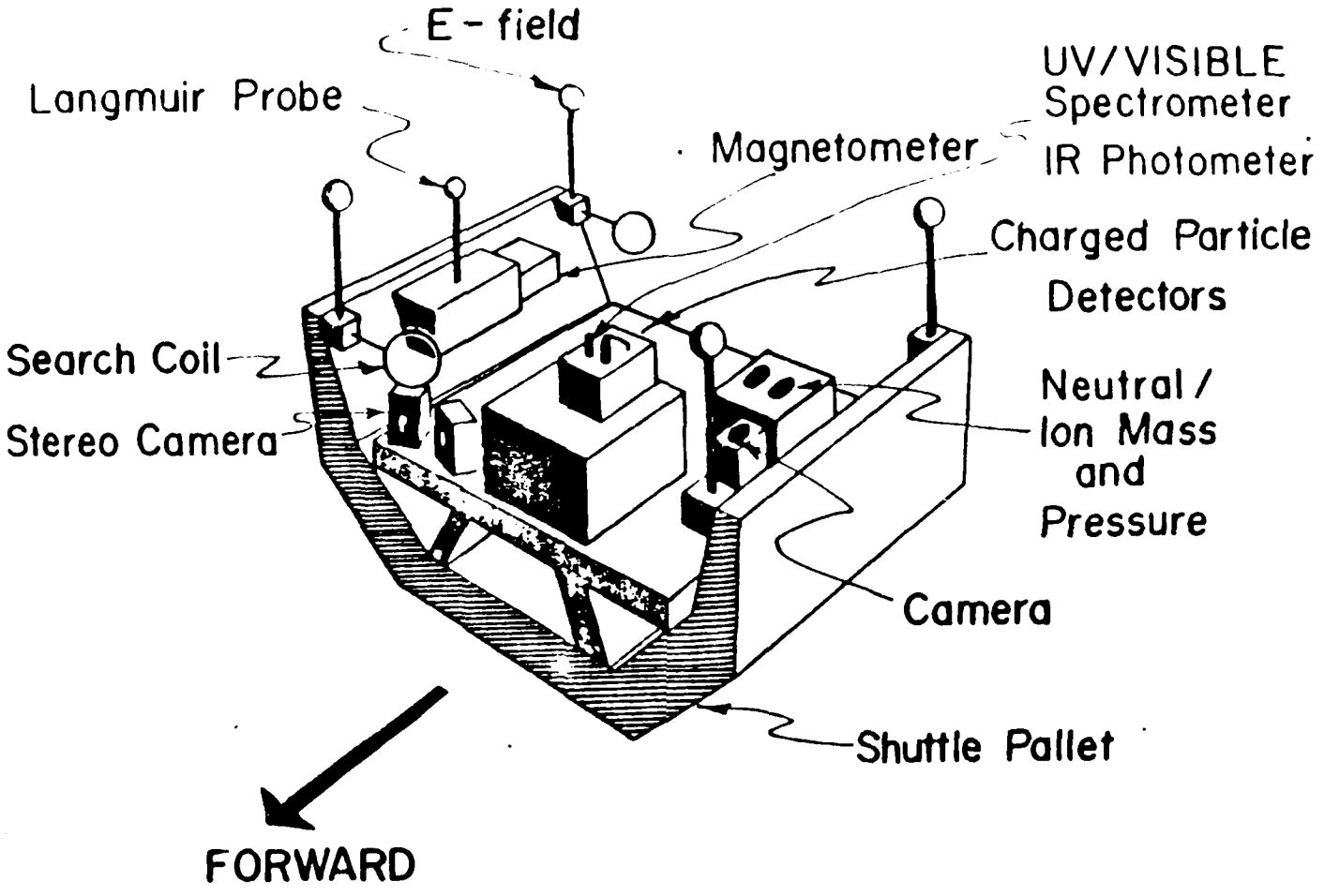

Table 1

Experiment Complement and Requirements

Item	Dimensions Stowed (cm)	Dimensions Deployed (cm)	Weight (kg)	Ejected	Recovery
Mass Spectrometer	N/A	15x7x7 6x6x6	12.7	N/A	N/A
Energetic Particle Det	N/A	25x25x30	14.2	N/A	N/A
UV/VIS Spectrometer	N/A	11x16x21	18.6	N/A	N/A
Stereo Cameras	N/A	TBD	33.6	N/A	N/A
Pressure Gauge	N/A	6x5x5 7x4x5	4.1	N/A	N/A
Near-IR Photometer	N/A	4x6x4	2.3	N/A	N/A
Plasma Probes	N/A	7x6x7 14x4x4	5.0	N/A	N/A
Magnetic Fields	N/A	7x6x7	5.0	N/A	N/A
Cameras	N/A	10x10x10	4.5	N/A	N/A

Nominal Power	150 - 200 watts
Peak Power	180 - 250 watts
Energy	6 - 10 kWh
Total Mass	100 - 150 kg
Real Time Data Rate	13 - 30 kbps
Data Storage	10^{10} bits

Payload Specialist Duties:

- Turning power ON/OFF and monitoring critical functions.
- During magnetically active periods when there are intense auroral features, the astronauts may be requested to photograph the displays using on-board cameras (still and TV). To this end, it may be necessary to have the astronauts change film canisters in addition to doing the photography.

B. The Free Floater EMP

The only meaningful way of determining the interaction of the Shuttle with the plasma and electromagnetic environment is to make measurements throughout the three-dimensional region in the vicinity of the Shuttle. One needs to get far enough from the Shuttle to avoid its own atmosphere of contaminants and explore the effects that the Shuttle has on waves, particles and fields.

The complement of experiments is basically the same as in the SACS package. The major difference is that it now has to be totally self-sufficient and recoverable. There are several possible candidate carriers but perhaps the closest and most readily available is the SPARTAN, currently in production at GSFC. It has all the desirable features of a free-floating, recoverable, Shuttle-compatible carrier, i.e., it has an approved safety package, structural analysis, support systems and STS interface, including grapple and release mechanism. It is a three-axis stabilized carrier but lacks translational ability. This is not a major drawback since the Shuttle could maneuver around it, if the SPARTAN could not be so enhanced.

The first SPARTAN will be released from the Shuttle this August 1984 and four others are currently in production or in the late planning stages. While the SPARTAN may not be the only available carrier (SPAS, PDP, Multi-probe are other possibilities), it is well conceived and a complete system which will be flight proven this year. It should be considered very seriously for the free-floating EMP. The full capabilities of SPARTAN are described in the attached document from GSFC.

Table 2: Revised May 23, 1985

MEASUREMENT REQUIREMENTS FOR ENVIRONMENTAL MONITORING

IN THE VICINITY OF THE SHUTTLE

Desired Measurement	Crucial Parameters	Possible Instrumentation
Ion Spectrum	1 eV → 10Kev	Langmuir Probe + LEPA
Electron Spectrum	~2 eV → 40Kev	LEPA
Ion Spectrum	15 Kev → 1 Mev	Solid State
Electron Spectrum	20 Kev → 150 Kev	Solid State
Ion Composition	Z = 1 → 32	Mass analyzer RPA or Faraday Cup w/ mass analyzer
Pressure of Neutral Ions	10^{-4} - 10^{-9}	Modified pressure gauge
$\vec{E}$, spectrum	DC → 1 MHz	Swept Frequency Analyzer
$\vec{B}$, spectrum	DC → 30 KHz	Triaxial Fluxgate magnetometers Triaxial Search Coil magnetometer
Plasma Impedance	Voltage & Current	Wire, or sphere, or $\vec{E}$ antenna
Camera	Spectral measurements of glow	35mm Camera w/grating
Plasma flow direction	~2 - 10^{0}	Several Faraday Cups on LEPA
Spacecraft Potential	± 10 volts, various places	Several Langmuir Probes

Appendix II

Radiation of Plasma Waves by a Conducting Body Moving Through a Magnetized Plasma

by A. Barnett and S. Olbert

We are studying the interaction between a moving conducting body and a magnetized plasma. It is well known that a large conducting body moving slowly across magnetic field lines radiates low frequency (Alfvén) waves (Drell, Foley & Ruderman (1965)). In this work we estimate the power radiated by a moving sphere or cylinder of arbitrary size at all frequencies.

Previous workers in the field of spacecraft interactions with plasmas concerned themselves primarily with computing the electrical charging of spacecraft. They used models which neglected the magnetic field and the "motional" electric field. Instead, they concentrated on detailed modeling of the electrical properties and geometry of the spacecraft. They computed the current balance by computing individual particle trajectories and applying the Liouville theorem. The magnetic field was neglected because its inclusion makes the particle trajectories prohibitively difficult to compute. For a small satellite in geosynchronous orbit, this type of model is adequate. For large structures in low Earth orbit, these models neglect the dominant effect.

The first work to concentrate on effects due to the magnetic field and the "motional" electric field was that of Drell, Foley & Ruderman. Using "cold plasma" theory in the MHD limit, they showed that a large conducting body in low Earth orbit radiates Alfvén waves, and proposed that the energy loss due to this mechanism was the cause of the anomalously fast rate of

decay of the orbit of the Echo I weather satellite. Their explanation did not gain wide acceptance, however, and it was not until direct in situ observation of the magnetic field perturbation and later of the plasma flow perturbation due to the Alfvén wave generated by the satellite Io in the Jovian magnetosphere that the phenomenon was first observed.

The present work is basically an extension of the DFR paper. We consider not only the MHD regime but also waves of higher frequencies. We formulate the problem in a self-consistent fashion for the passive state, and we estimate the power radiated and the total electric current of the system. We make certain simplifying assumptions, similar to those made by Drell et al: 1) The conducting body moves "slowly" relative to the sationary plasma ("slow" compared to c_A, the Alfvén speed of the ambient medium). 2) The scale lengths of the gradients in the unperturbed plasma and magnetic field are large compared to the size of the moving conductor so that, in effect, the unperturbed medium may be treated as uniform and homogeneous. 3) The velocity of the conductor, $\vec{V}$, remains constant and may be treated as a given perameter. Moreover, $\vec{V}$ lies in the plane perpendicular to the ambient magnetic field.

Although our work is closely related to the issue of "spacecraft charging" widely covered in the literature, our approach is vastly different from that taken by the workers in that field. We completely bypass the discussion of the microscopic details near the surface of the conductor and concentrate on the macroscpic collective effects relatively far from the body.

Our formulation is based upon the familiar procedures of plasma theory with one important modification: we augment the general equation for the electric field by a "source term" involving the electric current within

the moving conductor. More specifically, we start with the following equation in the $(\vec{k},\omega)$-Fourier space:

$$\vec{k} \times (\vec{k} \times \vec{E}) + \frac{\omega^2}{c^2} \tilde{K} \cdot \vec{E} = - \frac{4\pi i}{\omega} \vec{J}_s \qquad (1)$$

where $\vec{k}$ is the wave vector $\vec{E}$ is the electric field, $\tilde{K}$ is the dielectric tensor, ω is the angular frequency, c is the speed of light in vacuum, and $\vec{J}_s$ is the source current. Applying Ohm's law in the conductor, we can write an integral equation which determines $\vec{J}_s$ in a self-consistent manner. Since the integral equation is difficult to solve, we proceed to study solutions to Equation 1 for a known source current, and we infer the spatial dependence of the source current from physical arguments.

We begin by studying the dielectric tensor and the dispersion relation, including constraints on them imposed by our problem. We seek solutions which (a) do not depend on time when viewed from a frame of reference attached to the moving conductor and (b) involve only real propagation vectors $\vec{k}$ in the Fourier space. The latter constraint is directly coupled to the primary purpose of the work, namely, calculation of the energy loss of a moving conducting body solely due to the radiation of plasma waves. We find that both of the above conditions can be satisfied only by that mode of plasma waves that has nearly vanishing phase velocity for some specific direction and magnitude of the propagation vector $\vec{k}$. (By "nearly vanishing" we mean a phase velocity smaller than the velocity of the conductor.) The entire treatment is very reminiscent of the classical treatment of Cherenkov radiation produced by fast moving bodies in an ordinary diectric medium. Because of the enormous complexity of the

dielectric tensor of plasmas, we restrict our explicit evaluations to the cold plasma approximation. We believe that this approximation is sufficient for exploratory purposes. We do not aim at precision but rather to point out the existence of new phenomena.

We find, in the cold plasma approximation, that waves which satisfy the above stated conditions exist only in the following three frequency bands:

$$0 < \omega < \Omega_i \qquad 2a$$

$$\omega_{LH} < \omega < \Omega_e \qquad 2b$$

$$\omega_p < \omega < \omega_{UH} \qquad 2c$$

where Ω_i, Ω_e, ω_{LH}, ω_{UH}, and ω_p are, respectively, the ion and electron cyclotron frequencies, the lower and upper hybrid frequencies and the plasma frequency. The first band consists of the Alfvén waves, already studied by Drell et al. The other two bands are new. We find that the waves in band II are qualitatively very similar to the Alfvén waves, while the waves in band III are very different.

Finally, we estimate the total radiated power for a "passive" conducting sphere, and also for a conducting cylinder oriented such that the axis of the cylinder is parallel to the "motional" electric field. In both cases, we assume that the source current density is uniform everywhere inside the conducting body, and that it is in the direction of the "motional" electric field. The amplitude of the source current can then be computed using Poynting's Theorem and Ohm's law. Table I summarizes the results in several limits where simple analytic expressions are obtainable. In particular, for the case of a wire 10km long and less than 1mm in radius, we find the radiated power to be about 100 watts.

Impedence (Sphere)

Frequency Range	Size	Z (Ohm's)
$0 < \omega < \Omega_i$	$a >> \frac{V_s}{\Omega_i}$	$\frac{\mu_o c_A}{2\pi} = Z_o = .06\Omega$
	$a << \frac{V_s}{\Omega_i}$	$\frac{4\pi}{15} \frac{\Omega_i a}{V_s} Z_o$
$\omega L_H < \omega < \Omega_e$	$a >> \frac{V_s}{\omega_{LH}}$	$\frac{4\mu V_s c_A}{3\Omega_i^2 a^2} Z_o$
	$\frac{V_s}{\omega_{LH}} << a << \frac{V_s}{\Omega_e}$	$\frac{2\pi c_A}{3\Omega_i a} Z_o$
	$a << \frac{V_s}{\Omega_e}$	$\frac{3c_A}{8\pi\eta^2 V_s} Z_o$
$\omega_p < \omega < \omega_{UH}$	$a >> \frac{V_s}{\omega_p}$	$\frac{\eta^2 c_A V_s}{Za^2\Omega_i^2} Z_o$

Radiated Power

$$a >> \frac{V_s}{\Omega_i} \qquad \frac{32\pi a^2 E_o^2}{9 c_A \mu_o} = 1.4 \times 10^4 \left(\frac{a}{100_m}\right)^2 \text{ watts}$$

$$\frac{V_s}{\omega_{LH}} << a << \frac{V_s}{\Omega_e} \qquad \frac{16a^3 \Omega_i E_o^2}{3\mu_o c_A^2} = 4.1 \times 10^{-8} \left(\frac{a}{1\ cm}\right)^3 \text{ watts}$$

Cylinder radius b, length 2ℓ

Frequency	Size	
	$b \gg V_s/\Omega_i$, $\ell \ll b$ (disk)	$\frac{16}{3\pi}\frac{\ell}{b} Z_o$
	$b \gg V_s/\Omega_i$, $2\ell \gg b$	$\ln(\frac{2\ell}{b}) Z_o$
$0 < \omega < \Omega_i$	$b \ll V_s/\Omega_i$, $\ell \ll \frac{V_s}{2\Omega_i}$	$\frac{\pi \Omega_i \ell}{2V_s} Z_o$
	$b \ll V_s/\Omega_i$, $\ell \gg \frac{V_s}{2\Omega_i}$	$\ln(\frac{2\Omega_i \ell}{V_s}) Z_o$
$\omega_{LH} < \omega < \Omega_e$	$b \ll \frac{V_s}{\Omega_e}$, $\ell \gg \frac{V_s}{\omega_{LH}}$	$(\frac{2 c_A}{\pi \eta^2 V_s}) Z_o = 5 \times 10^4\ \Omega$

Power radiated, long wire

$$P_r = \frac{\pi^2 E^2 \ell^2 \eta^2 V_s}{c_A^2 \mu_o} = 100 \left(\frac{\ell}{10\text{km}}\right)^2 \text{ watts}$$

Reference
Drell, S.D., H.M. Foley, and M.P. Ruderman; Drag & Propulsion in the Ionosphere: An Alfvén Propulsion Engine in Space. JGR 70:3131 1965

Appendix III

PHASE AND GROUP VELOCITIES OF WAVES IN COLD PLASMA .

by

Zdzislaw E. Musielak

Center for Space Research
Massachusetts Institute of Technology
Cambridge, MA 02139 USA

October, 1984

TABLE OF CONTENTS

SECTION 1. INTRODUCTION

Phase and Group Velocities of Waves in Cold Plasma

This report presents results of a comprehensive analytical and numerical study of the dispersion relation for a "cold" plasma. Although the subject matter enjoys a time-honored familiarity for anyone interested in plasma waves, it appears that a unified presentation of phase and group velocities for all frequencies and for all directions of wave propagation is not available in the literature. Researchers in various fields dealing with plasmas (e.g. the earth's magnetosphere, the interplanetary medium, the solar corona, etc.) often need to know at a glance the magnitude of the phase or the group velocity for some preferred wave frequency and direction relative to the local magnetic field. The most convenient way to supply such information is by means of polar diagrams (sometimes also referred to as "Friedrichs' diagrams") and this is the form in which we have chosen to present the results of our calculations. The literature is replete with special examples of such diagrams, so that we need not dwell upon the pedagogical details of their construction. Nonetheless, for the convenience of the reader, we do summarize the basic equations needed for the derivation of the dispersion relation (see Section 2). In Section 3 we outline the mathematical formalism underlying the concept of the group velocity. Section 4 is devoted to the polar diagrams of both the phase and the group velocities. A brief discussion of some salient morphological features of the emerging patterns is also included. Section 4 contains, mostly in graphical form, additional information that elucidates the causal relations between the phase velocity graphs and those for the group velocities. Section 5 addresses in more detail the dependence of our results on the relative magnitude of the dimensionless parameters entering into calculations. In particular, the morphological changes of the polar diagrams resulting from the increase of the magnetic field strength are presented for various cases of special interest in astrophysics and solar physics.

SECTION 2. THE DISPERSION RELATION

Phase and Group Velocities of Waves in Cold Plasma

Following standard procedures (see, e.g., Stix 1962) we shall assume that the plasma is in the proper frame of reference (plasma velocity $\vec{V}_0$ and static electric field $\vec{E}_0$ are zero) and that the mean velocity, $\vec{V}_k$, of the particle of type "k", the electric field $\vec{E}$, the current density $\vec{j}$, etc. are infinitesimal perturbations. To derive the dispersion relation, we begin with the linearized equation for conservation of momentum for the k^{th} species of the form:

$$m_k \, \partial \vec{V}_k / \partial t = Z_k e \, (\vec{E} + \vec{V}_k \times \vec{B}_0 / c) \tag{1}$$

where $\vec{B}_0$ is the external, magnetic field, m_k and $Z_k e$ are the mass and charge of the k^{th} particle, respectively. We have neglected the effect of pressure ($1/n_k \, \nabla p \ll Z_k e \, \vec{V}_k \times \vec{B}_0 / c$); in other words we restrict ourselves to the cold plasma approximation. The gravity effect is unimportant in most applications (notably this is the case in earth's magnetosphere). Solving Eq. (1) for $\vec{V}_k$ allows us to construct the expression for the mobility tensor $\overleftrightarrow{M}$, which we define in dimensionless units for each type of particle

$$\vec{V}_k = (c/B_0) \, \overleftrightarrow{M}_k \cdot \vec{E} \tag{2}$$

where $\overleftrightarrow{M}_k$ is given by

$$\overleftrightarrow{M}_k = \begin{pmatrix} \frac{i}{2}\left(\frac{\varepsilon_k\Omega_k}{\omega + \varepsilon_k\Omega_k} + \frac{\varepsilon_k\Omega_k}{\omega - \varepsilon_k\Omega_k}\right), & -\frac{1}{2}\left(\frac{\varepsilon_k\Omega_k}{\omega + \varepsilon_k\Omega_k} - \frac{\varepsilon_k\Omega_k}{\omega - \varepsilon_k\Omega_k}\right), & 0 \\ -\frac{1}{2}\left(\frac{\varepsilon_k\Omega_k}{\omega + \varepsilon_k\Omega_k} - \frac{\varepsilon_k\omega_k}{\omega - \varepsilon_k\Omega_k}\right), & \frac{i}{2}\left(\frac{\varepsilon_k\omega_k}{\omega + \varepsilon_k\Omega_k} + \frac{\varepsilon_k\Omega_k}{\omega - \varepsilon_k\Omega_k}\right), & 0 \\ 0 \quad , & 0 \quad , & i\,\frac{\varepsilon_k\Omega_k}{\omega} \end{pmatrix} \tag{3}$$

ε_k gives the sign of the charge, and $\Omega_k = |\,(Z_k e \, B_0) \,/\, (m_k c)|$ is the cyclotron frequency for the k^{th} particle.

Having obtained the expression for the mobility tensor, we can calculate the dielectric tensor $\overleftrightarrow{K}$ defined by

Phase and Group Velocities of Waves in Cold Plasma

$$\overleftrightarrow{K} \cdot \vec{E} = \vec{E} + (4\pi i/\omega)\ \vec{j} \tag{4}$$

where the current density is given by

$$\vec{j} = \sum_k n_k Z_k e \vec{V}_k \tag{5}$$

with n_k being the number density. In terms of the dimensionless mobility tensor, Eq. (2), (3) and (4) may be combined to yield

$$\overleftrightarrow{K} = \overleftrightarrow{1} + i \sum_k (\varepsilon_k \pi_k^2) \overleftrightarrow{M}_k \ / (\omega \Omega_k) \tag{6}$$

where $\overleftrightarrow{1}$ is the unity matrix and the plasma frequency of the k^{th} species is given by

$$\pi_k \equiv ((4\pi n_k Z_k^2 e^2) / m_k)^{1/2}.$$

To obtain the dispersion relation we calculate the electric field E using Maxwell's equations. We have

$$\partial^2\vec{E}/\partial t^2 + \nabla \times (\nabla \times \vec{E}) = - 4\pi\ \partial\vec{j}/\partial t\ . \tag{7}$$

After Fourier transformation in time and space (assume homogeneous and infinite plasma), Eq. (7) becomes

$$\vec{k} \times (\vec{k} \times \vec{E}) + \omega^2/c^2 \overleftrightarrow{K} \cdot \vec{E} = 0 \tag{8}$$

where k is the propagation vector. Equation (8) is of the form $A_{ij} E_j = 0$, where the matrix A_{ij} is given by

$$A_{ij} = \begin{pmatrix} S-n^2\cos^2\theta & , -iD & , n^2\cos\theta \sin\theta \\ iD & , S-n^2 & , 0 \\ n^2\cos\theta \sin\theta & , 0 & , P-n^2\sin^2\theta \end{pmatrix} \tag{9}$$

The symbols S, R, L, D, P, and n are defined in a conventional way:

Phase and Group Velocities of Waves in Cold Plasma

$$S \equiv 1/2\ (R + L); \qquad D \equiv 1/2\ (R - L)$$

$$R = 1 - \sum_k (\Pi_k^2/\omega^2)\ \omega/(\omega + \varepsilon_k\omega_k) \tag{10}$$

$$L = 1 - \sum_k (\Pi_k^2/\omega^2)\ \omega/(\omega - \varepsilon_k\Omega_k) \tag{11}$$

$$P = 1 - \sum_k \Pi_k^2/\omega^2 \tag{12}$$

$$n = kc/\omega \tag{13}$$

For a two-component plasma, with electrons as negative ions, Eqs. (10), (11) and (12) reduce to

$$R = 1 - \omega_p^2/(\omega + \Omega_i)(\omega - \Omega_e) \tag{14}$$

$$L = 1 - \omega_p^2/(\omega - \Omega_i)(\omega + \Omega_e) \tag{15}$$

$$P = 1 - \omega_p^2/\omega^2 \tag{16}$$

where the plasma frequency, ω_p, is defined as

$$\omega_p = (\Pi_i^2 + \Pi_e^2)^{1/2} \tag{17}$$

From the condition for a nontrivial solution of Eq. (8) we obtain the familiar dispersion relation for the phase velocity (for references see Stix (1962)). Working out the algebra of det $(A_{ij})=0$ we find

$$U^4 - U^2C_A^2\ [(x-\sigma)\cos^2\theta - x-\sigma] + C_A^4\sigma[x\sin^2\theta - \psi\cos^2\theta] = 0 \tag{18}$$

where $U = \omega/k$ is the phase velocity, $C_A = B_0/(4\pi\rho)^{1/2}$ is the Alfven velocity for the case in which the magnetic energy is substantially less than the rest energy, and θ is the angle between $\vec{B}_0$ and $\vec{k}$. The dimensionless quantities x, σ and ψ are defined by

$$x = -\omega^2/\ (B_A^2(\omega^2 - \omega_p^2)) \tag{19}$$

$$\sigma = -\ ((\omega^2 - \omega_{LH}^2)\ (\omega^2 - \omega_{UH}^2))\ /\ (B_A^2(\omega^2 - \omega_{LC}^2)\ (\omega^2 - \omega_{UC}^2)) \tag{20}$$

Phase and Group Velocities of Waves in Cold Plasma

$$\psi = ((\omega^2 - \Omega_i^2)\,(\omega^2 - \Omega_e^2)) \,/\, (\beta_A^2(\omega^2 - \omega_{LH}^2)\,(\omega^2 - \omega_{UH}^2)) \qquad (21)$$

where ω_{LH}, ω_{UH}, ω_{LC} and ω_{UC} are the lower hybrid, the upper hybrid and the lower and upper cutoff frequencies, respectively. They are defined as

$$\omega_{LH}^2 = \frac{\Omega_i\Omega_e\,(\Omega_i^2 + \pi_i^2)}{\Omega_i\Omega_e + \Omega_i^2 + \pi_i^2} \qquad (22)$$

$$\omega_{UH}^2 = \Omega_i^2 + \Omega_e^2 + \omega_p^2 \qquad (23)$$

$$\omega_{LC,UC} = \sqrt{\omega_p^2 + \frac{1}{4}\,(\Omega_e^2 + \Omega_i^2)} \mp \frac{1}{2}\,(\Omega_e + \Omega_i). \qquad (24)$$

β_A is the ratio of C_A to the speed of light. Note that χ, σ and ψ are functions of ω and the characteristic plasma frequencies, but do not depend on θ. The solution of Eq. (18) yields for U^2/C^2:

$$\frac{U^2}{C^2} = \frac{1}{2}\,\beta_A^2[(\chi-\sigma)\,\cos^2\theta - \chi-\sigma \pm \sqrt{(\chi-\sigma)^2\,\sin^4\theta + 4\sigma(\sigma + \psi)\,\cos^2\theta}] \qquad (25)$$

Equation (25) shows that there are only two modes in the cold plasma approximation. We shall call them, respectively, the "plus" and the "minus" mode. In the literature these two modes go by a variety of different names depending on the frequency regime one happens to be interested in. The "plus" mode is variously referred to as the:

fast mode ($0 \leq \omega < \Omega_i$)

lower hybrid mode ($\Omega_i < \omega \leq \omega_{LH}$)

whistler mode ($\omega_{LH} < \omega < \Omega_e$)

electron cyclotron mode ($\omega \leq \Omega_e$)

Phase and Group Velocities of Waves in Cold Plasma

ordinary mode ($\omega > \omega_{LC}$)

as the frequency regime is changed; similarly, the "minus" mode is referred to as the:

Alfven mode ($0 \lesssim \omega < \Omega_i$)

ion cyclotron mode or ion whistler mode ($\omega \lesssim \Omega_i$)

upper hybrid mode or extraordinary mode ($\omega_p < \omega \leq \omega_{UH}$)

In order to unify our presentation, and simplify the nomenclature, we shall always refer to these modes as "plus" and "minus" modes.

The dispersion relation (Eq. 18) gives zero or infinity for the phase velocity when the dimensionless parameters go to a certain value. Stix (1962) terms the case $U \to 0$ a resonance, and the case $U \to \infty$ a cutoff. Resonances occur when the following criterion is satisfied:

$$\tan^2\theta = \frac{P}{S} = -\frac{(\omega^2 - \Omega_i^2)(\omega^2 - \Omega_e^2)(\omega^2 - \Omega_p^2)}{\omega^2(\omega^2 - \omega_{LH}^2)(\omega^2 - \omega_{UH}^2)} \tag{26}$$

After some algebra Eq. (26) becomes

$$\omega^6 - \omega^4 [\omega_{UH}^2 + (1 - \cos^2\theta)\omega_{LH}^2] + \omega^2 [(1 - \cos^2\theta)\, \omega_{LH}^2\, \omega_{UH}^2 + \Omega_p^2 \Omega_e^2 \cos^2\theta] - \Omega_i^2 \Omega_e^2 \omega_p^2 \cos^2\theta = 0 \tag{27}$$

where

$$\Omega_p^2 = \omega_p^2 + \Omega_i^2 + \frac{\omega_p^2 \Omega_i^2}{\Omega_e^2}$$

Phase and Group Velocities of Waves in Cold Plasma

The square roots of Eq. (27) are easy to find if we assume that $\omega < \Omega_e$ or $\omega < \omega_{UH}$. Solving Eq. (27) for these conditions, we obtain the general formulas for lower (Ω_{LR}), middle (Ω_{MR}) and upper (Ω_{UR}) resonance:

$$\Omega_{LR}^2 = \frac{\Omega_i^2 \Omega_e^2 \omega_p^2 \cos^2\theta}{[(1 - \cos^2\theta)\omega_{LH}^2 \omega_{UH}^2 + \Omega_p^2 \Omega_e^2 \cos^2\theta]} \tag{28a}$$

$$\Omega_{MR}^2 = \frac{[(1 - \cos^2\theta)\omega_{UH}^2 \omega_{LH}^2 + \Omega_p^2 \Omega_e^2 \cos^2\theta] + \sqrt{\Delta}}{2[\omega_{UH}^2 + (1 - \cos^2\theta)\omega^2 LH]} \tag{28b}$$

where

$$\Delta = [(1 - \cos^2\theta)\omega_{UH}^2 \omega_{LH}^2 + \Omega_p^2 \Omega_e^2 \cos^2\theta]^2 - 4[\omega_{UH}^2 + (1 - \cos^2\theta)\omega_{LH}^2]\Omega_i^2 \Omega_e^2 \omega_p^2 \cos^2\theta] ,$$

$$\Omega_{UR}^2 = \frac{1}{2}\omega_{UH}^2 \left[1 + \sqrt{1 - \frac{4\Omega_p^2 \Omega_e^2 \cos^2\theta}{\omega_{UH}^4}}\right]. \tag{28c}$$

From Equations (28a), (28b) and (28c), we can obtain the resonant frequencies for the particular physical situations.

The cutoffs occur when the following conditions are fulfilled:

$x \to \infty$ or $\sigma \to \infty$ or $\psi \to \infty$

Table 1 shows the dependence of the resonances and cutoffs on the angle θ.

Phase and Group Velocities of Waves in Cold Plasma

TABLE 1

Dependence of the resonances and cutoffs on the angle θ.

	Arbitrary Angle θ	θ = 0°	θ = 90°
Resonances	Ω_{LR}, Ω_{MR}, Ω_{UR}	Ω_i, Ω_e, ω_p	0, ω_{LH}, ω_{UH}
Cutoffs	ω_{LC}, ω_{UC}, ω_{LH}, ω_{UH}, ω_p	ω_{LC}, ω_{UC}, ω_{LH}, ω_{UH}	ω_{LC}, ω_{UC}, ω_p

Using the results from the first column of Table 1 we can strictly define the characteristic frequency regimes for arbitrary angles. The sketch below defines the regimes and shows the regions where the "plus" mode (indicated as +) and the "minus" mode (indicated as -) can exist. Symbols X indicate the regions where a given mode is evanescent.

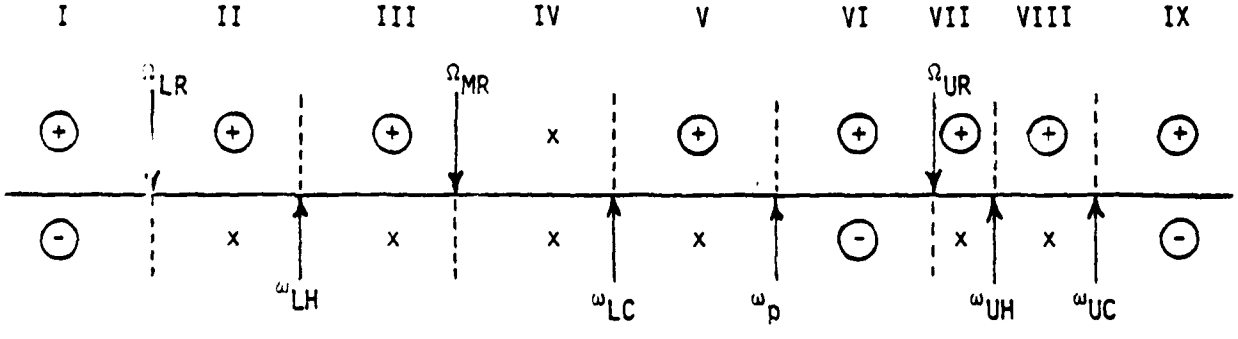

The ordering presented in this sketch (see Table 2) is typical for weak magnetic fields ($\omega^2_p >> \Omega_e^2$ or $\beta_A^2 < 0.001$), and change significantly when the magnetic field increases (see Section 6 for a more detailed discussion). Table 2 presents values of the resonances and cutoffs ($\theta = 0$) for earth's magnetosphere ($\beta_A = 0.001$ and electron density $n_e = 3.6\times10^5$).

TABLE 2

The resonances and cutoffs for the earth's magnetosphere with $\beta_A = 0.001$, B = 0.33G and $n_e = 3.6\times10^5$ cm^{-3}.

Ω_i	ω_{LH}	Ω_e	ω_{LC}	ω_p	ω_{UH}	ω_{UC}
1.96×10^2	3.33×10^4	5.80×10^6	3.11×10^7	3.39×10^7	3.44×10^7	3.69×10^7

Phase and Group Velocities of Waves in Cold Plasma

SECTION 3. GROUP VELOCITY

Phase and Group Velocities of Waves in Cold Plasma

The group velocity of a wave, $\vec{U}_g$, is defined in general by equation

$$\vec{U}_g = \nabla_k \omega \tag{29}$$

In dispersive and anisotropic media the direction and the magnitude of $\vec{U}_g$ are different from those of $\vec{U}$. The sketch below defines the pertinent symbols relating $\vec{U}_g$ to $\vec{U}$.

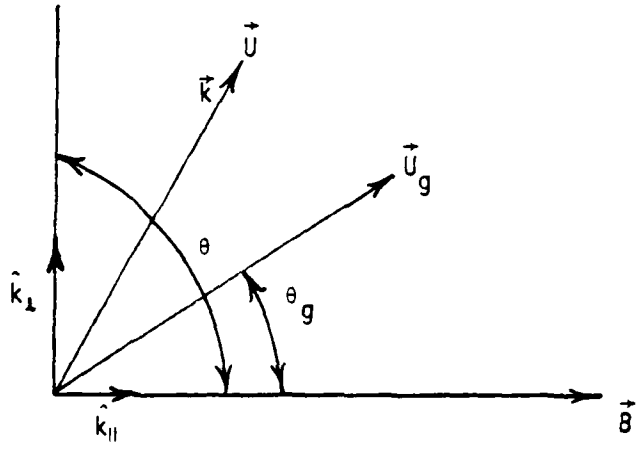

Since ω may be looked upon as a function of $k_\parallel$ and $k_\perp$ ($\vec{k} = k_\parallel \hat{k}_\parallel + k_\perp \hat{k}_\perp$) Eq. (29) implies that

$$\vec{U}_g = \frac{\partial \omega}{\partial k_\perp} \hat{k}_\perp + \frac{\partial \omega}{\partial k_\parallel} \hat{k}_\parallel . \tag{30}$$

For the explicit evaluation of $\partial\omega/\partial k_\perp$ and $\partial\omega/\partial k_\parallel$ we need the dispersion relation

$$F(\omega, k_\parallel, k_\perp) = 0 \tag{31}$$

obtainable from Eq. (18). We then have

Phase and Group Velocities of Waves in Cold Plasma

$$\frac{\partial F}{\partial \omega}\, d\omega + \frac{\partial F}{\partial k_{\parallel}}\, dk_{\parallel} + \frac{\partial F}{\partial k_{\perp}}\, dk_{\perp} = 0 \tag{32}$$

and

$$\vec{U}_g = -\left(\frac{\partial}{\partial k_{\parallel}}\hat{k}_{\parallel} + \frac{\partial F}{\partial k_{\perp}}\hat{k}_{\perp}\right)\frac{1}{F_\omega} \tag{33}$$

where $F_\omega = \partial F/\partial\omega$. For the modes considered here we find from Eqs. (32) and (33) the following expression for the group velocity:

$$\vec{U}_g = \frac{C_A^2\sigma}{F_u}\left\{\left[C_A^2\,(\psi\cos^2\theta - \chi\sin^2\theta) - U^2\right]\frac{\vec{k}}{k} + \right.$$

$$\left. + \left[C_A{}^2\psi - U^2\right]\frac{\vec{k}_{\parallel}}{k} - \frac{\chi}{\sigma}\left[C_A{}^2\sigma + U^2\right]\frac{\vec{k}_{\perp}}{k}\right\} \tag{34}$$

where

$$F_u \equiv k^{-3} F_\omega = 2U^3 + UC_A{}^2[2\sigma\cos^2\theta + (\chi + \sigma)\sin^2\theta +$$

$$+ \frac{1}{2}(\sigma_A + \sigma_B)(1 + \cos^2\theta + \frac{C_A{}^2}{U^2}\,(\chi\sin^2\theta - \psi\cos^2\theta)) +$$

$$+ (1 - \chi\beta_A{}^2)(1 + \sigma\frac{C_A{}^2}{U^2})\,\chi\sin^2\theta -$$

$$- \frac{C_A{}^2}{U^2}(\psi_A + \nu_B)\sigma\cos^2\theta] \tag{35}$$

and

$$\sigma_A = \frac{1}{2} \quad \frac{\omega\Omega_i\Omega_e\ (2\omega + \Omega_e - \Omega_i)}{[\Omega_i\ \Omega_e - \beta_A{}^2(\omega - \Omega_i)(\omega + \Omega_e)]^2} \quad ,$$

$$\sigma_B = \frac{1}{2} \quad \frac{\omega\Omega_i\Omega_e\ (2\omega - \Omega_e + \Omega_i)}{[\Omega_i\ \Omega_e - \beta_A{}^2(\omega - \Omega_i)(\omega - \Omega_e)]^2} \quad ,$$

$$\psi_A = \quad \frac{\omega^2\ \Omega_i\Omega_e}{(\omega^2 - \Omega_i{}^2)(\omega^2 - \Omega_e{}^2)} \quad ,$$

$$\psi_B = \psi_A \quad \frac{(\omega^2\Omega_i\Omega_e)(2\omega^2 - \Omega_e{}^2 - \Omega_i{}^2)}{(\omega^2 - \Omega_i{}^2)(\omega^2 - \Omega_e{}^2)} \quad .$$

Introducing the polar angle θ_g shown in the sketch above, we can calculate, according to Eq. (34), the components of $\vec{U}_g$ parallel and perpendicular to $\vec{B}_0$. Then we have

$$U_{\parallel} \equiv U_g \cos\theta_g = \frac{C_A{}^2\sigma}{F_u}\,[C_A{}^2(\psi(1 + \cos^2\theta) - \chi \sin^2\theta) - 2U^2]\cos\theta$$

$$U_{\perp} \equiv U_g \sin\theta_g = \frac{C_A{}^2\sigma}{F_u}\,[C_A{}^2(\psi \cos^2\theta - \chi(1 + \sin^2\theta)) - U^2(1 - \frac{\chi}{\sigma})]\sin\theta \qquad (36)$$

The above equations yield then, with the help of Eq. (18),

$$\tan\theta_g = \frac{U^4 - U^2C_A{}^2\ (\chi - \sigma)\cos^2\theta - C_A{}^4\ \sigma\chi}{U^4 + U^2C_A{}^2\ (\chi - \sigma)\sin^2\theta + C_A{}^4\ \sigma\chi^-}\tan\theta \qquad (37)$$

Phase and Group Velocities of Waves in Cold Plasma

and

$$U_g^2 = \frac{1}{F_u^2}\left[U^8 + \frac{1}{2}U^2C_A^2(\chi - \sigma)\left[\frac{1}{2}U^2C_A^2(\chi - \sigma) + C_A^4\sigma(\chi + \psi)\right]\sin^2 2\theta + \right.$$

$$+ C_A^4\sigma\left[2U^4(\chi + \psi) + C_A^4\sigma(\psi^2 - \chi^2)\cos^2\theta + \right. \tag{38}$$

$$\left. \left. + C_A^4\sigma\chi\left[C_A^4\sigma\chi - 2U^4\right]\right]\right].$$

Since the general equations for the group velocity are cumbersome, it is instructive to derive simplified expressions for $\vec{U}_g$ and U_g^2 in the MHD limit ($\omega << \Omega_i$). Thus we get $\chi \to 0$, $\sigma \approx -1$, $\psi \approx 1$, $(\sigma_A + \sigma_B) \to 0$, $(\psi_A + \psi_B) \to 0$ and

$$U_g = \frac{U^4 \frac{\vec{k}}{k}}{U[2U^2 - C_A^2]}\ , \tag{39}$$

which yields

$$U_g^2 \approx C_A^2;\ \tan\theta_g = \tan\theta \qquad \text{for the fast mode}$$

and

$$U_g^2 \approx C_A^2;\ \theta_g = 0 \qquad \text{for the Alfven mode.}$$

SECTION 4. POLAR DIAGRAMS FOR PHASE AND GROUP VELOCITY

Phase and Group Velocities of Waves in Cold Plasma

The solutions of the dispersion relation for the phase and group velocity (Eqs. 25, 37 and 38) are plotted as the polar diagrams. For numerical calculations it is convenient to redefine the dimensionless parameters that were introduced in Eqs. (25), (37) and (38). After defining the mass ratio as $\zeta \equiv (m_e/m_i)^{1/2}$, we have

$$X \equiv \frac{f^2}{1 - f^2\beta_A^2} \tag{40}$$

$$\sigma \equiv \frac{1}{2}\left[\frac{1}{\frac{\zeta}{(f-\zeta)(1+f\zeta)} - \beta_A^2} - \frac{1}{\frac{\zeta}{(f+\zeta)(1-f\zeta)} + \beta_A^2}\right] \tag{41}$$

$$\psi \equiv \frac{1}{\frac{\zeta^2(f^2-1)}{(f^2-\zeta^2)(1-f^2\zeta^2)} + \beta_A^2}\,, \tag{42}$$

and

$$\sigma_A \equiv \frac{1}{2}\,\frac{f\zeta}{(f-\zeta)(1+f\zeta)}\,\frac{1+2f\zeta-\zeta^2}{[\zeta^2 - \beta_A^2(f-\zeta)(1+f\zeta)]} \tag{43}$$

$$\sigma_B \equiv \frac{f\zeta}{(f+\zeta)(1-f\zeta)}\,\frac{2f\zeta+\zeta^2-1}{[\zeta^2 + \beta_A^2(f+\zeta)(1-f\zeta)]} \tag{44}$$

$$\psi_A \equiv (\psi\beta_A^2 - 1)\,\psi\,\frac{2f^2}{(f^2-1)} \tag{45}$$

$$\psi_B \equiv (1 - \psi\beta_A^2) \frac{2f^2}{(f^2 - 1)} \left(\frac{1}{\zeta^2} - 2f^2 - \zeta^2\right) , \tag{46}$$

where $f = \omega/(\Omega_i\Omega_e)^{1/2}$. Now Eqs. (25), (37), (38) and (40)+(46) represent a convenient form for calculations because $\vec{U}$, $\vec{U}_g$ and θ_g are functions of ω and two physical parameters β_A and ζ. Thus, holding β_A and ζ fixed we construct a family of polar diagrams for $\vec{U}$ and $\vec{U}_g$ for various frequencies. We plot the polar diagrams using different normalization of f for different regimes of frequency:

I and II: $f \equiv f_i\ \zeta \equiv (\omega/\Omega_i)\zeta$

III: $f \equiv f_{LH}\omega_R \equiv (\omega/\omega_{LH})\ \omega_R \equiv (\omega/\omega_{LH})\ ((\Omega_i^2 + \Pi_i^2) / (\Omega_i^2 + \Pi_i^2 + \Omega_i\Omega_e))^{1/2}$

IV: $f \equiv f_e\ \zeta^{-1} \equiv (\omega/\Omega_e)\zeta^{-1}$

V and VI: $f \equiv f_p\beta_A^{-1} \equiv (\omega/\omega_p)\ \beta_A^{-1}$.

The results presented in this section are typical for the earth's magnetosphere, where $\zeta = 1/171.4$ and $\beta_A = 10^{-3}$. Figures 4.1 through 4.5 show the polar diagrams for the phase velocity of the "plus" mode in the different frequency regions. The diagrams for the group velocity of the "plus" mode are presented on Figures 4.6 through 4.10. The next four figures show the diagrams for U and U_g of the "minus" mode. As one sees from Figures 4.1 through 4.14, there are several general trends in the behavious of the modes. The polar diagrams for the "plus" mode present the "evolution" of loci of the phase velocity, from a sphere (Fig. 4.1) through two distinct spheres that are surfaces of revolution about the symmetry axis (Fig. 4.2); these evolve eventually to small aspect ratio lobes (Figs. 4.3a and 4.3b) which are narrowly confined in. The symmetry axis is defined by direction of the magnetic field that is along the abscissa axis. For frequencies just above ω_{LC}, a sphere appears again (Fig. 4.4) and becomes slightly deformed in the regime VI (Fig.

4.5). The loci of the group velocity evolve from a sphere (Fig. 4.6) through a "pre-whistler" shape (Fig. 4.7) to the characteristic whistler cusp (Fig. 4.8a). However, the behavior of the loci in the regime is more complex than in the other frequency regions. The group velocity locus can be plotted as one topologically complex curve, but for presentation it is convenient to distinguish two different shapes: the whistler cusp (its evolution is shown on Fig. 4.8a) and the "expanding lobes" (Fig. 4.8b). When the frequency increases the whistler cusp becomes deformed and disappears completely at $\omega = \Omega_e/2$; as Fig. 4.8c shows for higher frequencies the lobe dominates (region III is discussed later in this section). The group velocity loci in regimes V and VI evolve from a sphere (Fig. 4.9) to a tiny shape limited to the direction perpendicular to $\vec{B}$ (Fig. 4.10).

The next four figures demonstrate the behavior of the "minus" mode. Figures 4.11 and 4.12 show that the phase velocity does not change its characteristic shape, but, that during the evolution the loci shape becomes smaller and disappears at the critical frequencies Ω_i and ω_{UH}. The group velocity loci (Figures 4.13 and 4.14) show the ion whistler cusp in the regime I and the cone shape (regime VI) that is deformed when the frequency approaches ω_{UH}. The angle θ_g reaches the maximum value at 12° (for $f_i \approx 0.85$) in regime I and the minimum value at 12° (for $f_p \approx 1.005$) in regime VI.

The "plus" mode is the only one that can exist in the region III; in this region the group velocity loci have topologically complex structure that strongly depends on frequency. The series of Figures 4.15 through 4.25 present the changes of U and U_g (plotted together) for increasing frequency. One sees the characteristic whistler cusp ($f_{LH} \ll 1$); where the line that is plotted along $\vec{B}$ (and ties the origin to the ends of the cusps) marks the initial stage of formation of the lobes (Figures 4.15 and 4.16). Generally this "line" is split and the split angle is as small as 0.017° for $f_{LH} = 1.01$. When the frequency increases, the split angle increases also, and the lobe becomes the significant feature on the diagrams (Fig. 4.17 through 4.22) instead of the whistler cusp. The critical point occurs for $\omega = \Omega_e/2$ (or $f_{LH} = 86$) when the whistler cusp disappears (Fig. 4.23) and expanding lobe can be seen only (Figs. 4.24 and 4.25). Therefore, it is convenient to divide the region III into two subregions: IIIA ($\omega < \Omega_e/2$) and IIIB ($\omega > \Omega_e/2$). The angle θ_g

reaches the maximum at 76.5° for $f_{LH} = 170$ or $f_e = 0.98$ (subregion IIIB), however the maximum angle for the whistler cusp never exceeds 19.29° (subregion IIIA).

Phase and Group Velocities of Waves in Cold Plasma

SECTION 5. DEPENDENCE OF THE DISPERSION RELATIONS ON THE

MAGNETIC FIELD STRENGTH AND DENSITY OF PLASMA

The general equations for the phase and group velocity (Eqs. 25, 37 and 38) contain only two dimensionless parameters: ζ and β_A. These parameters influence the results by changing the values of the characteristic frequencies and thus changing the widths of the regimes. Generally, ζ affects all the characteristic frequencies except Ω_e and ω_p and consequently the change of the frequency regimes. However, the change of β_A not only implies the change of the width of the regimes but can also lead to a redefinition of the upper and lower limits of these regimes. The cutoff frequencies ω_{LC} and ω_{UC} are the most important parameters for changing the width of the regimes. Table 3 shows the dependence of ω_{LC} on β_A and ζ and the "vanishing" regime in the various cases.

TABLE 3

Dependence of the cutoff ω_{LC} on the changes of β_A

β_A^2	ω_{LC}	ω_p^2	Vanishing regime
$<< \frac{1}{2}\zeta^2$	$\approx\omega_p$	$>> \Omega_e^2$	V
$\frac{1}{2}\zeta^2$	$\Omega_{MR} = \Omega_e$	$2\Omega_e^2$	IV
ζ $\frac{2}{3}$	$\approx\omega_{LH}$ $\approx\omega_{LH}$	$\Omega_e\sqrt{\Omega_i\Omega_e}$ $\frac{2}{3}\quad \Omega_i\Omega_e$	III
1.0	$\Omega_{LR} = \Omega_i$	$\Omega_i\Omega_e$	II
2.0	0	$\frac{1}{2}\Omega_i\Omega_e$	I

In Section 2 we defined the nine frequency regimes for the particular physical conditions typical for the earth's magnetosphere. Now, we are interested in how the ordering and the classification will be altered when β_A increases. Table 4 presents a sequence of inequalities for β_A and shows the changes of the bounds of the regimes. As one sees from Table 4 a significant reordering of the regimes is necessary as β increases.

TABLE 4

Dependence on the bounds of the frequency regime on β_A.

Regime	$\beta_A \leq 0.001$	$0.001 < \beta_A^2 \leq 0.01$	$0.01 < \beta_A^2 \leq 0.1$	$0.1 < \beta_A^2 \leq 1.0$
I	0, Ω_{LR}	0, Ω_{LR}	0, Ω_{LR}	0, ω_{LC}
II	Ω_{LR}, ω_{LH}	Ω_{LR}, ω_{LH}	Ω_{LR}, ω_{LC}	Vanishes
III	ω_{LH}, Ω_{MR}	ω_{LH}, ω_{LC}	Vanishes	Vanishes
IV	Ω_{MR}, ω_{LC}	Vanishes	Vanishes	Vanishes
V	ω_{LC}, ω_p	ω_{LC}, ω_p	ω_{LC}, ω_p	ω_{LC}, Ω_{LR}
VI	ω_p, Ω_{UR}	ω_p, Ω_{MR}	ω_p, Ω_{MR}	ω_p, Ω_{MR}

Let us consicer the results of calculations that were made for β_A varying between 0.0005 and 0.05 and for $\zeta = 1/171.4$ (for oxygen). The polar diagrams

for the group velocity are presented on Figs. 5.1 and 5.2, and show the independence of the shape of the loci on β_A as long as the regime is not disturbed by ω_{LC}. Figure 5.2 presents the disturbance of regime III by ω_{LC} that becomes the new "bound" for this regime. For frequencies higher than ω_{LC} but less than Ω_e the behavior of the group velocity is typical for regime V (see Section 4).

Now, we consider the results for two different mass ratios: $\zeta_o = 1/171.4$ (for oxygen) and $\zeta_h = 1/42.85$ (for hydrogen) and for $\beta_A = 0.1$, 0.03, 0.01, 0.005 and 0.001 where the changes of n_e and B are treated independently. The values of β_A that were chosen can be identified with different astrophysical objects such as the atmospheres of magnetic white dwarfs, the atmospheres of magnetic (A_p) stars, and the solar atmosphere (e.g., chromosphere and coronae above sunspots). The results are presented on θ_g versus θ diagrams that give direct information about the connections between the direction of $\vec{k}$ and $\vec{U}_g$. The series of the diagrams (Figs. 5.3 through 5.6 for hydrogen and Figs. 5.7 through 5.10 for oxygen) are plotted for the two constant frequencies $\omega = 5\times10^5$ and $\omega = 5\times10^6$. In addition, the calculations were carried out for the given β_A but with constant n_e ($= 1.0\times1.0^{10}cm^{-3}$) or constant B (= 5 G). The mode frequency was held fixed and the values of B and n_e were chosen for convenience of presentation for the various frequency regimes. The θ_g versus θ diagrams (Figs. 5.3 through 5.6 and 5.7 through 5.10) present changes of the behavior of the group velocity for different β_A; a comparison of Figs. 5.3 with 5.7 and 5.4 with 5.8 shows the results for the different ζ. Several features of these diagrams merit special emphasis:

1. the "formation" of the whistler mode from the almost ideal MHD fast mode for decreasing β_A (Figs. 5.4, 5.7 and 5.8), or the reverse process for increasing β_A;

2. a similar evolution can be seen for decreasing ζ (compare Figs. 5.3 with 5.7 or 5.4 with 5.8);

3. the absence of one or two curves in Figs. 5.5, 5.6, and 5.9 is caused by the independence of the shape of the loci on the specific values of β_A;

4. the crossing of the bound between regimes III and V is shown on Fig. 5.6 and 5.9; Fig. 5.10 presents the crossing of the bounds between regimes III-V and V-VI (regime IV does not exist for $\beta_A > 0.001$).

SECTION 6. SUMMARY

Phase and Group Velocities of Waves in Cold Plasma

In this report we derived the general dispersion relations (Eqs. 25, 37 and 38) for the phase and group velocity in the "cold" plasma approximation. The dispersion relations were obtained as a function of the physical parameters: ζ, β_A, frequency and the direction of wave propagation. In this approximation, there are only two clearly distinct modes: "plus" and "minus". Using the general definitions of the resonant (Eqs. 28a, b, c) and cutoff (Eqs. 22, 23 and 24) frequencies, we classified the various frequency regimes, and showed in which regimes the modes become evanescent. The general definitions of the resonant and cutoff frequencies allowed us to show their dependence on the direction of propagation (Table 1) and on the physical parameters (Table 4).

The polar and θ_g versus θ diagrams that are presented in the report show the distinct behavior of the "plus" and "minus" modes in different frequency regimes. Each particular frequency domain is characterized by a typical shape of the phase or group velocity loci. This shape is independent of the physical parameters ζ and β_A (Fig. 26) that change the width of the regimes in frequency space, the identity of the regimes, as well as of the value of the phase or group velocity.

A particular physical condition ($\beta_A \approx 0.001$) gives the maximum number (nine according to our definition) of distinct regimes of behavior. The "plus" mode can propagate in eight of these frequency domains, but the propagation of the "minus" mode is admissible in only three of them. There is only one regime (IV) where both modes are evanescent. Either an increase or decrease in β_A causes a decrease in the number of distinct regimes of behavior.

In region II, we showed (Fig. 4.7) that the "plus" mode exhibits a degeneracy in group velocity (i.e., there exist three distinct group velocities for one very specific angle θ_g); this degeneracy never occurs in the direction of the magnetic field. One can also see the degeneracy for one angle θ_g in Figs. 4.20 and 4.21. However, in these latter cases, the physical picture is more complicated, and will be discussed in a separate paper. Generally, the "plus" mode never exhibits the U_g degeneracy for one θ_g except in some portion of Region II.

Several characteristic angles θ_g were found for the modes. The transport of energy by the "plus" mode is restrictd to angles 19.29° and 76.5° for sub-regimes III A and III B, respectively. The minus mode can transport energy at less than the angle θ_g = 12° in Regime I and only above the angle $\theta_g \simeq 12°$ in Regime VI. The coincidence will be also discussed in a separate paper.

Phase and Group Velocities of Waves in Cold Plasma

ACKNOWLEDGEMENTS

I would like to thank Stanislaw Olbert and Tom Chang for their discussions and advice during the preparation of this report, John Belcher and Robert Rosner for a critical reading of the manuscript and very useful comments and suggestions. This work was supported under AFGL Contract F19628-83-K-0030.

REFERENCES

Stix, T. H., 1962, "The Theory of Plasma Waves", McGraw-Hill, New York

FIGURE CAPTIONS

Figure 4.1 The "plus" mode in the earth's magnetosphere. We show the polar diagrams for the phase velocity in Regime I and for frequencies f_i = 0.05, 0.35, 0.5, 0.75, 0.85 and 1.0 (correspond with the curves from the internal to the external one, respectively). The magnetic field is along the abscissa axis.

Figure 4.2 The same as Fig. 4.1 but for Regime II and for frequencies f_i = 1.1, 3.5, 8.5, 17.0, 25.0, 33.0 and 41.0.

Figure 4.3a The same as Fig. 4.1 but for subregime III A and for frequencies f_{LH} = 1.1, 2.0, 5.0, 10.0, 25.0, 50.0 and 86.0.

Figure 4.3b The same as Fig. 4.1 but for subregime III B and for frequencies f_{LH} = 170.0, 150.0, 120.0, 100.0 and 86.0.

Figure 4.4 The same as Fig. 4.1 but for Regime V and for frequencies f_p = 0.96, 0.95, 0.94, 0.93 and 0.92.

Figure 4.5 The same as Fig. 4.1 but for regime VI and for frequencies f_{UH} = 0.995, 0.994, 0.993, 0.992, 0.991 and 0.990.

Figure 4.6 The plus mode is the earth's magnetosphere. We show the polar diagrams for the group velocity in Regime I and for frequencies f_i = 0.05, 0.35, 0.5, 0.75, 0.85 and 1.0 (correspond with the curves from the internal to the external one, respectively). The magnetic field is along the abscissa axis.

Figure 4.7 The same as Fig. 4.6 but for Regime II and for frequencies f_i = 1.10, 3.5, 8.5, 17.0, 25.0, 33.0 and 41.0.

Figure 4.8a The same as Fig. 4.6 but for subregime III A and for frequencies f_{LH} = 2.0, 5.0, 10.0, 25.0 and 50.0. The evolution of the whistler cusp only is presented.

Figure 4.8b The same as Fig. 4.6 but for subregime III A and for frequencies f_{LH} = 2.0, 5.0, 10.0, 25.0 and 50.0. The splitting of the "line" for increasing frequency is shown.

Figure 4.8c The same as Fig. 4.6 but for subregime III B and for frequencies f_{LH} = 170.0, 150.0, 120.0, 100.0 and 86.0.

Figure 4.9 The same as Fig. 4.6 but for regime V and for frequencies f_{UH} = 0.96, 0.95, 0.94, 0.93 and 0.92.

Figure. 4.10 The same as Fig. 4.6 but for regime VI and for frequencies f_{UH} = 0.995, 0.994, 0.993, 0.992, 0.991 and 0.990.

Figure 4.11 The "minus" mode in the earth's magnetosphere. We show the polar diagrams for the phase velocity in regime I and for frequencies f_i = 0.99, 0.95, 0.85, 0.75, 0.50, 0.35 and 0.05 (decreasing from the internal to the external curves, respectively). The magnetic field is along the abscissa axis.

Figure 4.12 The same as Fig. 4.11 but for regime VI and for frequencies f_{UH} = 0.995, 0.994, 0.992, 0.990 and 0.899.

Figure 4.13 The "minus" mode in the earth's magnetosphere. We show the polar diagrams for the group velocity in the regime I and for frequencies f_i = 0.99, 0.95, 0.85, 0.75, 0.50, 0.35 and 0.05 (decreasing from the internal to the external curves, respectiveiy). The magnetic field is along the abscissa axis.

Figure 4.14 The same as Fig. 4.13 but for regime VI and for frequencies f_{UH} = 0.995, 0.994, 0.992, 0.990 and 0.899.

Figure 4.15 The "plus" mode in the earth's magnetosphere. We show the polar diagrams for the phase and group velocities in regime III and for frequency f_{LH} = 1.01. The magnetic field is along the abscissa axis.

Figure 4.16 The same as Fig. 4.15 but for f_{LH} = 1.1.

Figure 4.17 The same as Fig. 4.15 but for f_{LH} = 2.0.

Figure 4.18 The same as Fig. 4.15 but for f_{LH} = 10.0.

Figure 4.19 The same as Fig. 4.15 but for f_{LH} = 15.0.

Figure 4.20 The same as Fig. 4.15 but for f_{LH} = 20.0.

Figure 4.21 The same as Fig. 4.15 but for f_{LH} = 50.0.

Figure 4.22 The same as Fig. 4.15 but for f_{LH} = 70.0.

Figure 4.23 The same as Fig. 4.15 but for f_{LH} = 86.0.

Figure 4.24 The same as Fig. 4.15 but for f_{LH} = 120.0.

Figure 4.25 The same as Fig. 4.15 but for f_{LH} = 170.0.

Figure 5.1 Propagation of the "plus" mode with constant frequency ω = 1330.0 s^{-1} (Regime II) through the earth's magnetosphere with β_A = 0.005, 0.01, 0.015, 0.025, 0.035, 0.040 and 0.050 but for constant the magnetic field, B = 0.33G. Increasing β_A runs from the internal to the external curves, respectively. The magnetic field is along the abscissa axis.

Figure 5.2 The same as Fig. 5.1 but for $\omega = 8.5 \times 10^5$ s^- (Regime III). The change of the shape of the loci during the propagation is caused by the crossing of the bound between regimes III and V ($\omega_{LC} < \Omega_e$).

Figure 5.3 The θ_g versus θ diagram for the "plus" mode with constant frequency $\omega = 5 \times 10^5$ s^{-1}. The curves (from the bottom of figure) present the dependence of θ_g on θ for the values of β_A = 0.001, 0.005, 0.01, 0.03, and 0.1 in a hydrogen atmosphere. The number density is constant and equal to $n_e = 1.0 \times 10^{10}$ cm^{-3}.

Figure 5.4 The same as Fig. 5.3 but for $\omega = 5 \times 10^6$ s^{-1}.

Figure 5.5 The same as Fig. 5.3 but for B = 5 G.

Figure 5.6 The same as Fig. 5.3 but for $\omega = 5 \times 10^6$ s^{-1} and for B = 5 G.

Figure 5.7 The same as Fig. 5.3 but for an oxygen atmosphere.

Figure 5.8 The same as Fig. 5.3 but for $\omega = 5 \times 10^6$ s^{-1} and for an oxygen atmosphere.

Figure 5.9 The same as Fig. 5.3 but for B = 5 G and for an oxygen atmosphere.

Figure 5.10 The same as Fig. 5.3 but for $\omega = 5 \times 10^6$ and for B = 5 G and for oxygen atmosphere.

FIGURES

Phase and Group Velocities of Waves in Cold Plasma

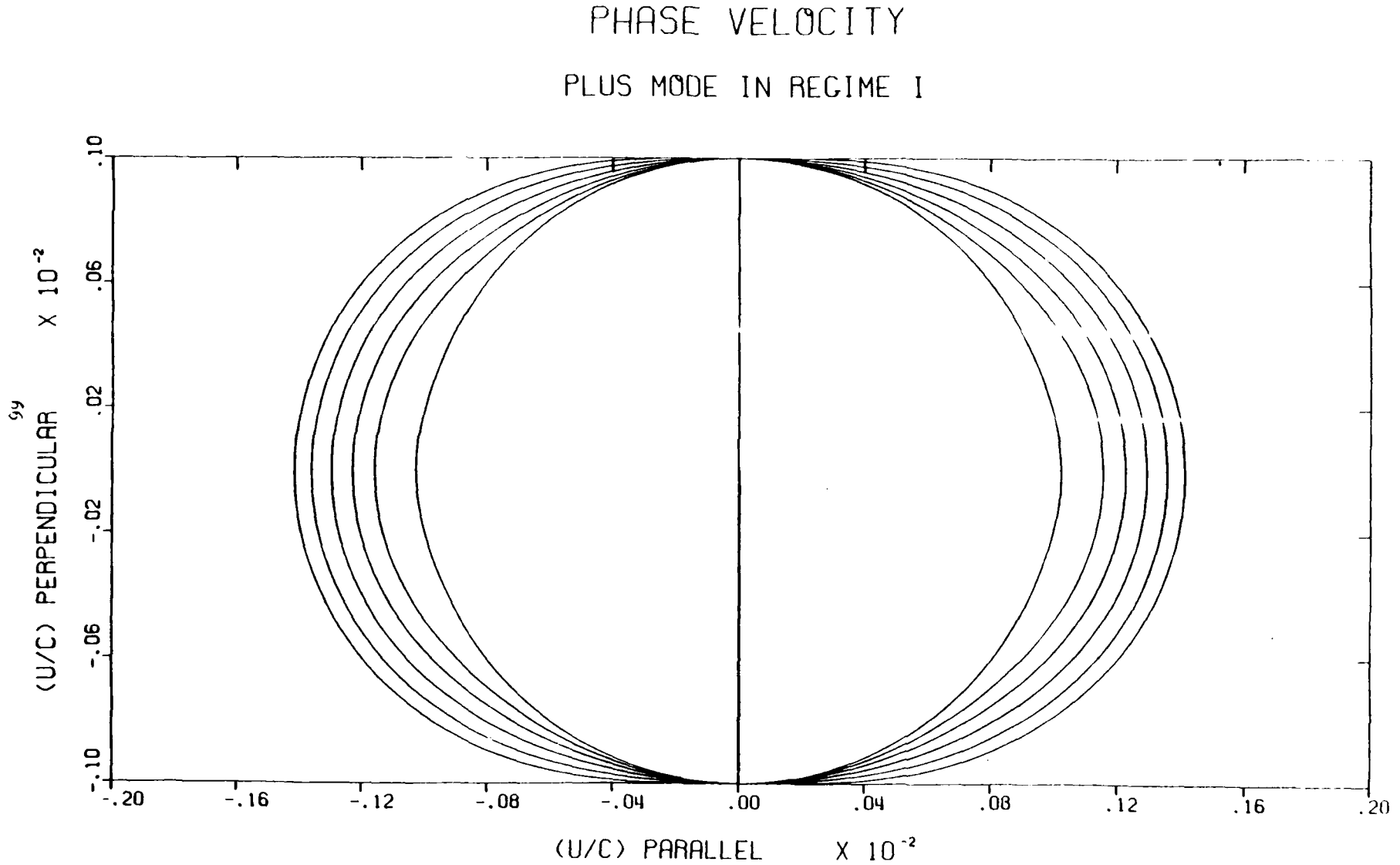
PHASE VELOCITY
PLUS MODE IN REGIME I
(U/C) PERPENDICULAR $_{gy}$ X 10^{-2}
.10
.06
.02
-.02
-.06
-.10
-.20
-.16
-.12
-.08
-.04
.00
.04
.08
.12
.16
.20
(U/C) PARALLEL X 10^{-2}

Figure 4.1

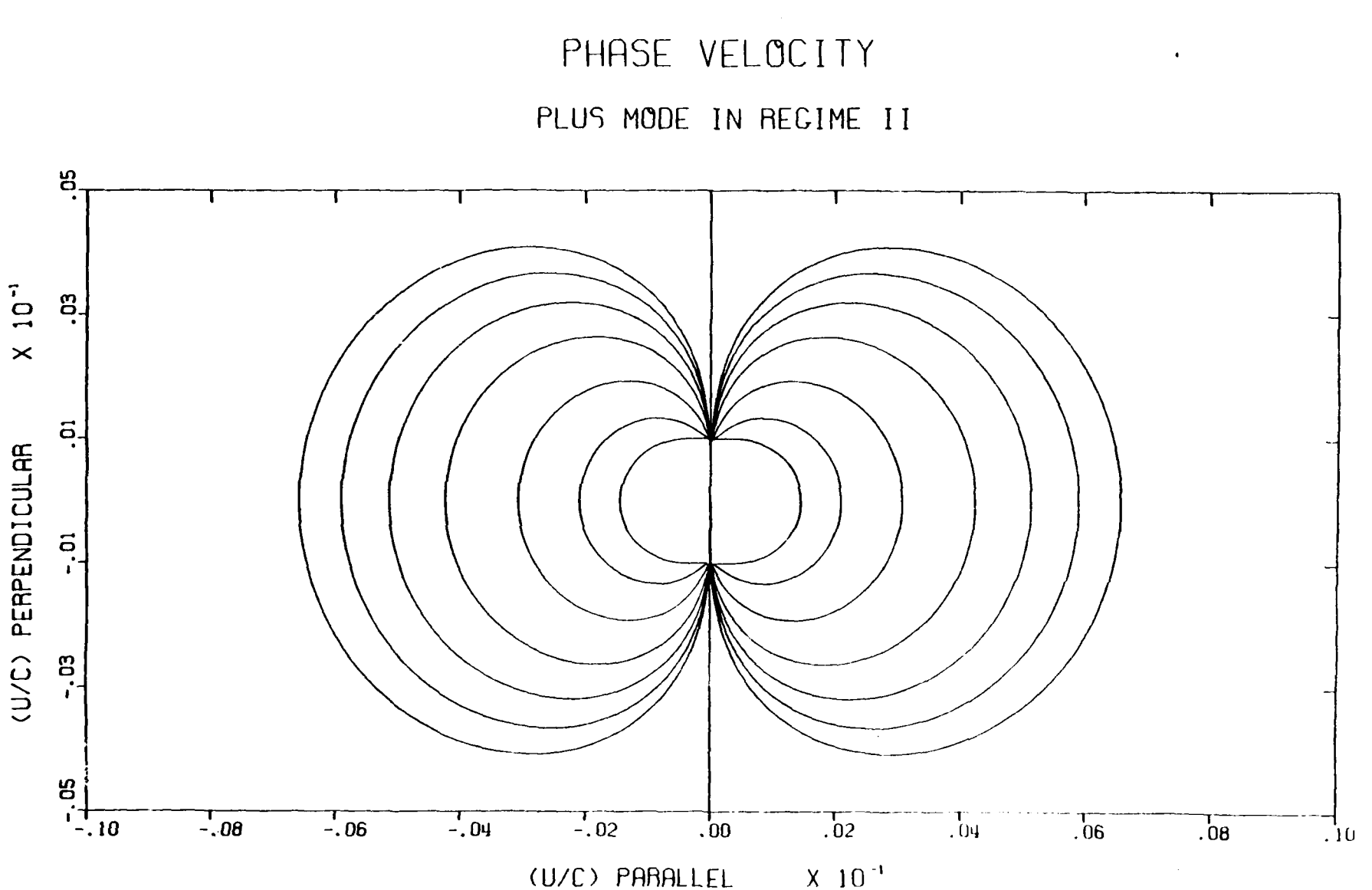
PHASE VELOCITY
PLUS MODE IN REGIME II
(U/C) PERPENDICULAR X 10⁻¹
.05
.03
.01
-.01
-.03
-.05
-.10
-.08
-.06
-.04
-.02
.00
.02
.04
.06
.08
.10
(U/C) PARALLEL X 10⁻¹

Figure 4.2

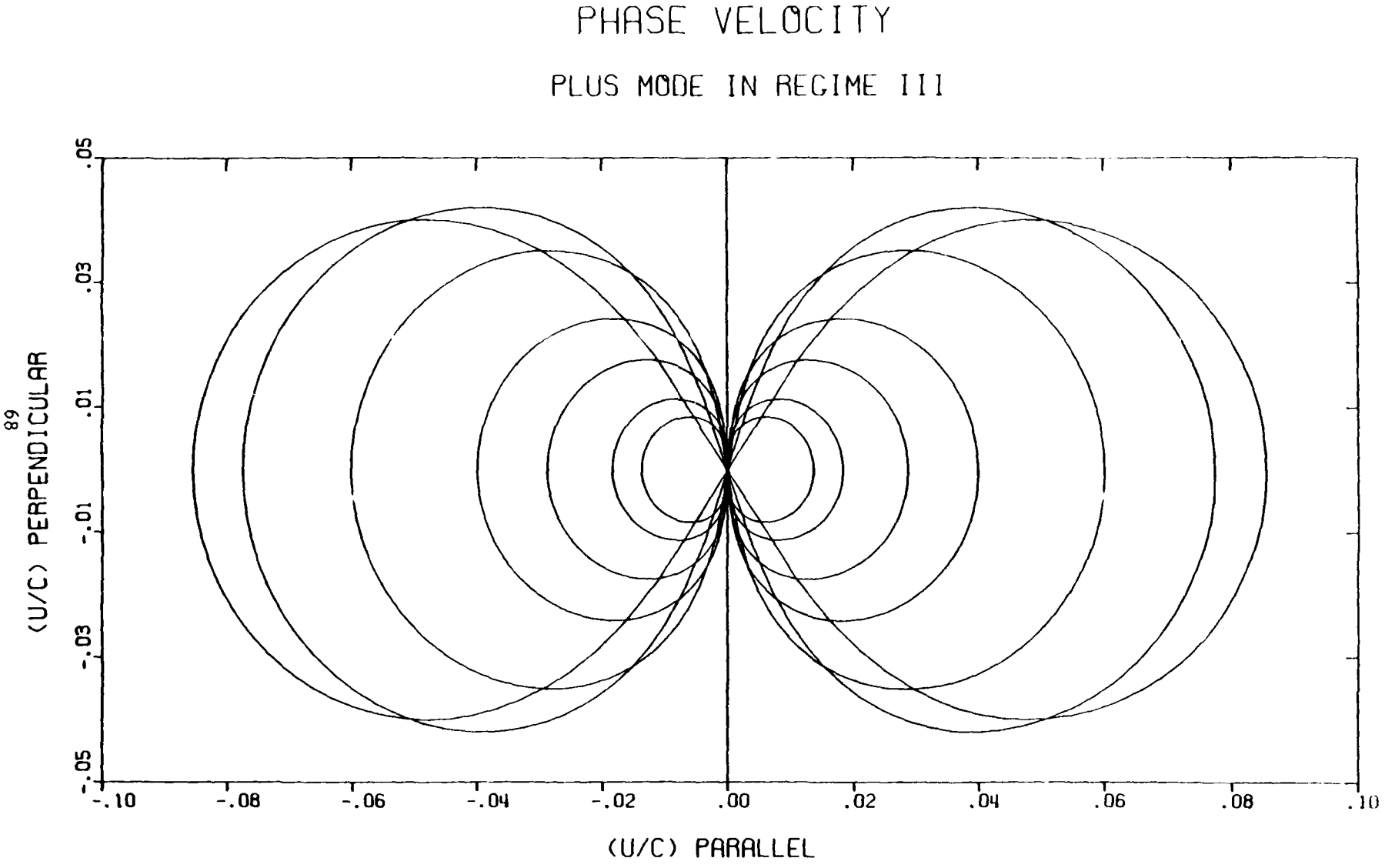
PHASE VELOCITY
PLUS MODE IN REGIME III
(U/C) PERPENDICULAR
.05
.03
.01
-.01
-.03
-.05
-.10
-.08
-.06
-.04
-.02
.00
.02
.04
.06
.08
.10
(U/C) PARALLEL

Figure 4.3a

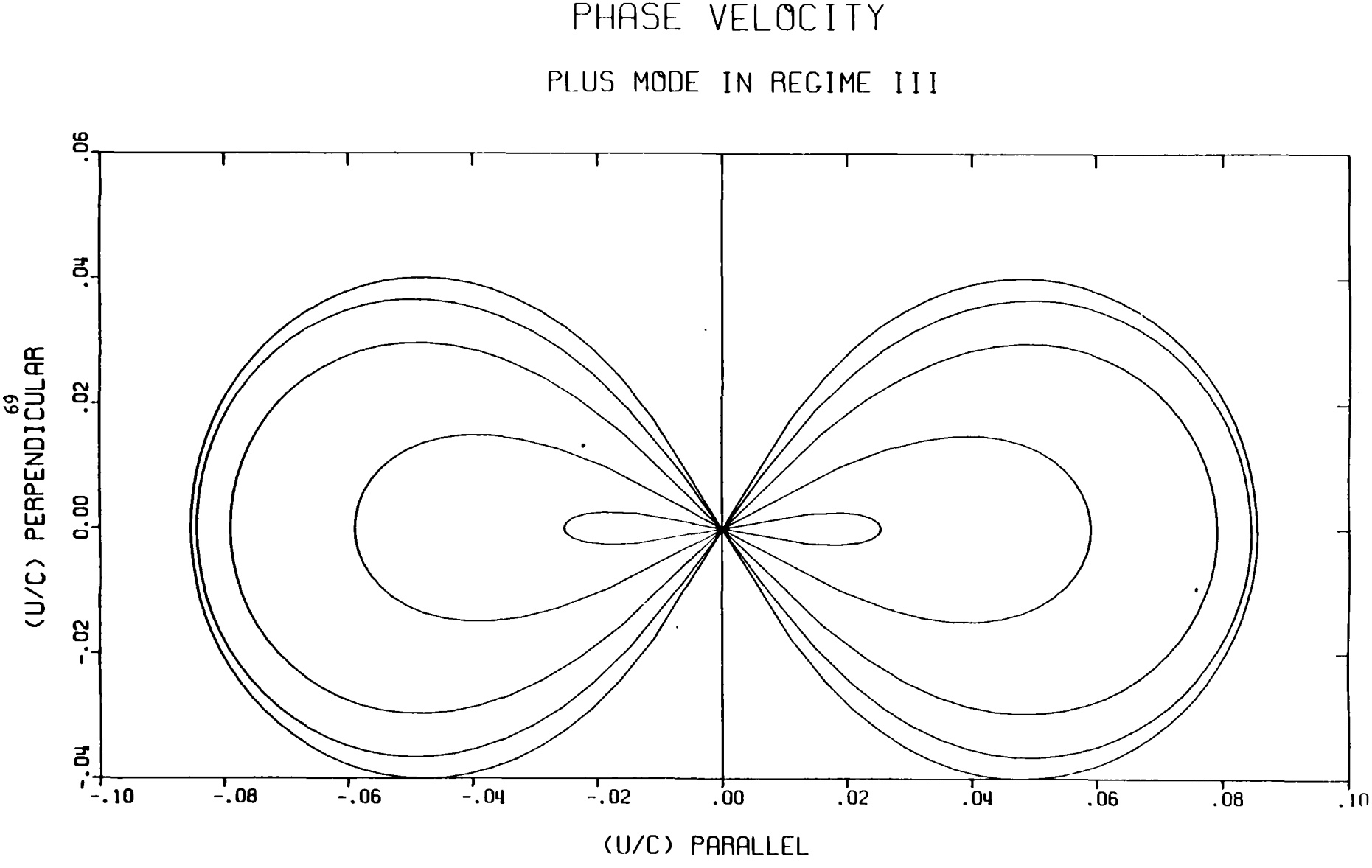
PHASE VELOCITY
PLUS MODE IN REGIME III
(U/C) PERPENDICULAR
.06
.04
.02
0.00
-.02
-.04
-.10
-.08
-.06
-.04
-.02
.00
.02
.04
.06
.08
.10
(U/C) PARALLEL

Figure 4.3b

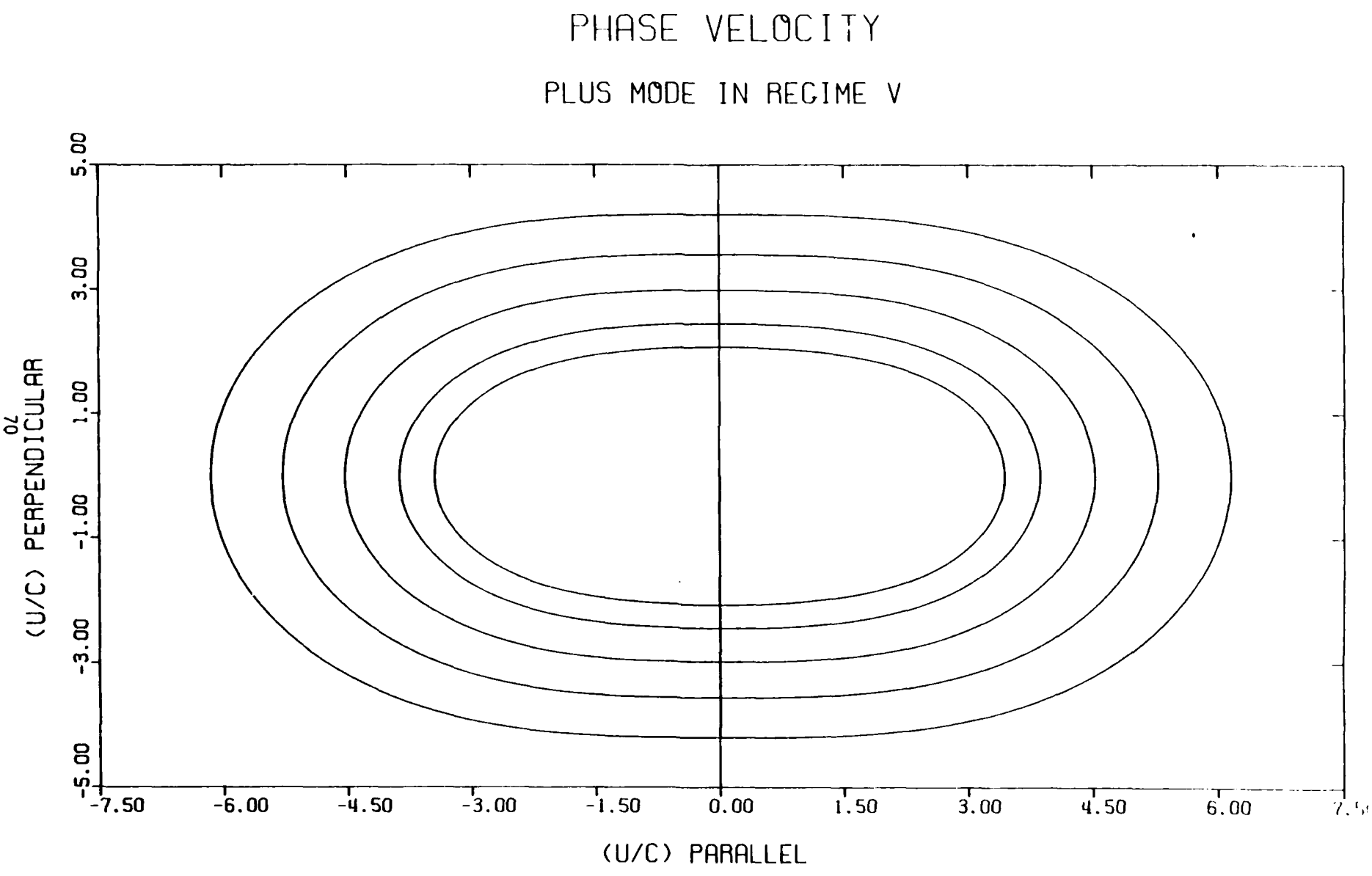
PHASE VELOCITY
PLUS MODE IN REGIME V
(U/C) PERPENDICULAR
0Z
5.00
3.00
1.00
-1.00
-3.00
-5.00
-7.50
-6.00
-4.50
-3.00
-1.50
0.00
1.50
3.00
4.50
6.00
(U/C) PARALLEL

Figure 4.4

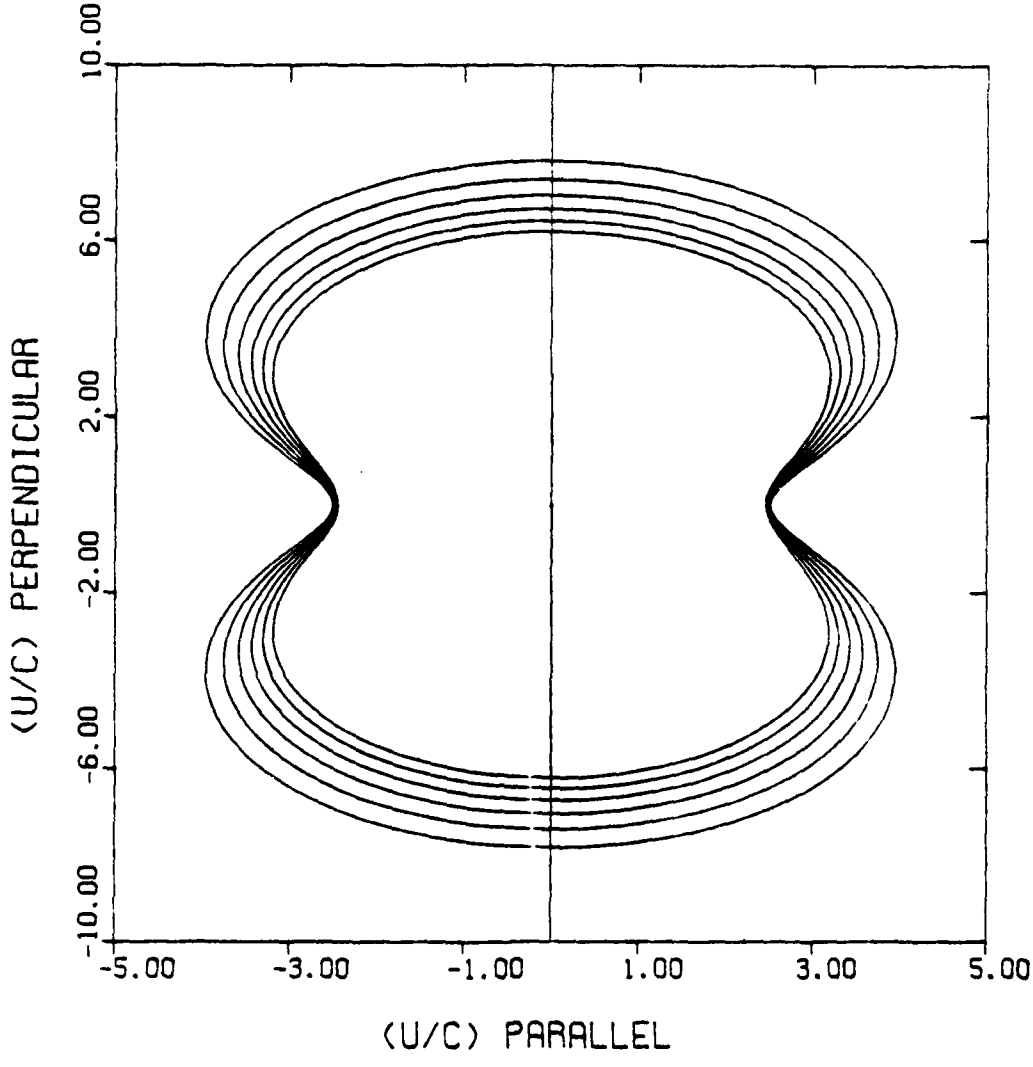
PHASE VELOCITY
PLUS MODE IN REGIME VI
(U/C) PERPENDICULAR
10.00
6.00
2.00
-2.00
-6.00
-10.00
-5.00
-3.00
-1.00
1.00
3.00
5.00
(U/C) PARALLEL

Figure 4.5

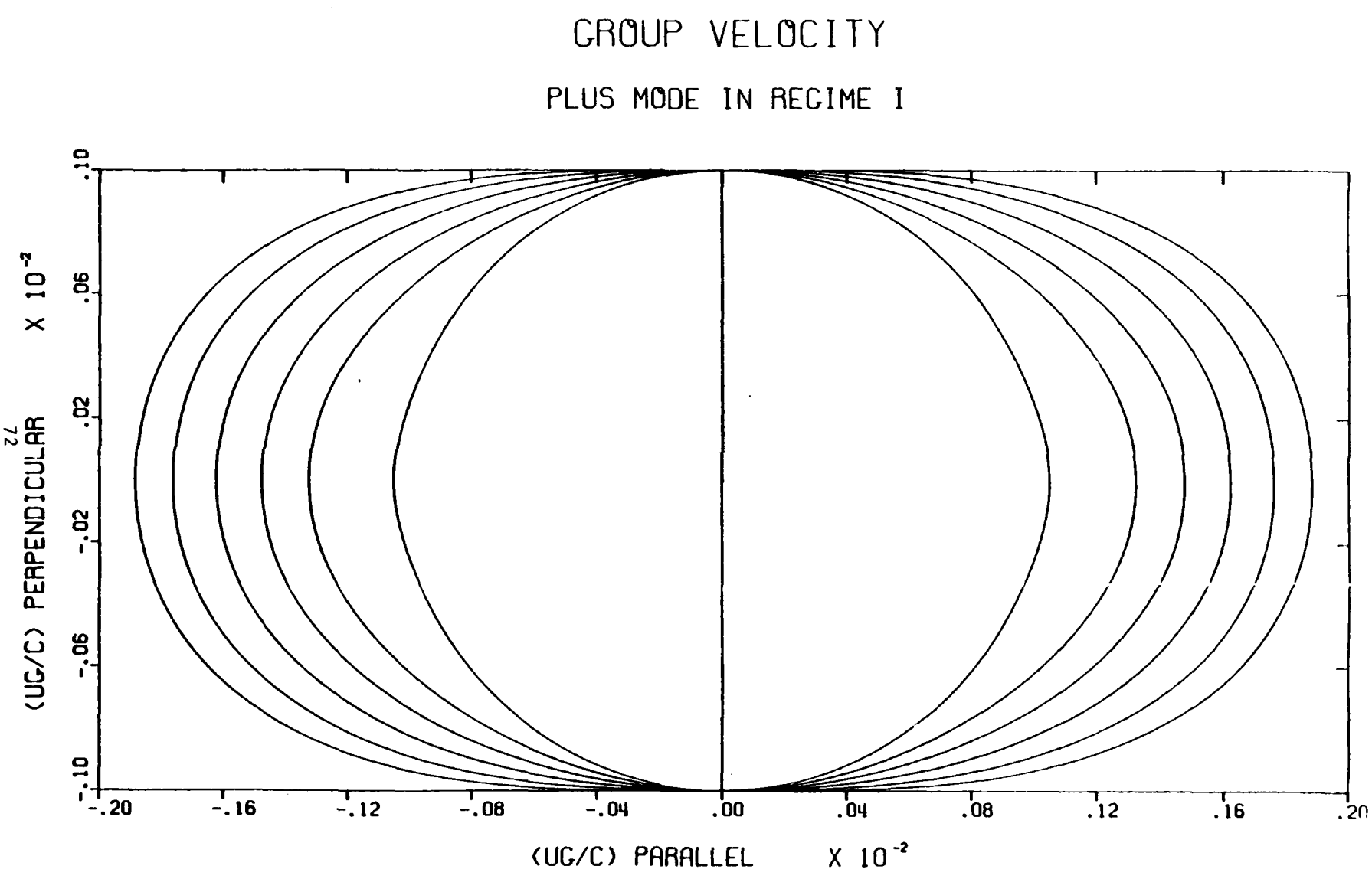
GROUP VELOCITY
PLUS MODE IN REGIME I
(UG/C) PERPENDICULAR X 10^-2
.10
.06
.02
-.02
-.06
-.10
-.20
-.16
-.12
-.08
-.04
.00
.04
.08
.12
.16
.20
(UG/C) PARALLEL X 10^-2

Figure 4.6

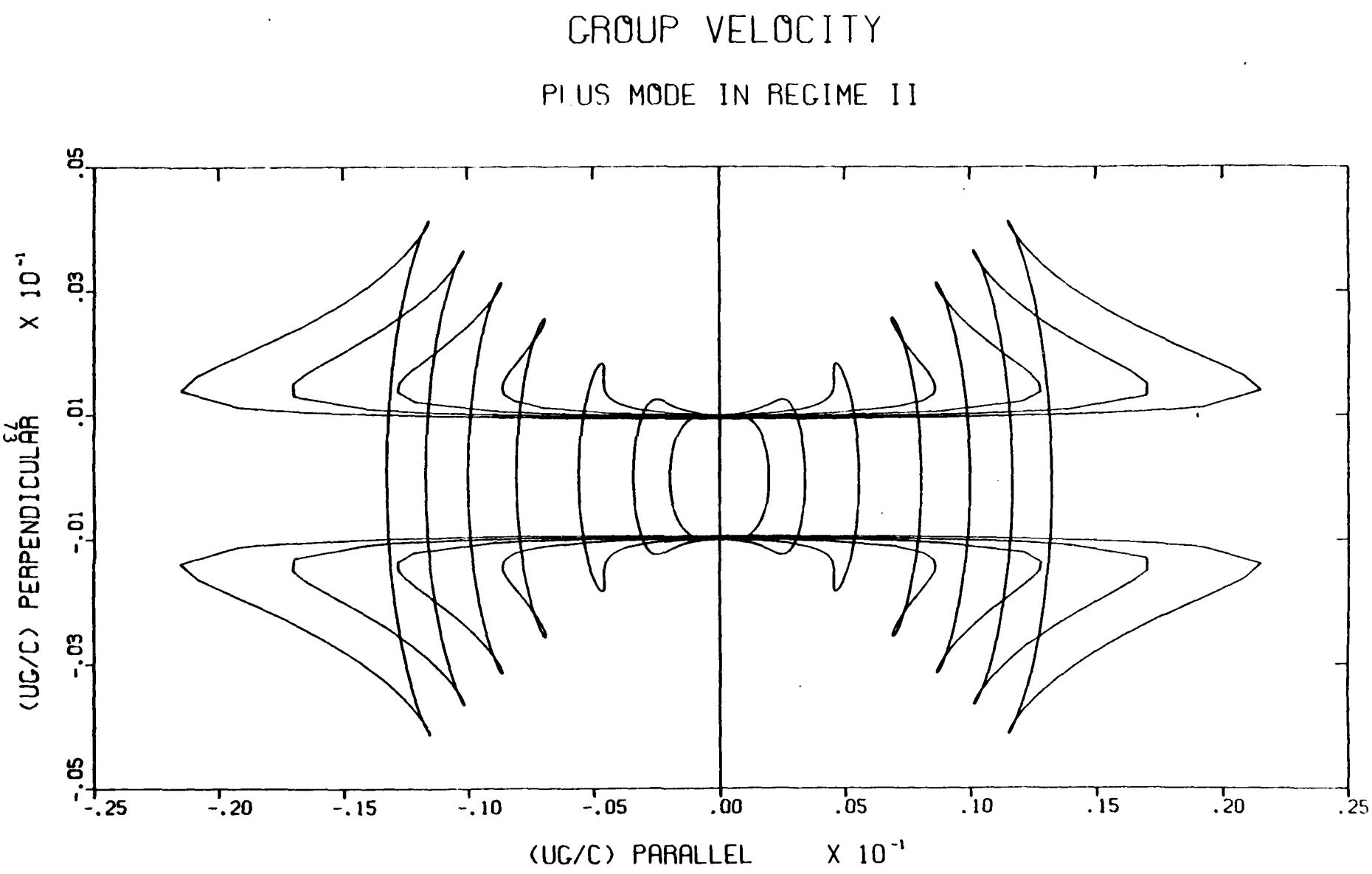
GROUP VELOCITY
PLUS MODE IN REGIME II
(UG/C) PERPENDICULAR X 10⁻¹
.05
.03
.01
-.01
-.03
-.05
-.25
-.20
-.15
-.10
-.05
.00
.05
.10
.15
.20
.25
(UG/C) PARALLEL X 10⁻¹

Figure 4.7

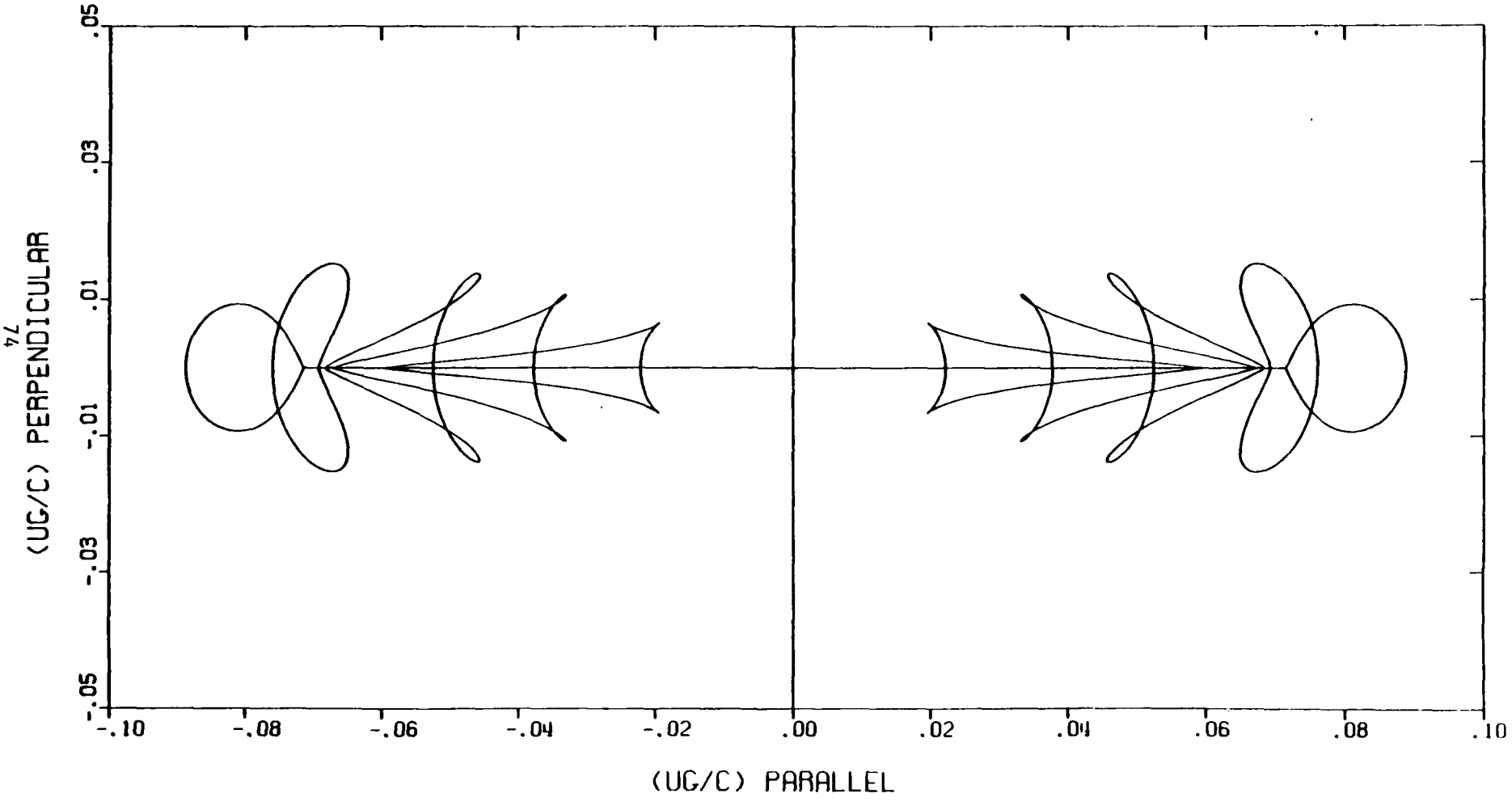
GROUP VELOCITY
PLUS MODE IN REGIME III
(UG/C) PERPENDICULAR
.05
.03
.01
-.01
-.03
-.05
-.10
-.08
-.06
-.04
-.02
.00
.02
.04
.06
.08
.10
(UG/C) PARALLEL

Figure 4.8a

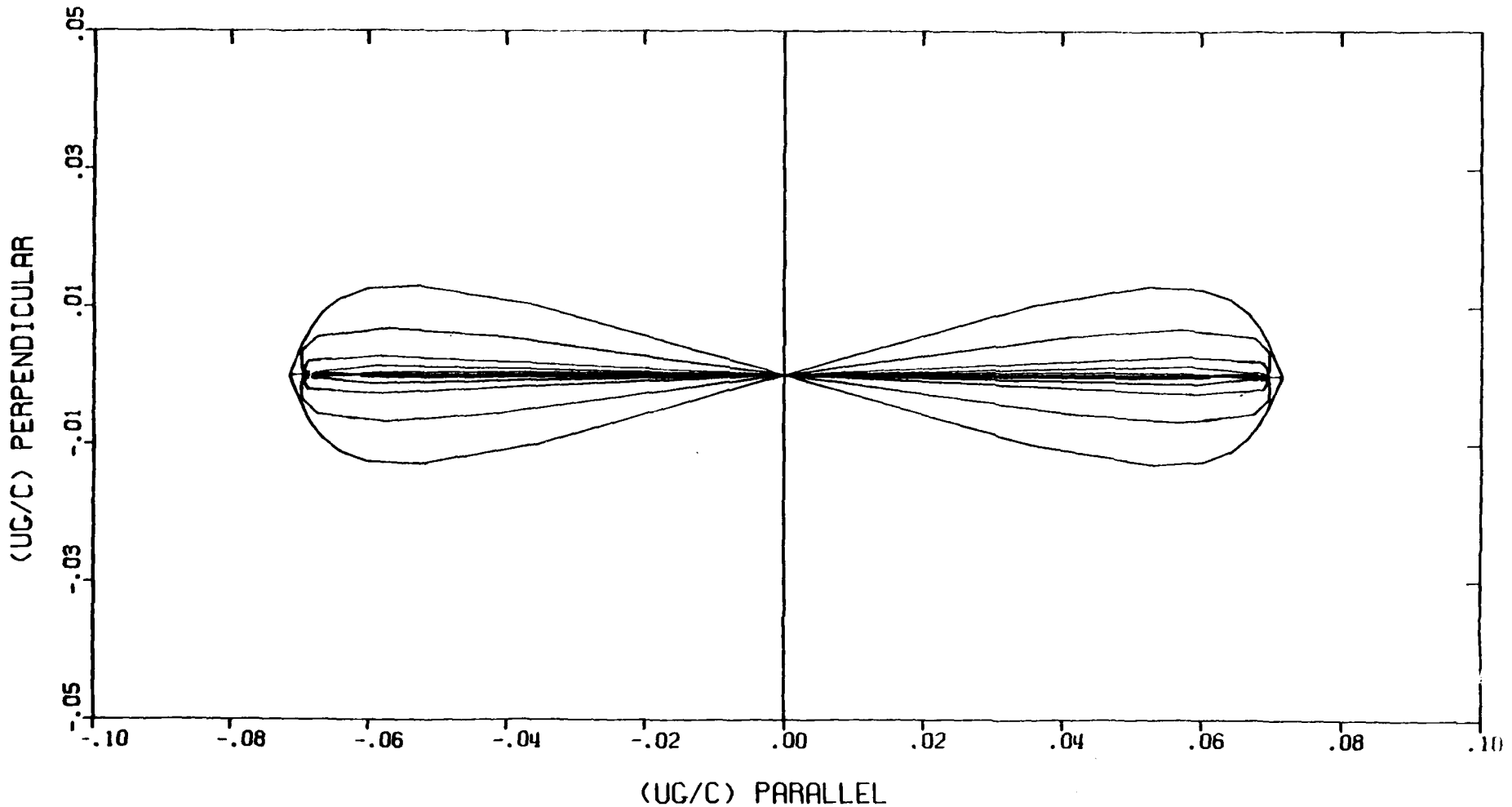
GROUP VELOCITY
PLUS MODE IN REGIME III
(UG/C) PERPENDICULAR
.05
.03
.01
-.01
-.03
-.05
-.10
-.08
-.06
-.04
-.02
.00
.02
.04
.06
.08
.10
(UG/C) PARALLEL

Figure 4.8b

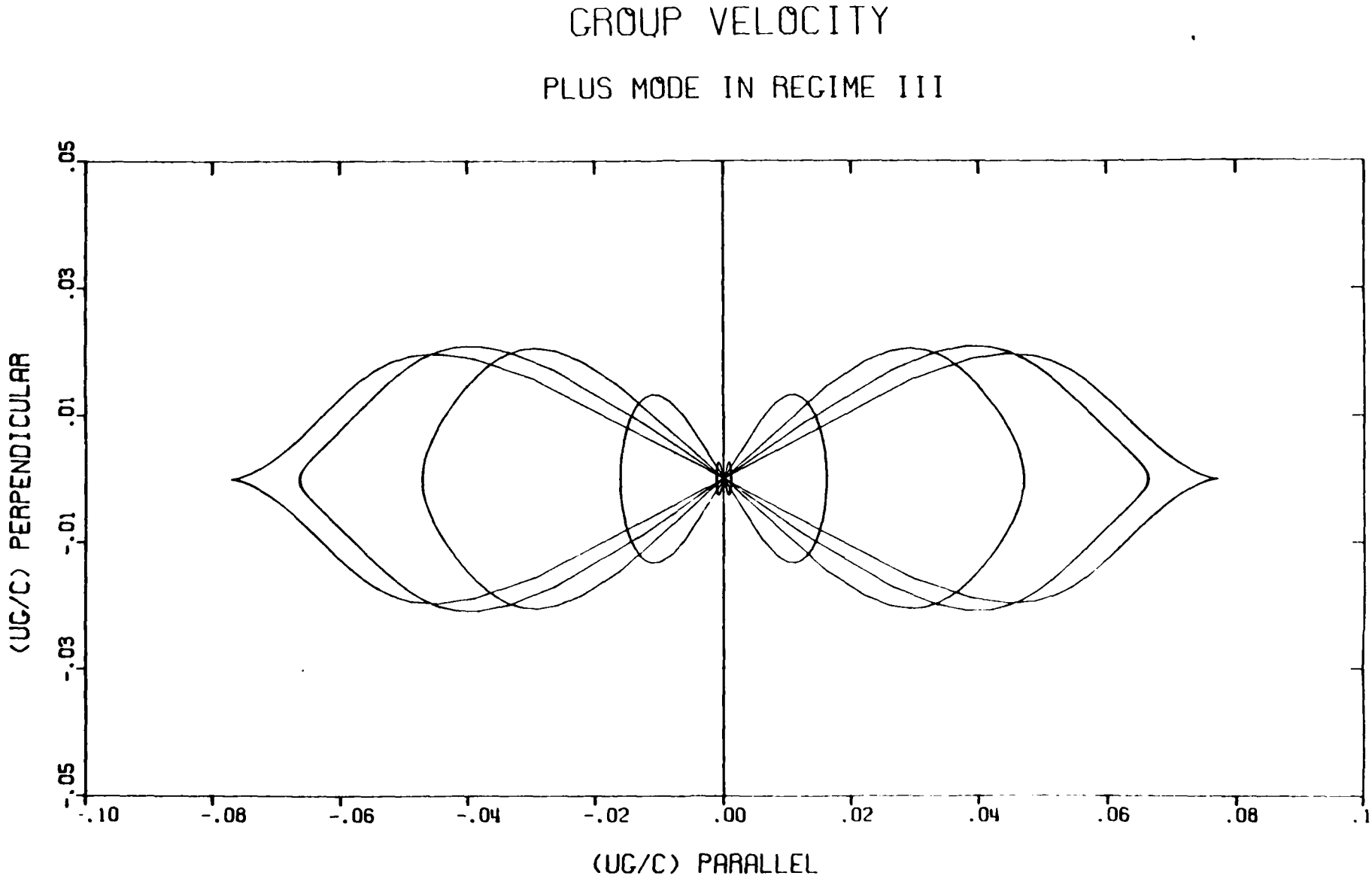
GROUP VELOCITY
PLUS MODE IN REGIME III
(UG/C) PERPENDICULAR
.05
.03
.01
-.01
-.03
-.05
-.10
-.08
-.06
-.04
-.02
.00
.02
.04
.06
.08
.1
(UG/C) PARALLEL

Figure 4.8c

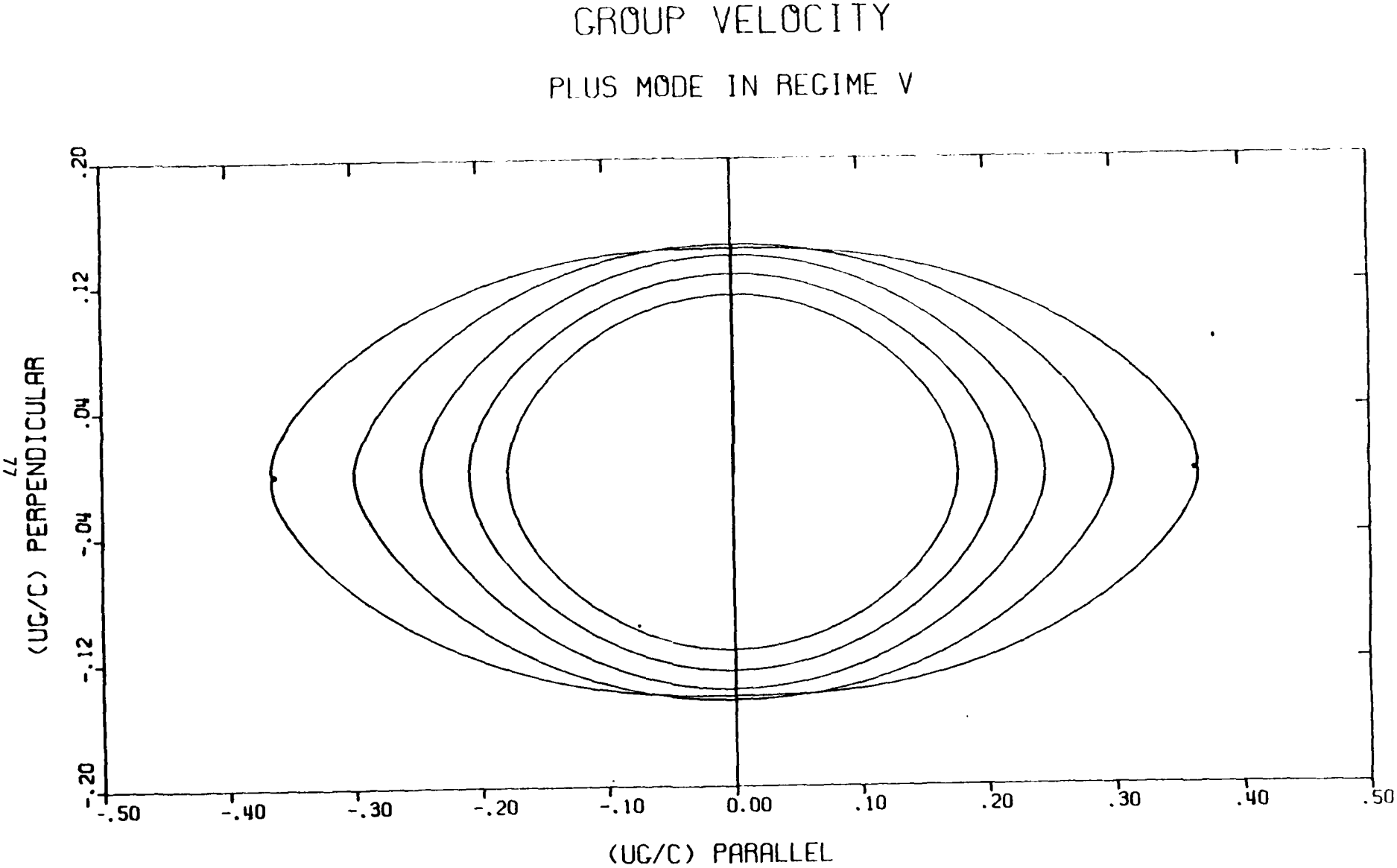
GROUP VELOCITY
PLUS MODE IN REGIME V
(UG/C) PERPENDICULAR
(UG/C) PARALLEL
.20
.12
.04
-.04
-.12
-.20
-.50
-.40
-.30
-.20
-.10
0.00
.10
.20
.30
.40
.50

Figure 4.9

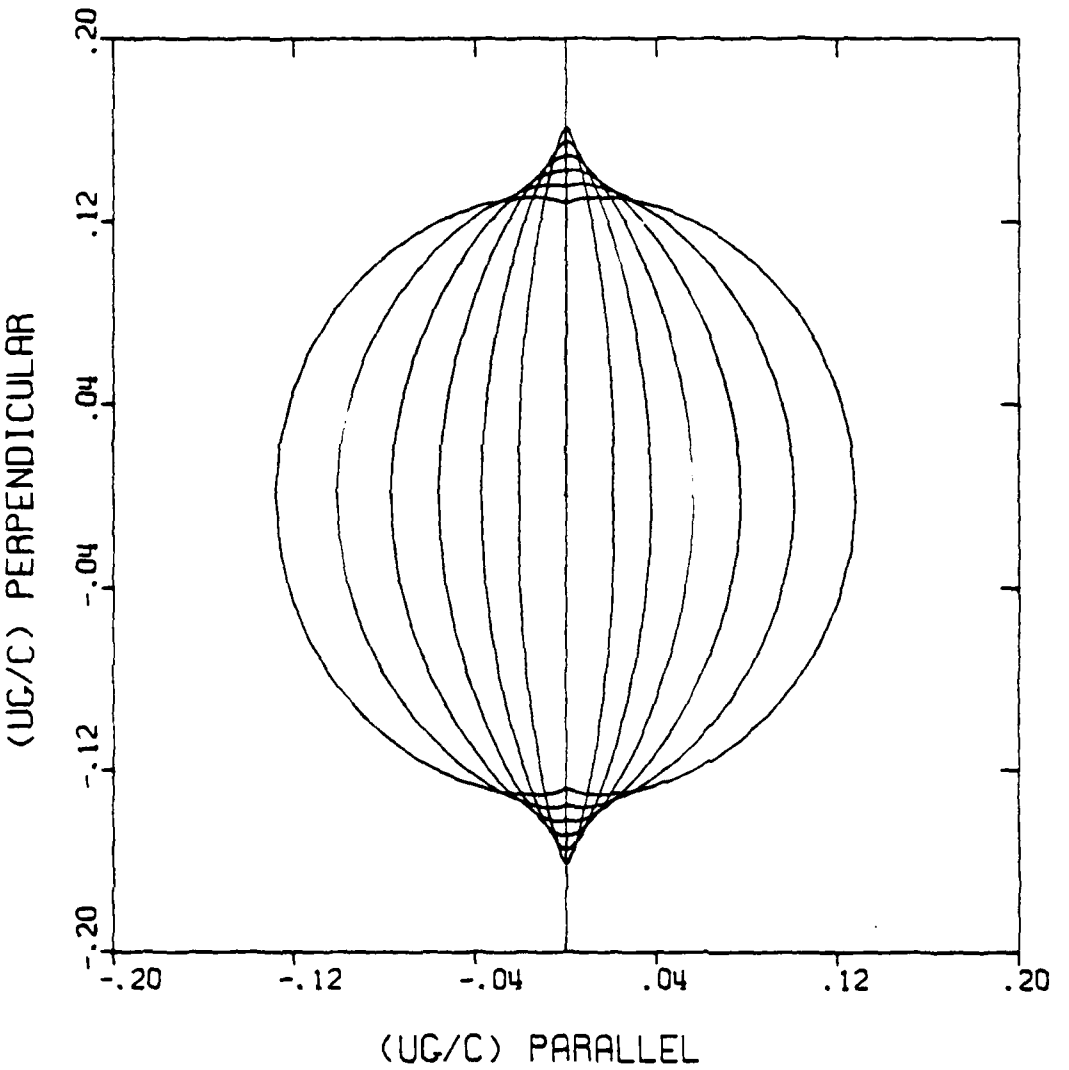
GROUP VELOCITY
PLUS MODE IN REGIME VI
(UC/C) PERPENDICULAR
.20
.12
.04
-.04
-.12
-.20
-.20
-.12
-.04
.04
.12
.20
(UC/C) PARALLEL

Figure 4.10

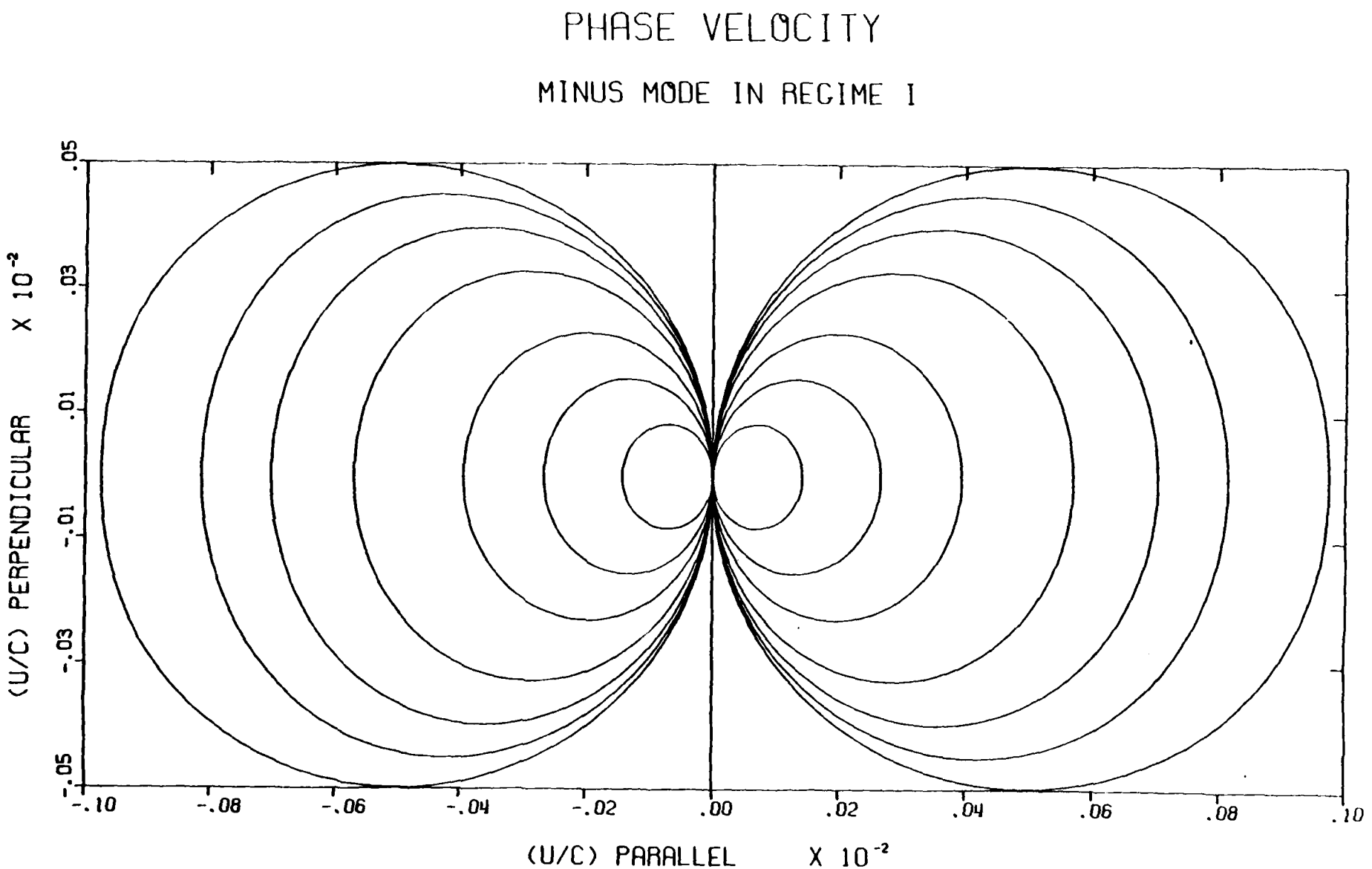
PHASE VELOCITY
MINUS MODE IN REGIME I
(U/C) PERPENDICULAR X 10⁻²
.05
.03
.01
-.01
-.03
-.05
-.10
-.08
-.06
-.04
-.02
.00
.02
.04
.06
.08
.10
(U/C) PARALLEL X 10⁻²

Figure 4.11

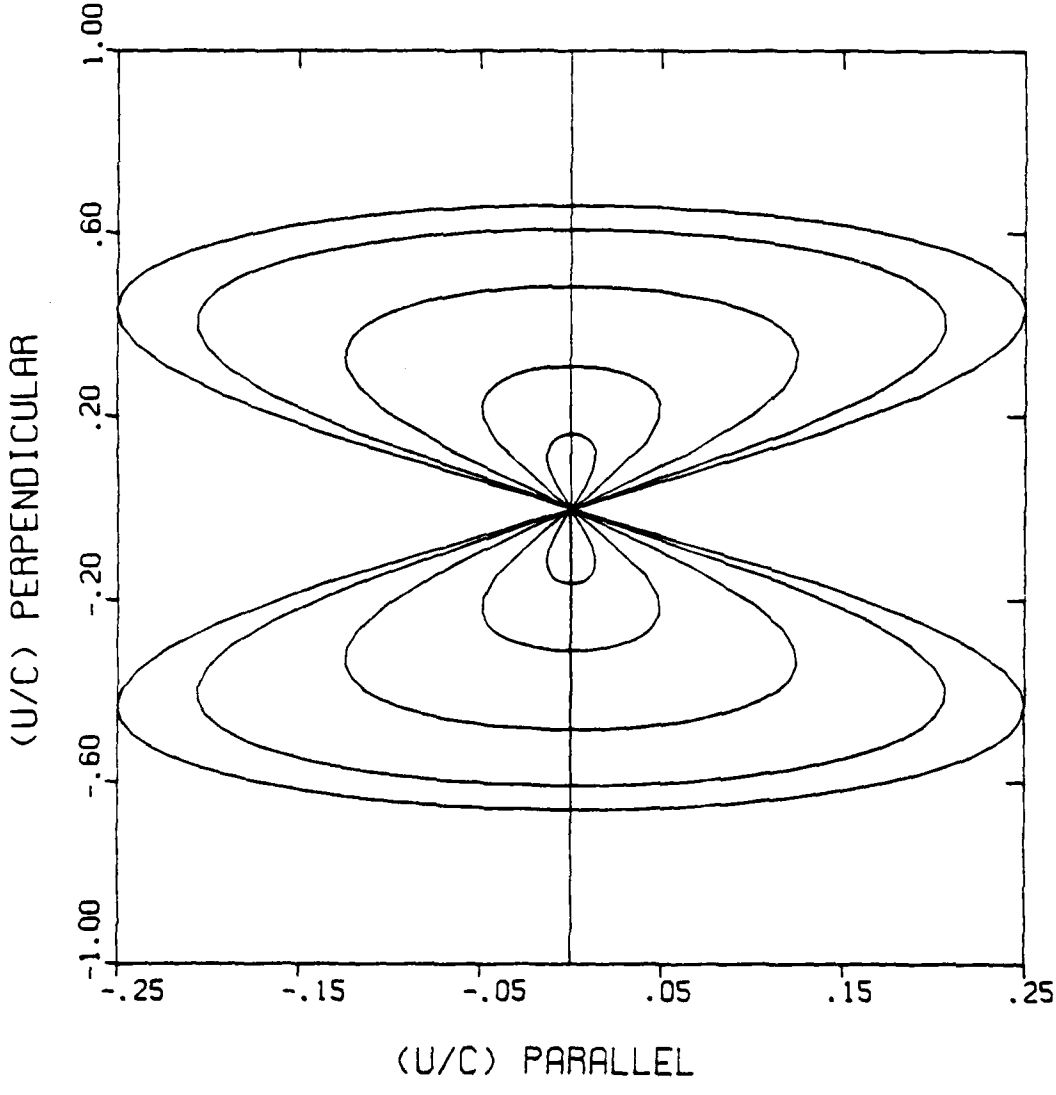
PHASE VELOCITY
MINUS MODE IN REGIME VI
(U/C) PERPENDICULAR
1.00
.60
.20
-.20
-.60
-1.00
-.25
-.15
-.05
.05
.15
.25
(U/C) PARALLEL

Figure 4.12

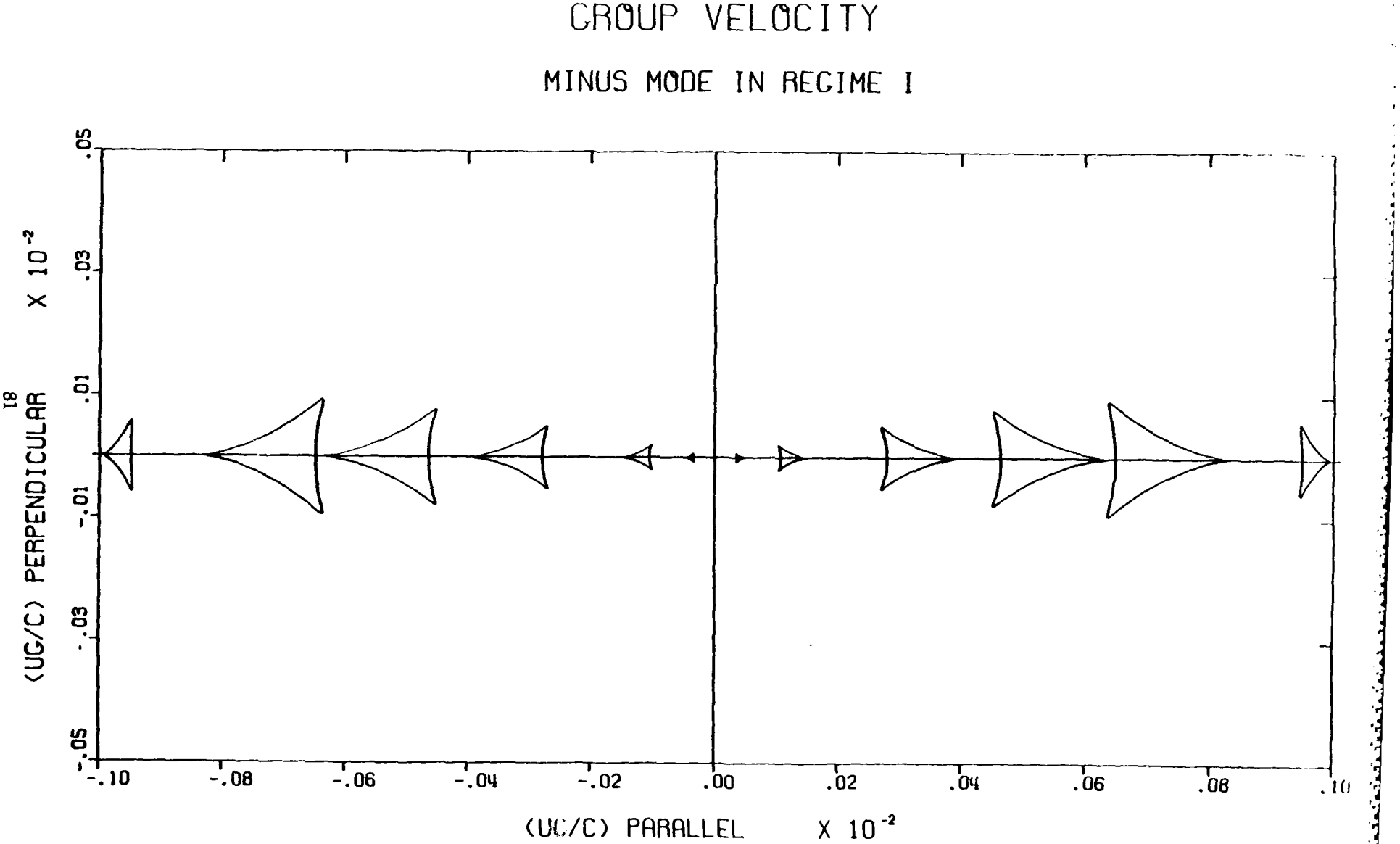
GROUP VELOCITY
MINUS MODE IN REGIME I
(UG/C) PERPENDICULAR X 10⁻²
.05
.03
.01
-.01
-.03
-.05
-.10
-.08
-.06
-.04
-.02
.00
.02
.04
.06
.08
.10
(UC/C) PARALLEL X 10⁻²

Figure 4.13

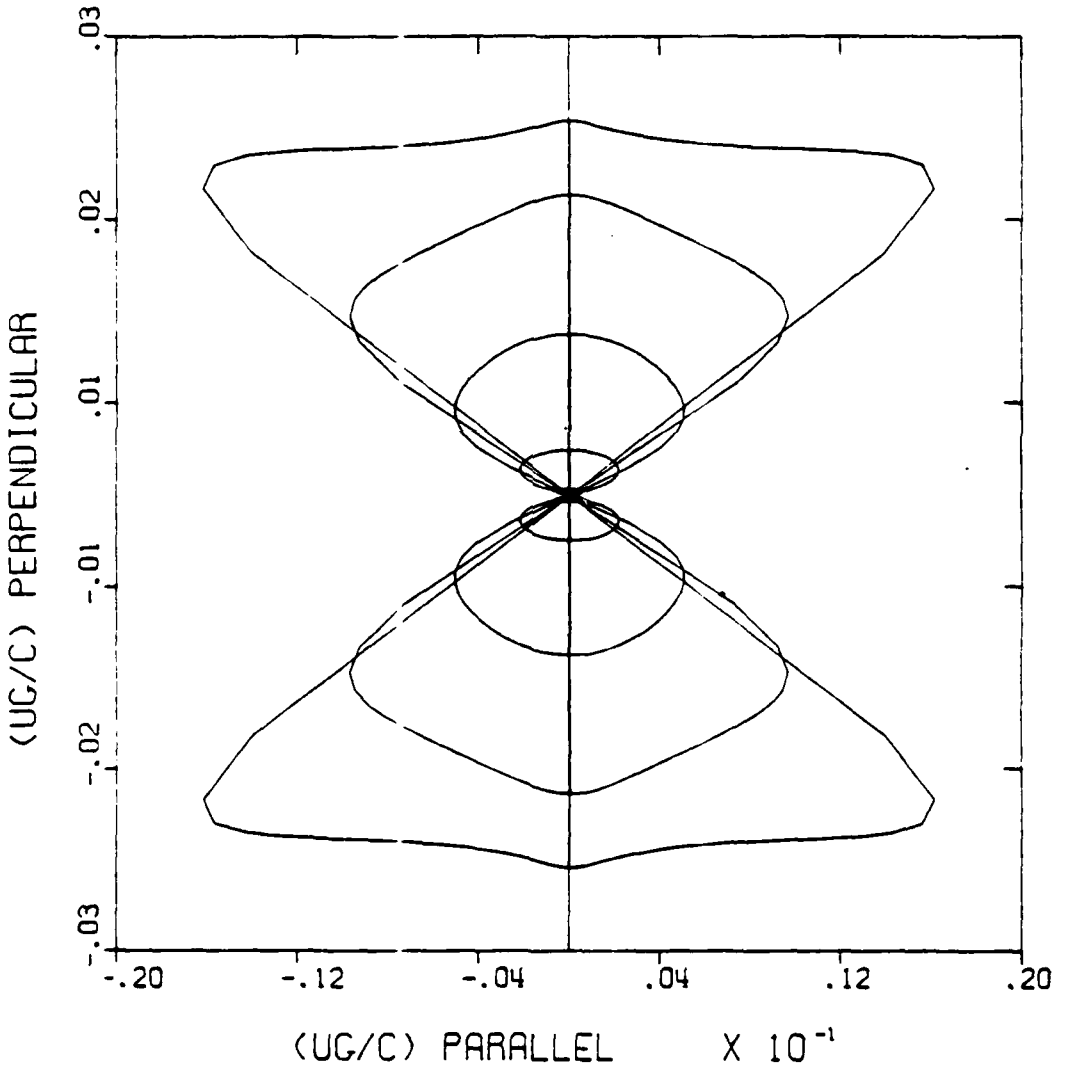
GROUP VELOCITY
MINUS MODE IN REGIME VI
(UG/C) PERPENDICULAR
.03
.02
.01
-.01
-.02
-.03
-.20
-.12
-.04
.04
.12
.20
(UG/C) PARALLEL X 10⁻¹

Figure 4.14

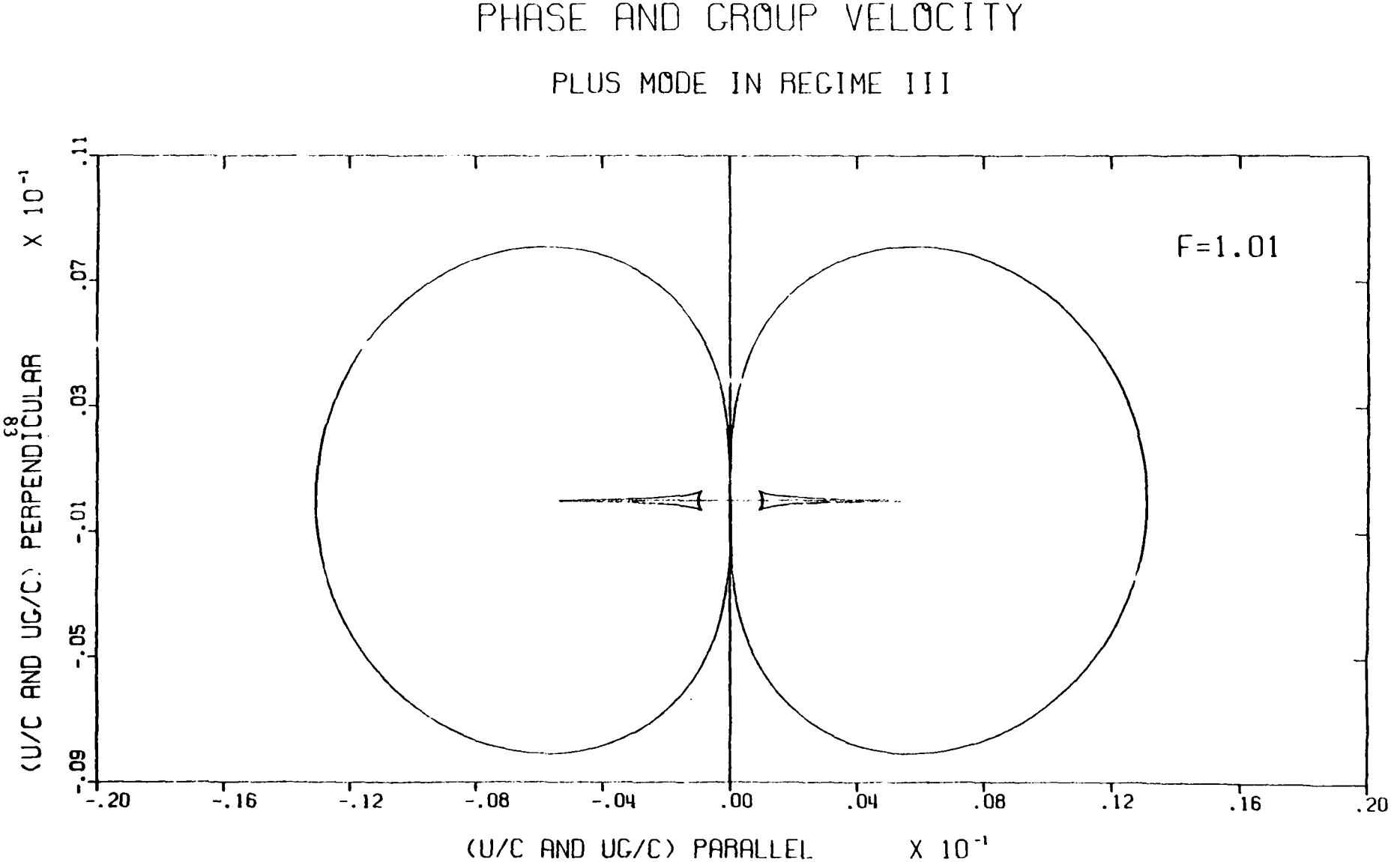
PHASE AND GROUP VELOCITY
PLUS MODE IN REGIME III
F=1.01
(U/C AND UG/C) PERPENDICULAR X 10⁻¹
(U/C AND UG/C) PARALLEL X 10⁻¹
.11
.07
.03
-.01
-.05
-.09
-.20
-.16
-.12
-.08
-.04
.00
.04
.08
.12
.16
.20

Figure 4.15

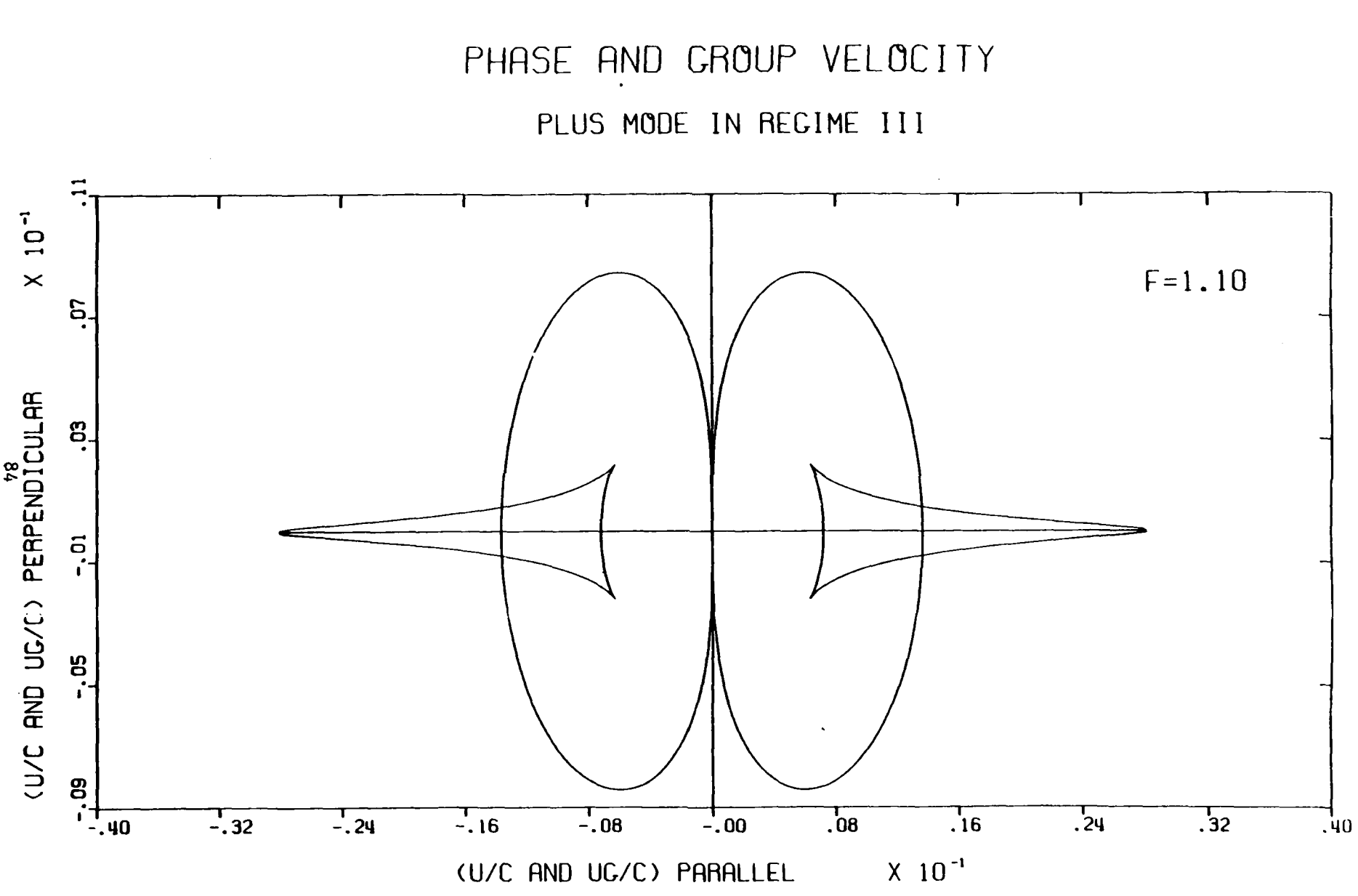
PHASE AND GROUP VELOCITY
PLUS MODE IN REGIME III
F=1.10
(U/C AND UG/C) PERPENDICULAR X 10⁻¹
(U/C AND UG/C) PARALLEL X 10⁻¹
.11
.07
.03
-.01
-.05
-.09
-.40
-.32
-.24
-.16
-.08
-.00
.08
.16
.24
.32
.40

Figure 4.16

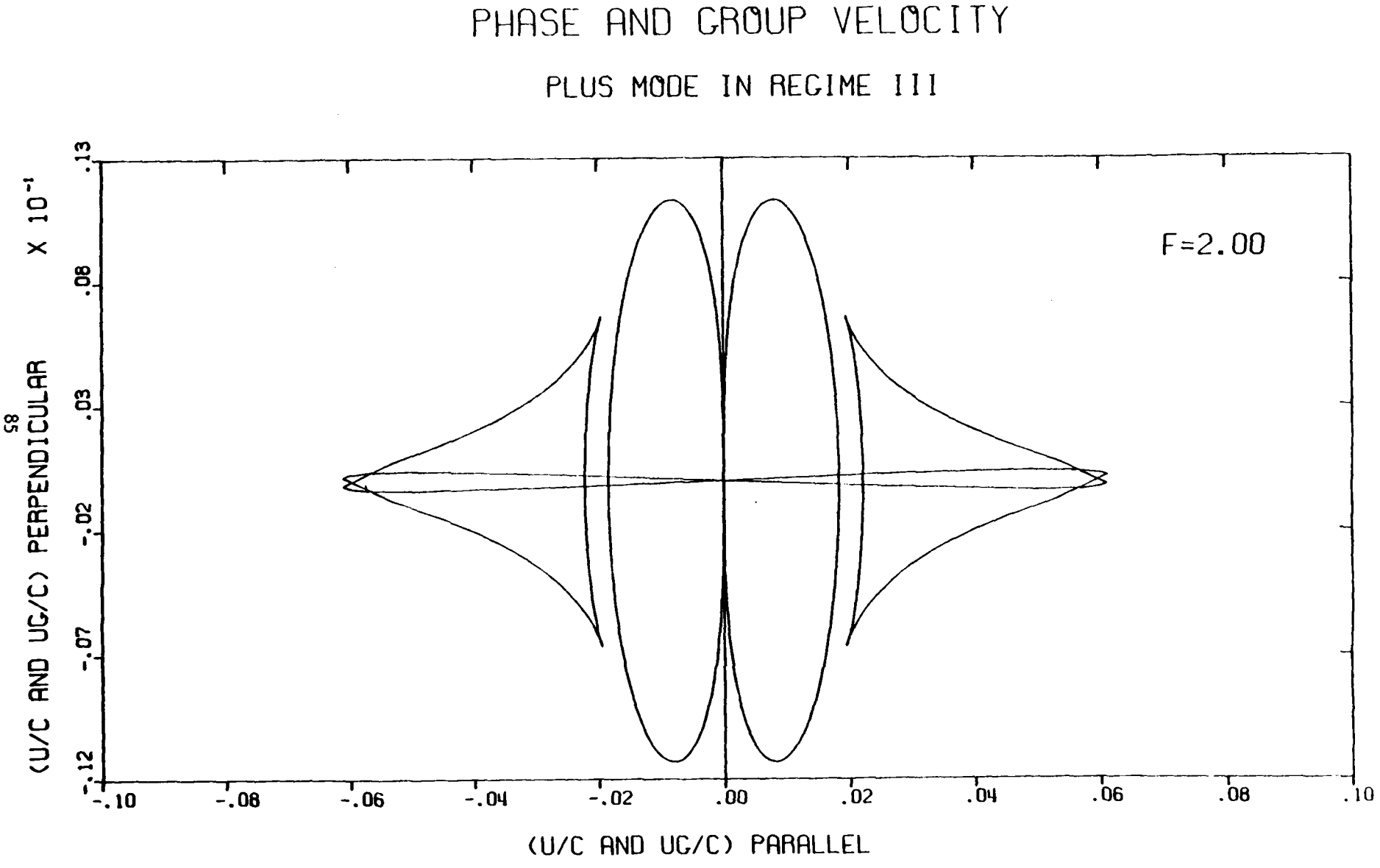
PHASE AND GROUP VELOCITY
PLUS MODE IN REGIME III
F=2.00
(U/C AND UG/C) PERPENDICULAR X 10⁻¹
(U/C AND UG/C) PARALLEL
.13
.08
.03
-.02
-.07
-.12
-.10
-.08
-.06
-.04
-.02
.00
.02
.04
.06
.08
.10

Figure 4.17

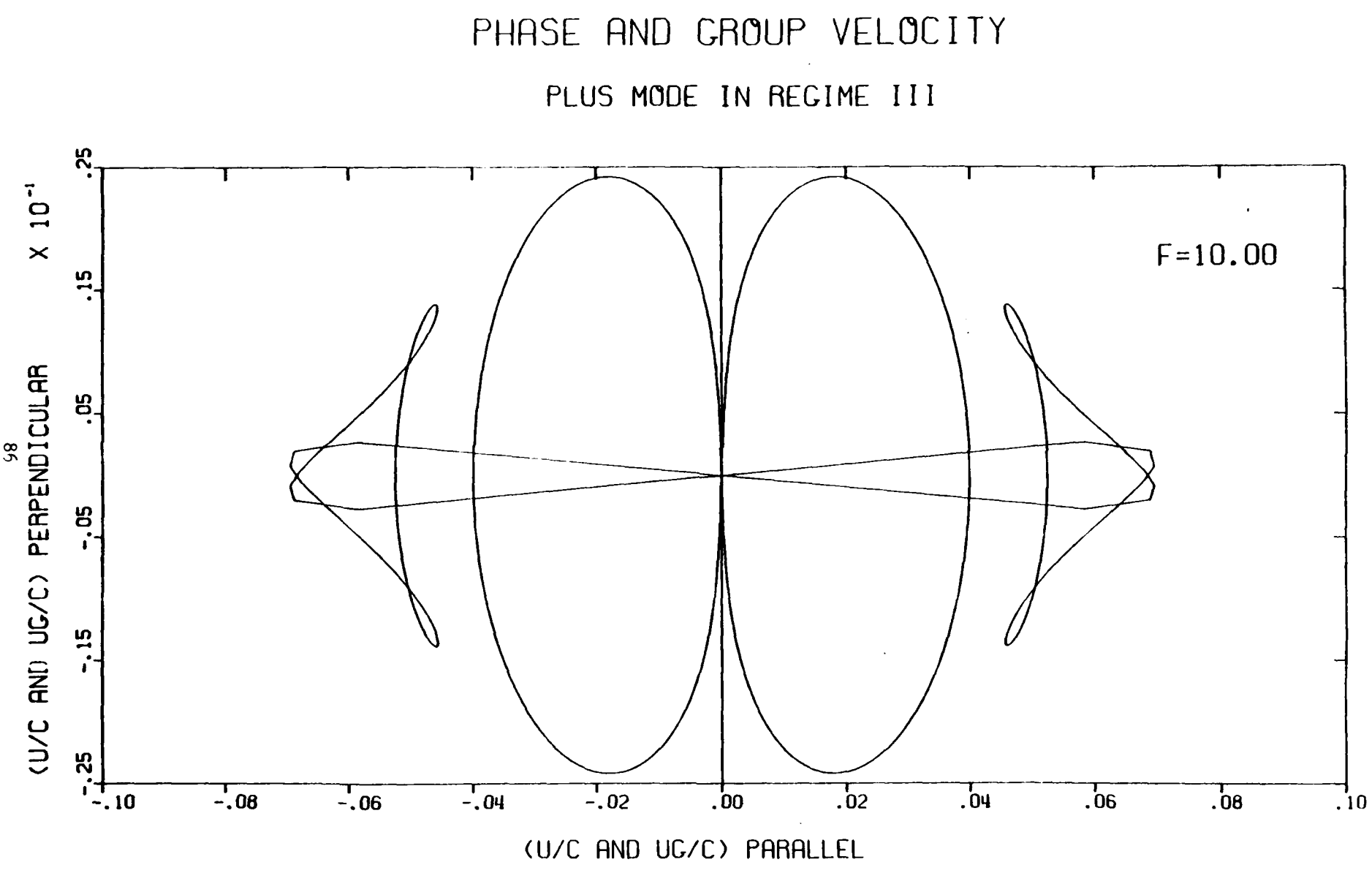
PHASE AND GROUP VELOCITY
PLUS MODE IN REGIME III
F=10.00
(U/C AND UG/C) PERPENDICULAR X 10⁻¹
.25
.15
.05
-.05
-.15
-.25
-.10
-.08
-.06
-.04
-.02
.00
.02
.04
.06
.08
.10
(U/C AND UG/C) PARALLEL

Figure 4.18

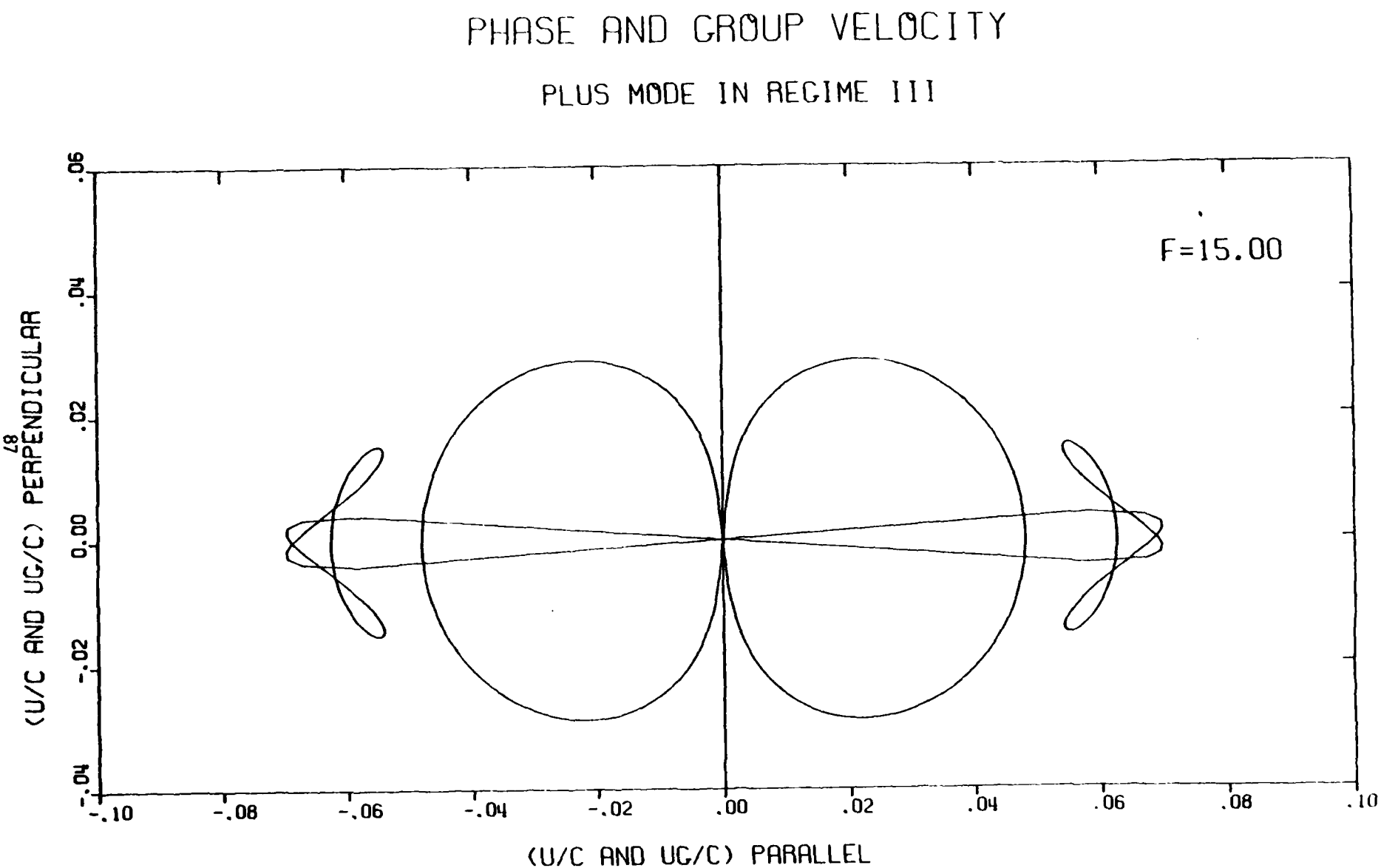
PHASE AND GROUP VELOCITY
PLUS MODE IN REGIME III
F=15.00
(U/C AND UG/C) PERPENDICULAR
.06
.04
.02
0.00
-.02
-.04
-.10
-.08
-.06
-.04
-.02
.00
.02
.04
.06
.08
.10
(U/C AND UG/C) PARALLEL

Figure 4.19

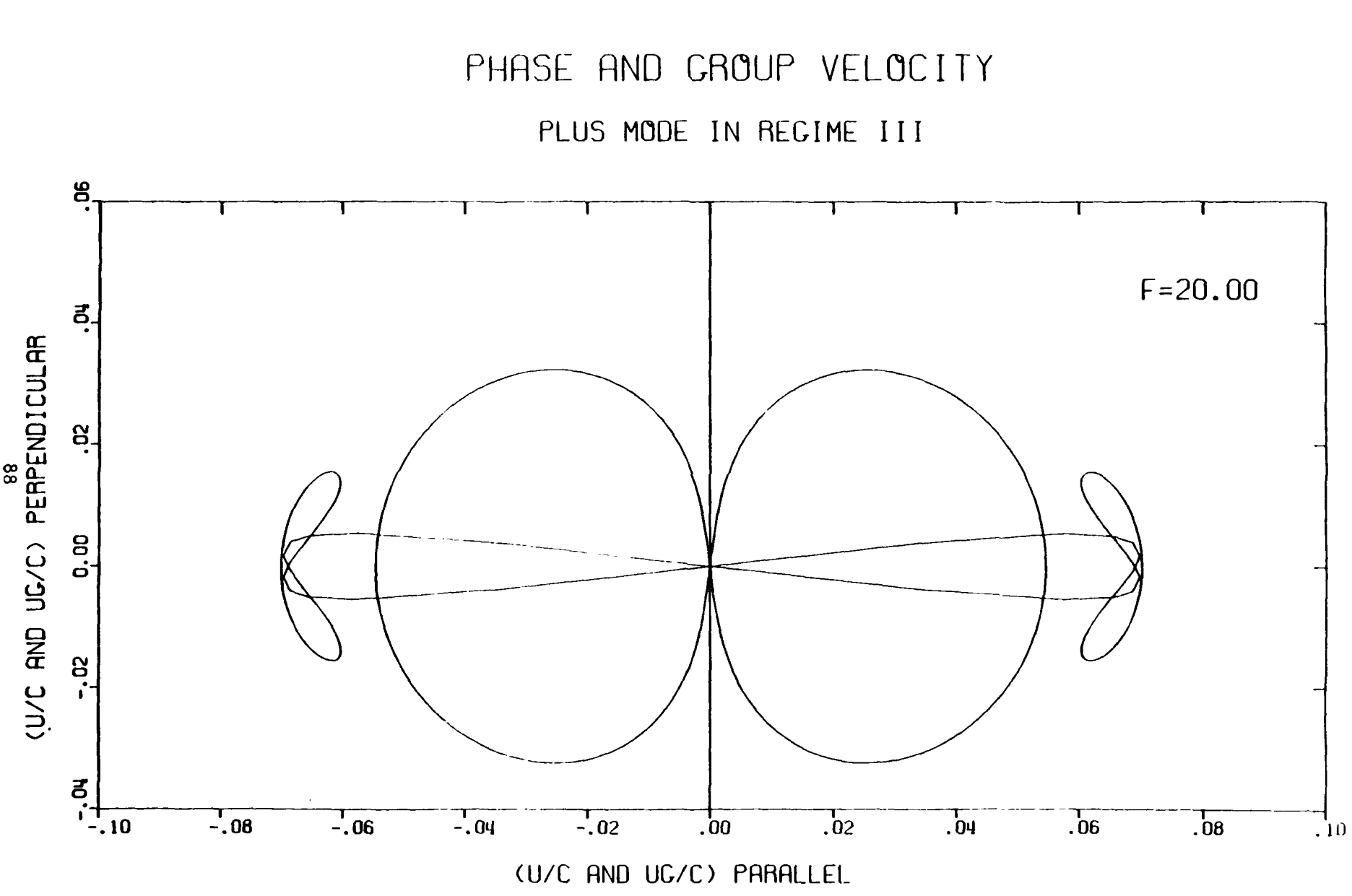
PHASE AND GROUP VELOCITY
PLUS MODE IN REGIME III
F=20.00
(U/C AND UG/C) PERPENDICULAR
(U/C AND UG/C) PARALLEL
.06
.04
.02
0.00
-.02
-.04
-.10
-.08
-.06
-.04
-.02
.00
.02
.04
.06
.08
.10

Figure 4.20

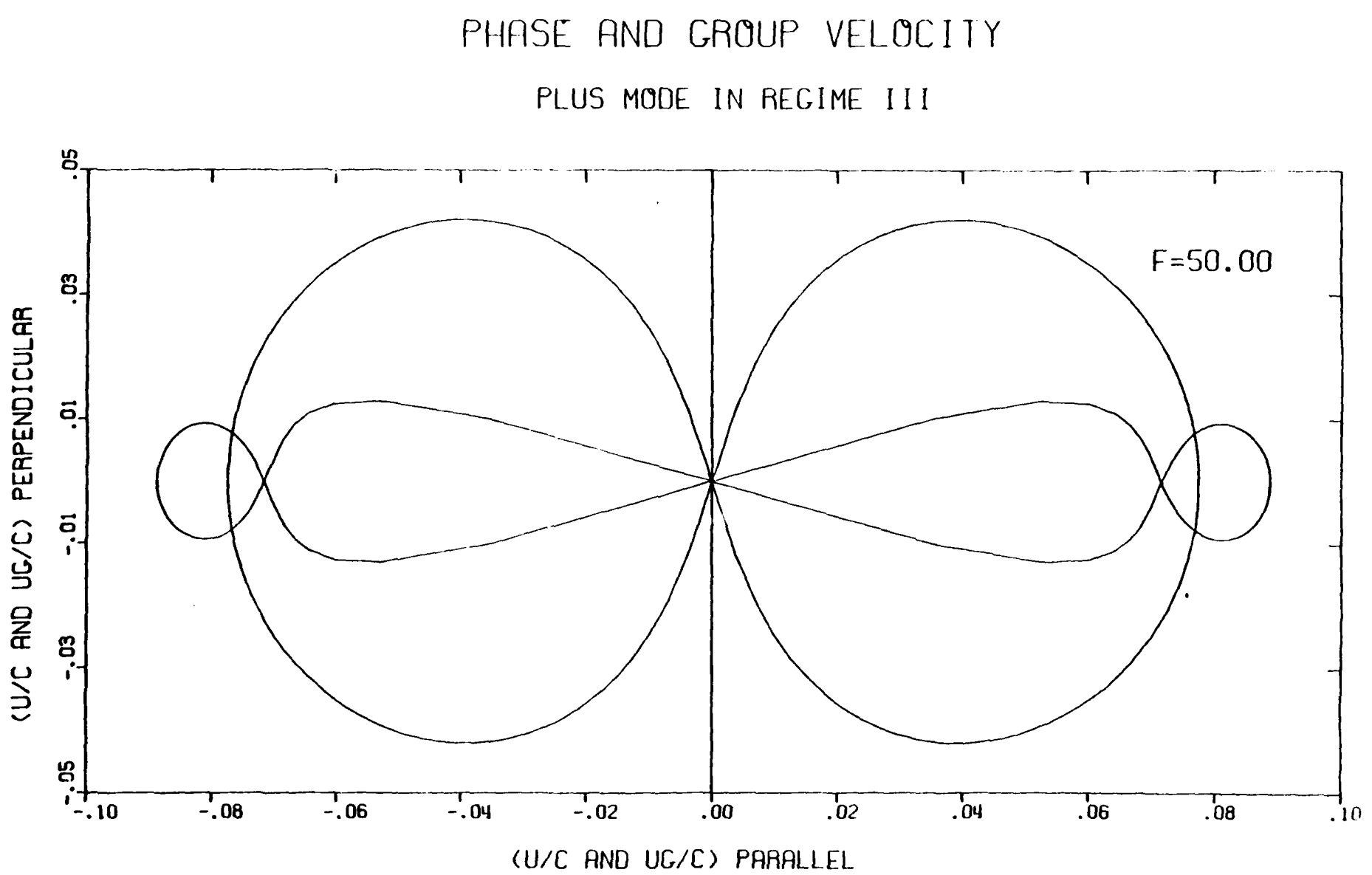
PHASE AND GROUP VELOCITY
PLUS MODE IN REGIME III
F=50.00
(U/C AND UG/C) PERPENDICULAR
.05
.03
.01
-.01
-.03
-.05
-.10
-.08
-.06
-.04
-.02
.00
.02
.04
.06
.08
.10
(U/C AND UG/C) PARALLEL

Figure 4.21

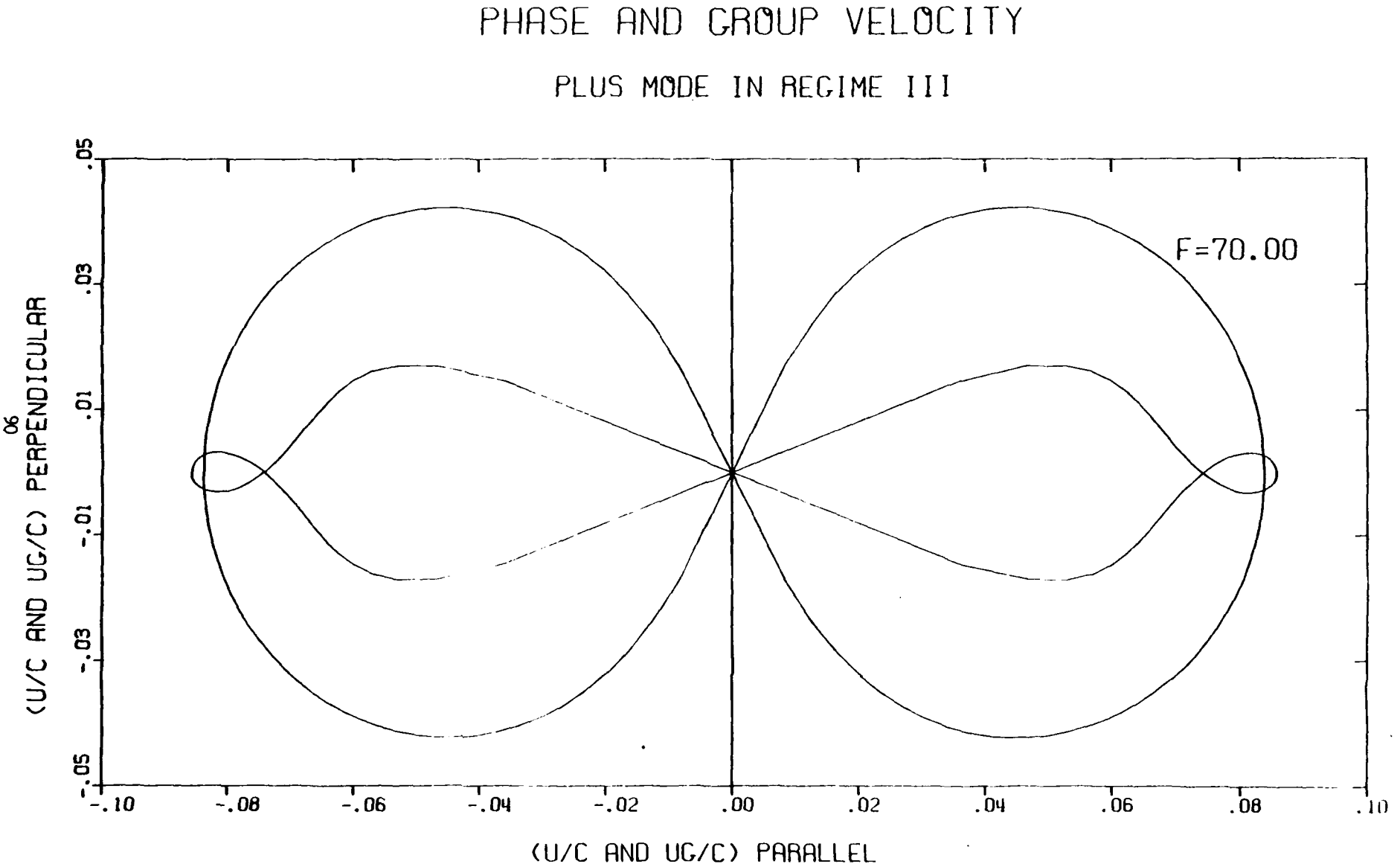
PHASE AND GROUP VELOCITY
PLUS MODE IN REGIME III
F=70.00
(U/C AND UG/C) PERPENDICULAR
06
.05
.03
.01
-.01
-.03
-.05
-.10
-.08
-.06
-.04
-.02
.00
.02
.04
.06
.08
.10
(U/C AND UG/C) PARALLEL

Figure 4.22

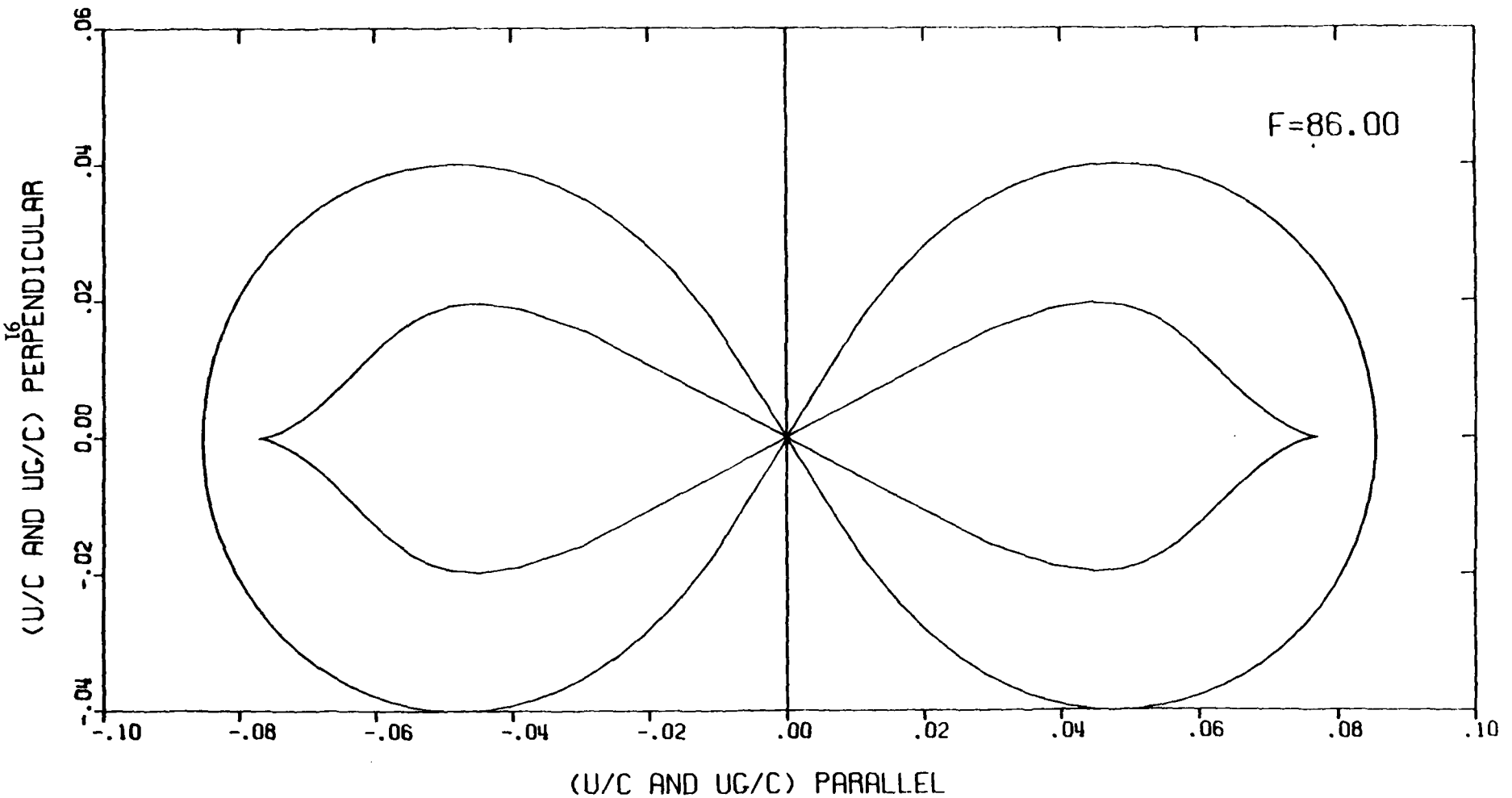
PHASE AND GROUP VELOCITY
PLUS MODE IN REGIME III
F=86.00
(U/C AND UG/C) PERPENDICULAR
16
.06
.04
.02
0.00
-.02
-.04
-.10
-.08
-.06
-.04
-.02
.00
.02
.04
.06
.08
.10
(U/C AND UG/C) PARALLEL

Figure 4.23

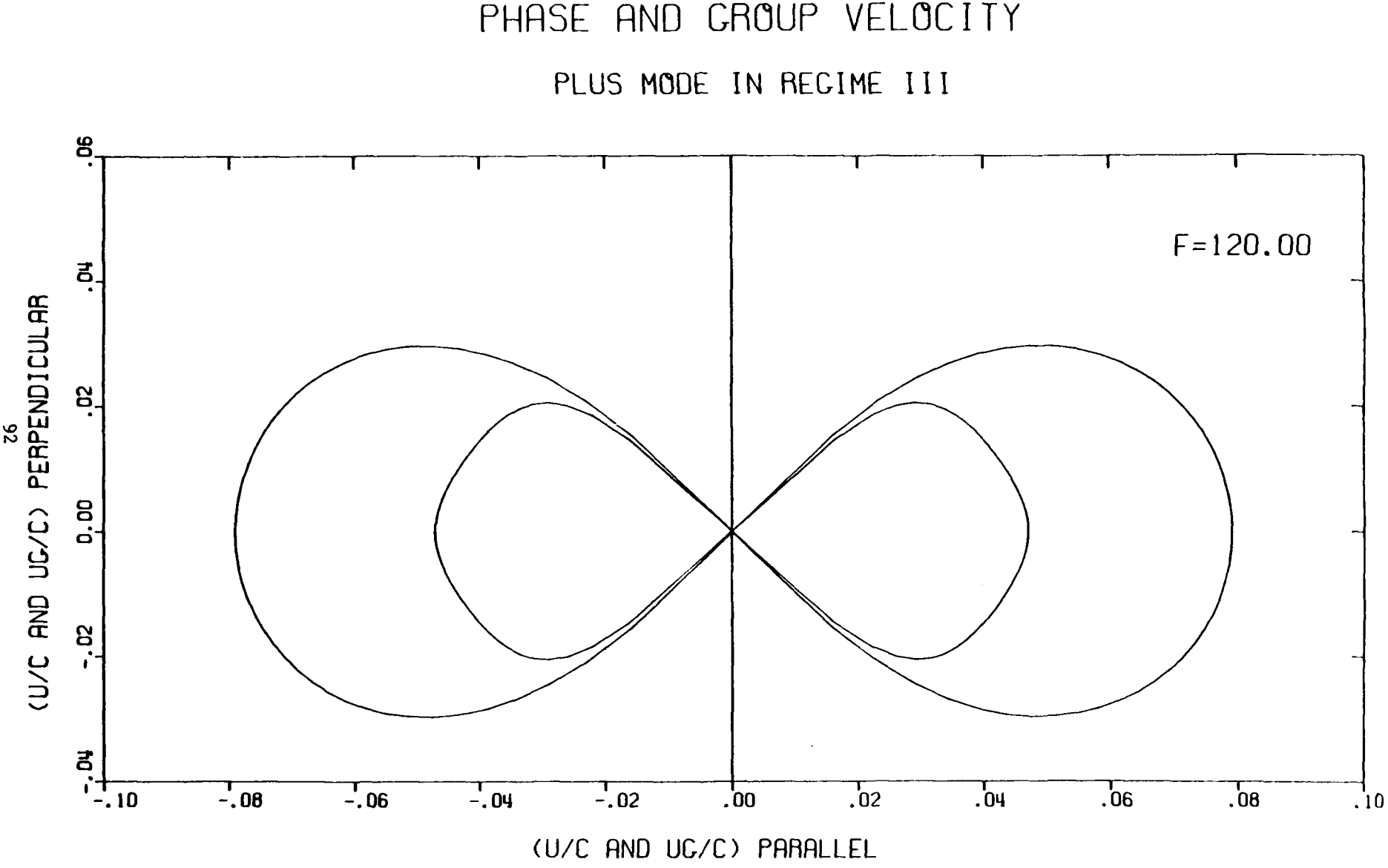
PHASE AND GROUP VELOCITY
PLUS MODE IN REGIME III
F=120.00
(U/C AND UG/C) PERPENDICULAR
92
.06
.04
.02
0.00
-.02
-.04
-.10
-.08
-.06
-.04
-.02
.00
.02
.04
.06
.08
.10
(U/C AND UG/C) PARALLEL

Figure 4.24

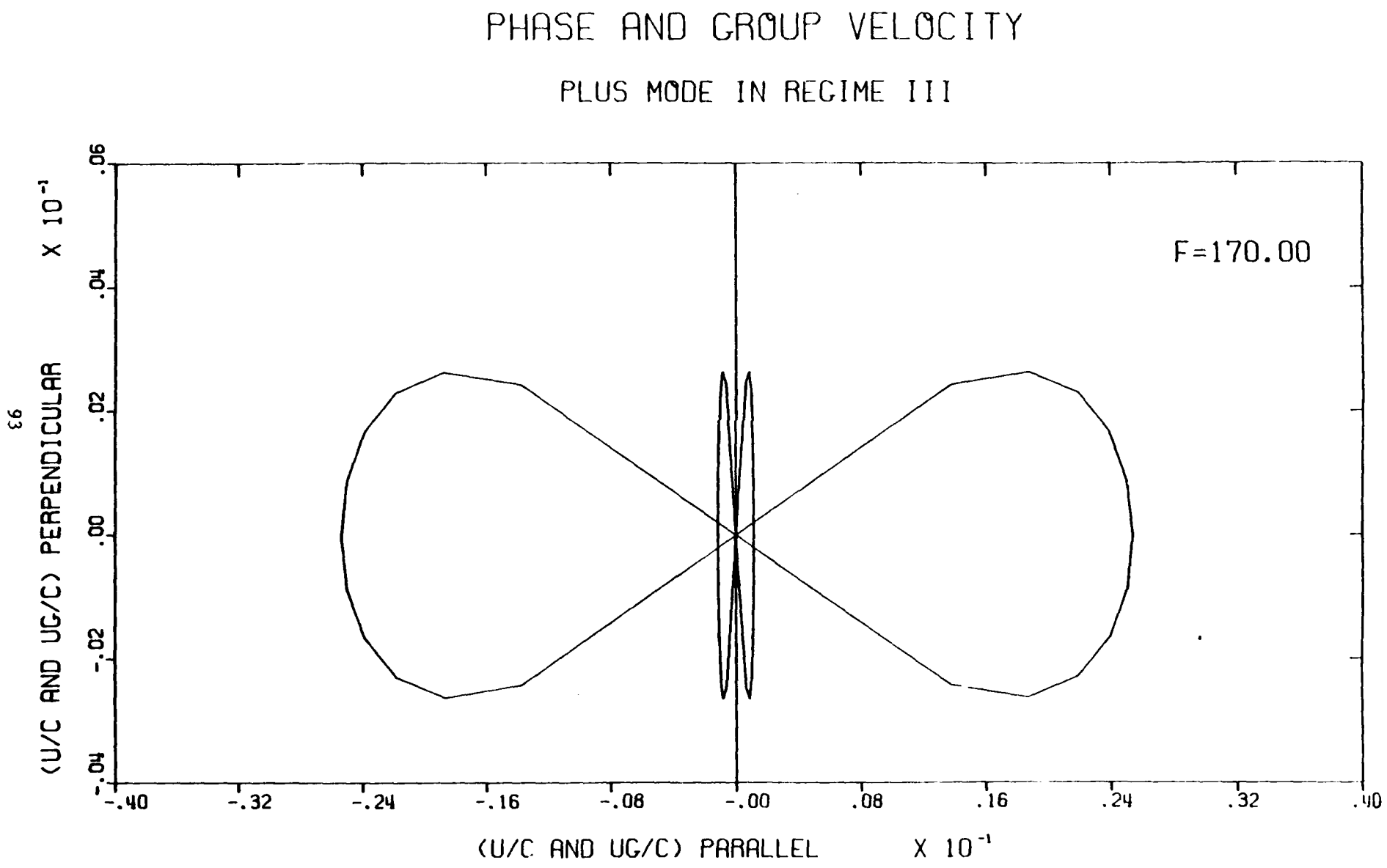
PHASE AND GROUP VELOCITY
PLUS MODE IN REGIME III
F=170.00
(U/C AND UG/C) PERPENDICULAR X 10⁻¹
(U/C AND UG/C) PARALLEL X 10⁻¹
.06
.04
.02
.00
-.02
-.04
-.40
-.32
-.24
-.16
-.08
-.00
.08
.16
.24
.32
.40

Figure 4.25

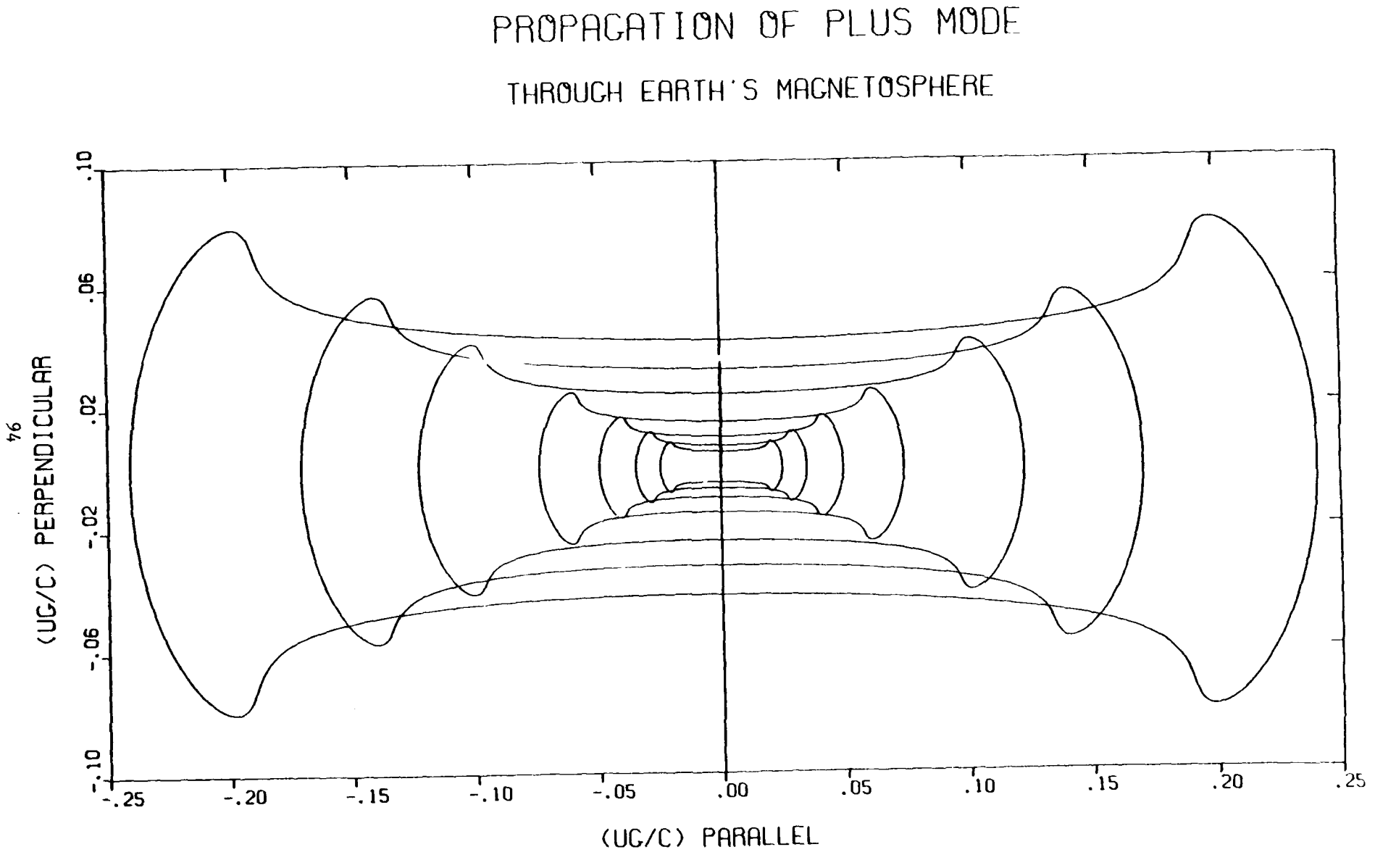
PROPAGATION OF PLUS MODE
THROUGH EARTH'S MAGNETOSPHERE
(UG/C) PERPENDICULAR
.10
.06
.02
-.02
-.06
-.10
-.25
-.20
-.15
-.10
-.05
.00
.05
.10
.15
.20
.25
(UC/C) PARALLEL

Figure 5.1

AD-A164 561 DEFINITION STUDY OF A COORDINATED GROUP OF EXPERIMENTS TO MEASURE AND MON..(U) MASSACHUSETTS INST OF TECH CAMBRIDGE CENTER FOR SPACE RESEARC.. H S BRIDGE ET AL. 2/2

UNCLASSIFIED SEP 85 AFGL-TR-85-0238 F19628-83-K-0030 F/G 22/1 NL

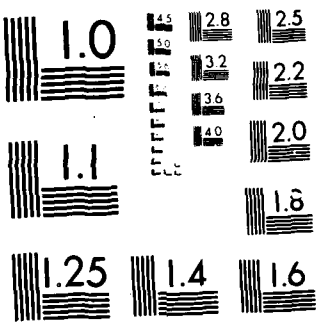

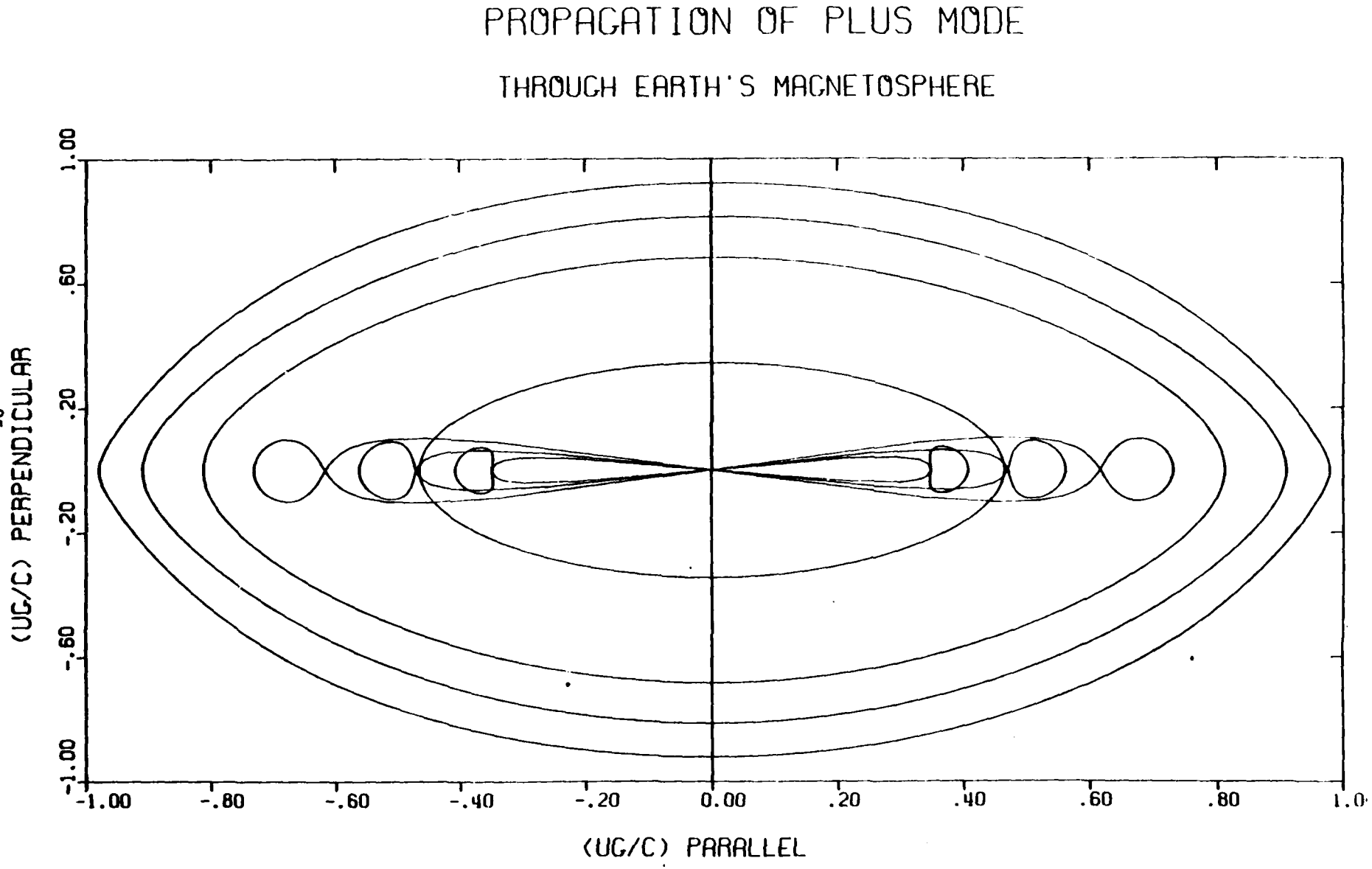
PROPAGATION OF PLUS MODE
THROUGH EARTH'S MAGNETOSPHERE
(UG/C) PERPENDICULAR
S6
1.00
.60
.20
-.20
-.60
-1.00
-1.00
-.80
-.60
-.40
-.20
0.00
.20
.40
.60
.80
1.0
(UG/C) PARALLEL

Figure 5.2

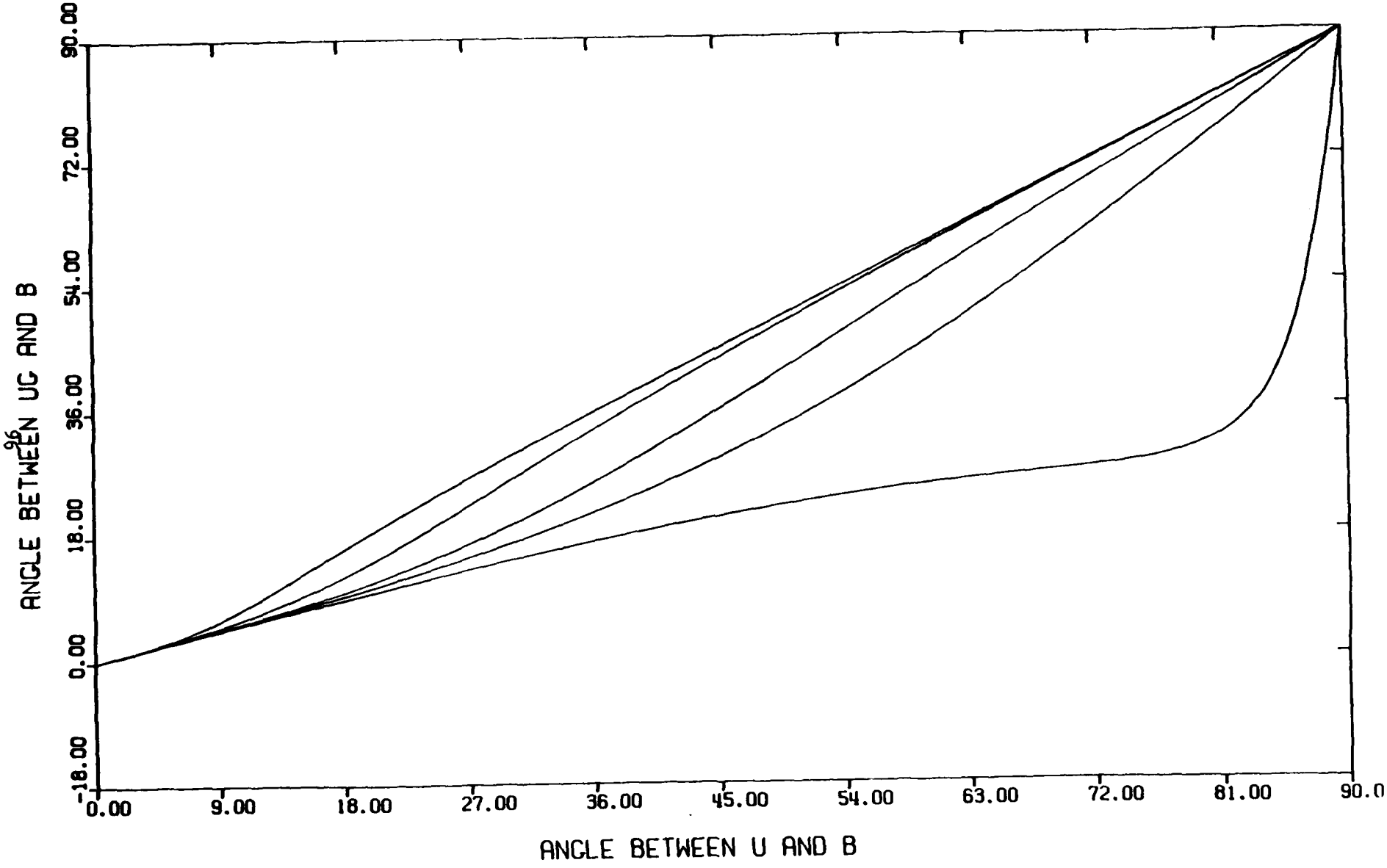
90.00
72.00
54.00
36.00
18.00
0.00
-18.00
ANGLE BETWEEN UC AND B
0.00
9.00
18.00
27.00
36.00
45.00
54.00
63.00
72.00
81.00
90.0
ANGLE BETWEEN U AND B

Figure 5.3

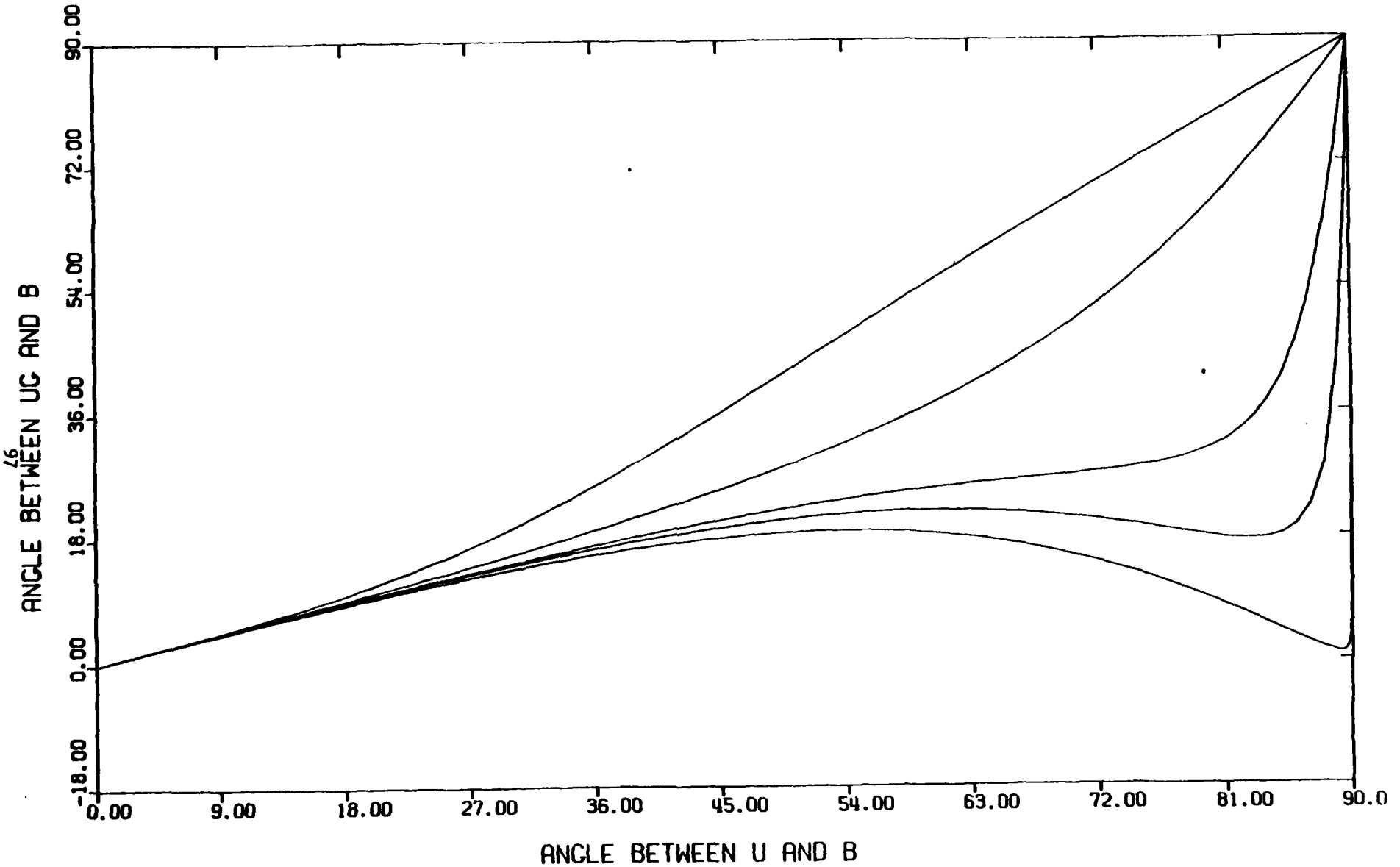
ANGLE BETWEEN UG AND B
90.00
72.00
54.00
36.00
18.00
0.00
-18.00
0.00
9.00
18.00
27.00
36.00
45.00
54.00
63.00
72.00
81.00
90.0
ANGLE BETWEEN U AND B

Figure 5.4

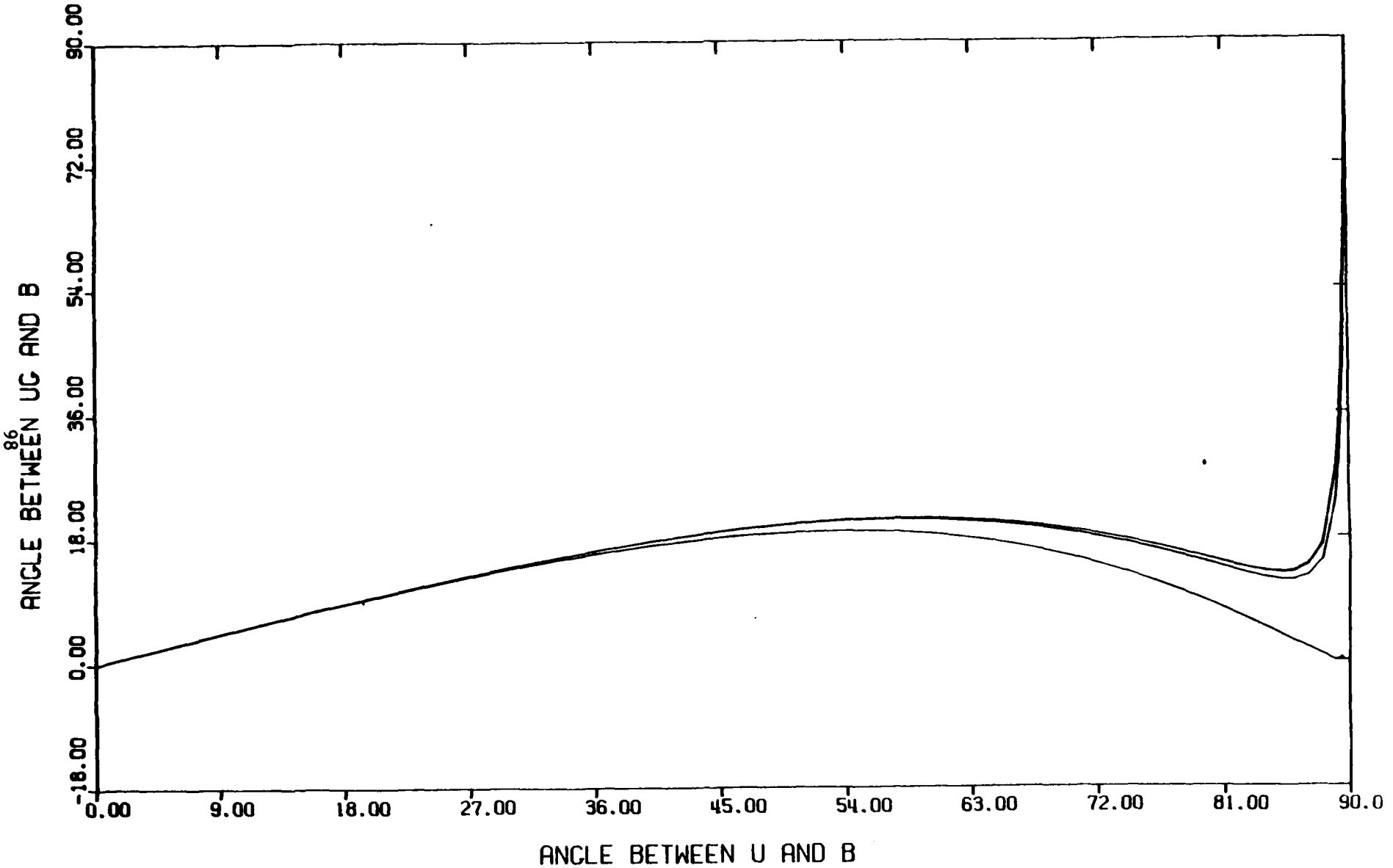
90.00
72.00
54.00
36.00
18.00
0.00
-18.00
ANGLE BETWEEN UG AND B
0.00
9.00
18.00
27.00
36.00
45.00
54.00
63.00
72.00
81.00
90.0
ANGLE BETWEEN U AND B

Figure 5.5

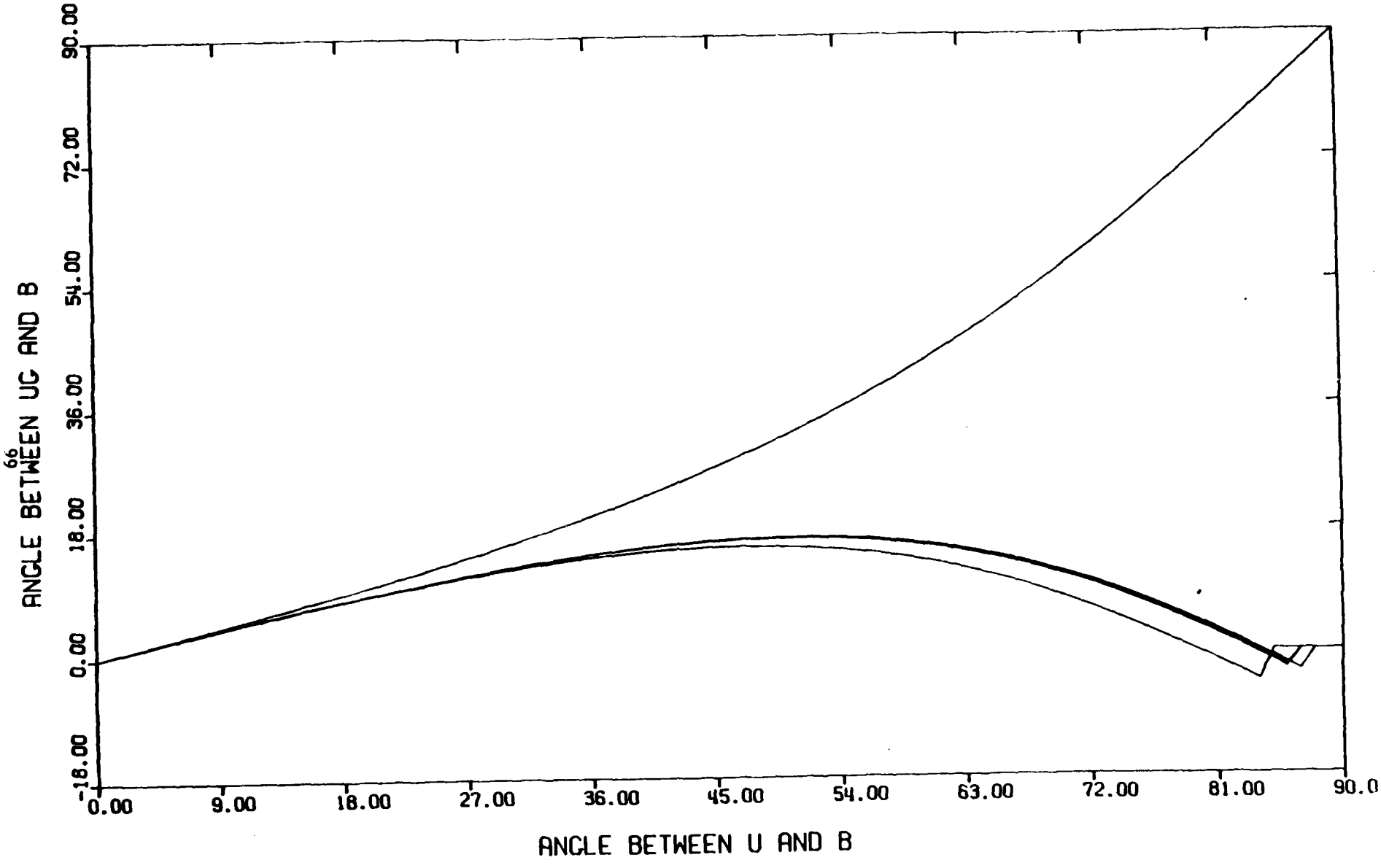
90.00
72.00
54.00
36.00
18.00
0.00
-18.00
ANGLE BETWEEN UG AND B
0.00
9.00
18.00
27.00
36.00
45.00
54.00
63.00
72.00
81.00
90.0
ANGLE BETWEEN U AND B

Figure 5.6

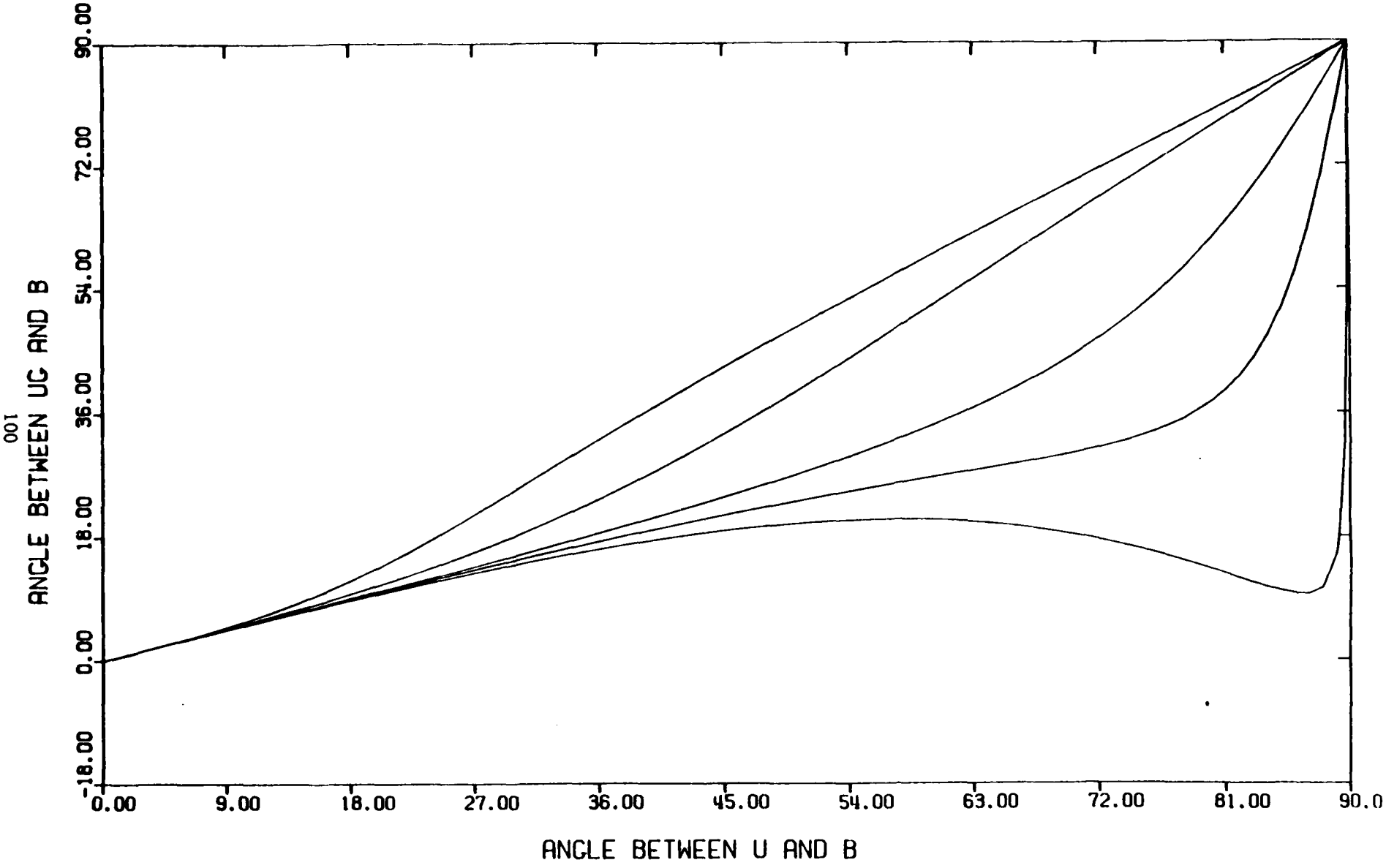
ANGLE BETWEEN UC AND B
100
90.00
72.00
54.00
36.00
18.00
0.00
-18.00
0.00
9.00
18.00
27.00
36.00
45.00
54.00
63.00
72.00
81.00
90.0
ANGLE BETWEEN U AND B

Figure 5.7

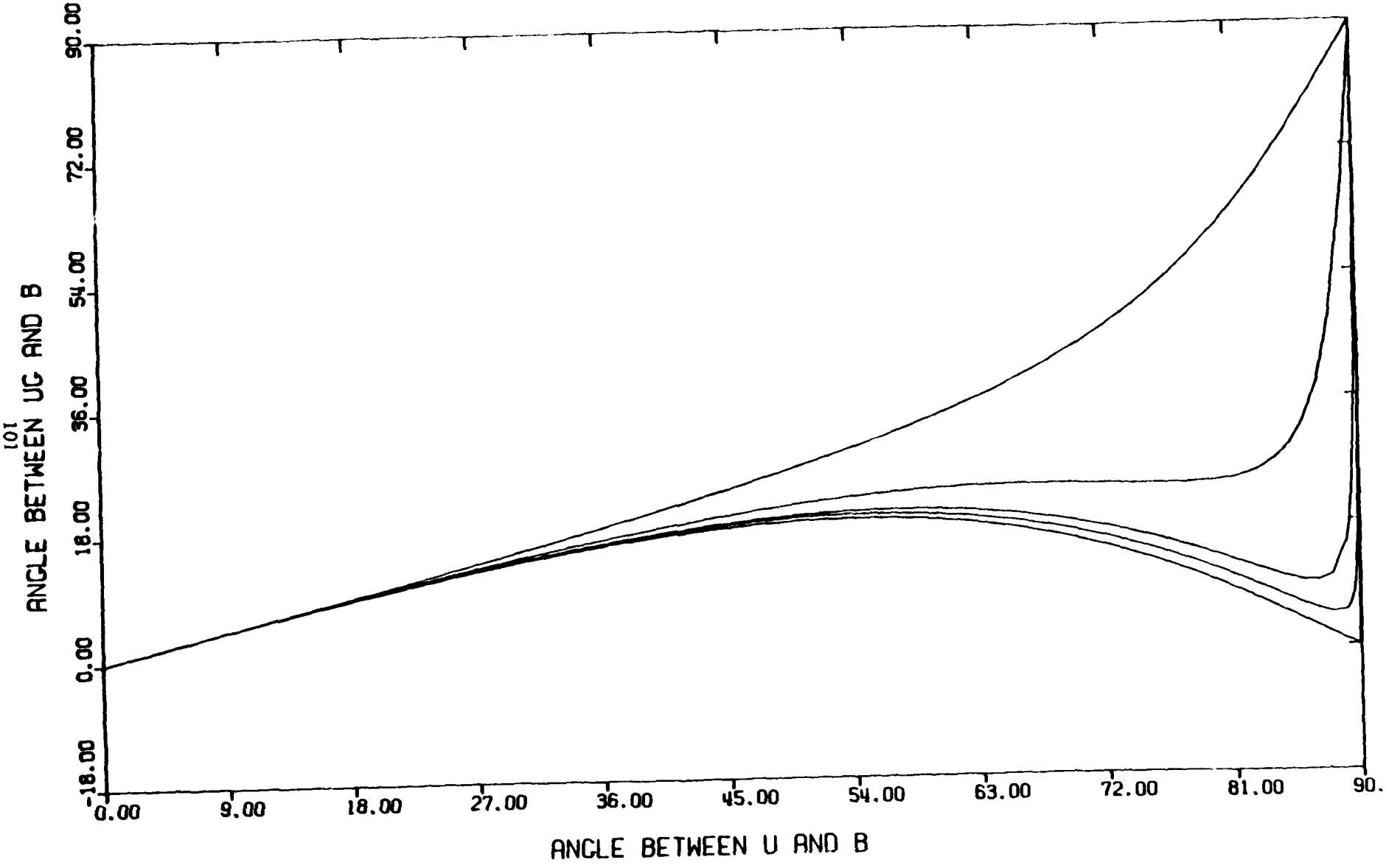
ANGLE BETWEEN UC AND B
90.00
72.00
54.00
36.00
18.00
0.00
-18.00
0.00
9.00
18.00
27.00
36.00
45.00
54.00
63.00
72.00
81.00
90.
ANGLE BETWEEN U AND B

Figure 5.8

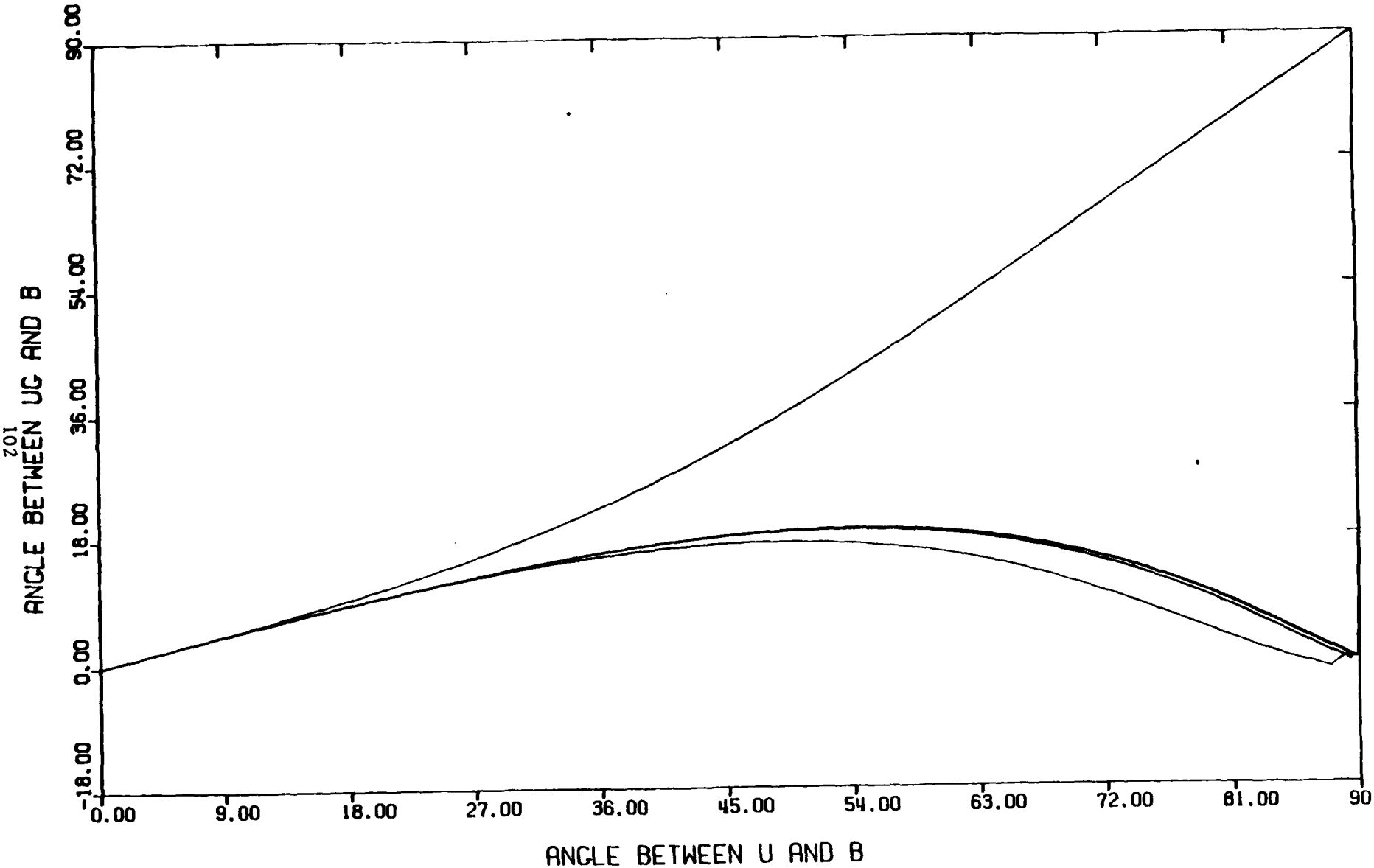
ANGLE BETWEEN UG AND B
102
90.00
72.00
54.00
36.00
18.00
0.00
-18.00
0.00
9.00
18.00
27.00
36.00
45.00
54.00
63.00
72.00
81.00
90.
ANGLE BETWEEN U AND B

Figure 5.9

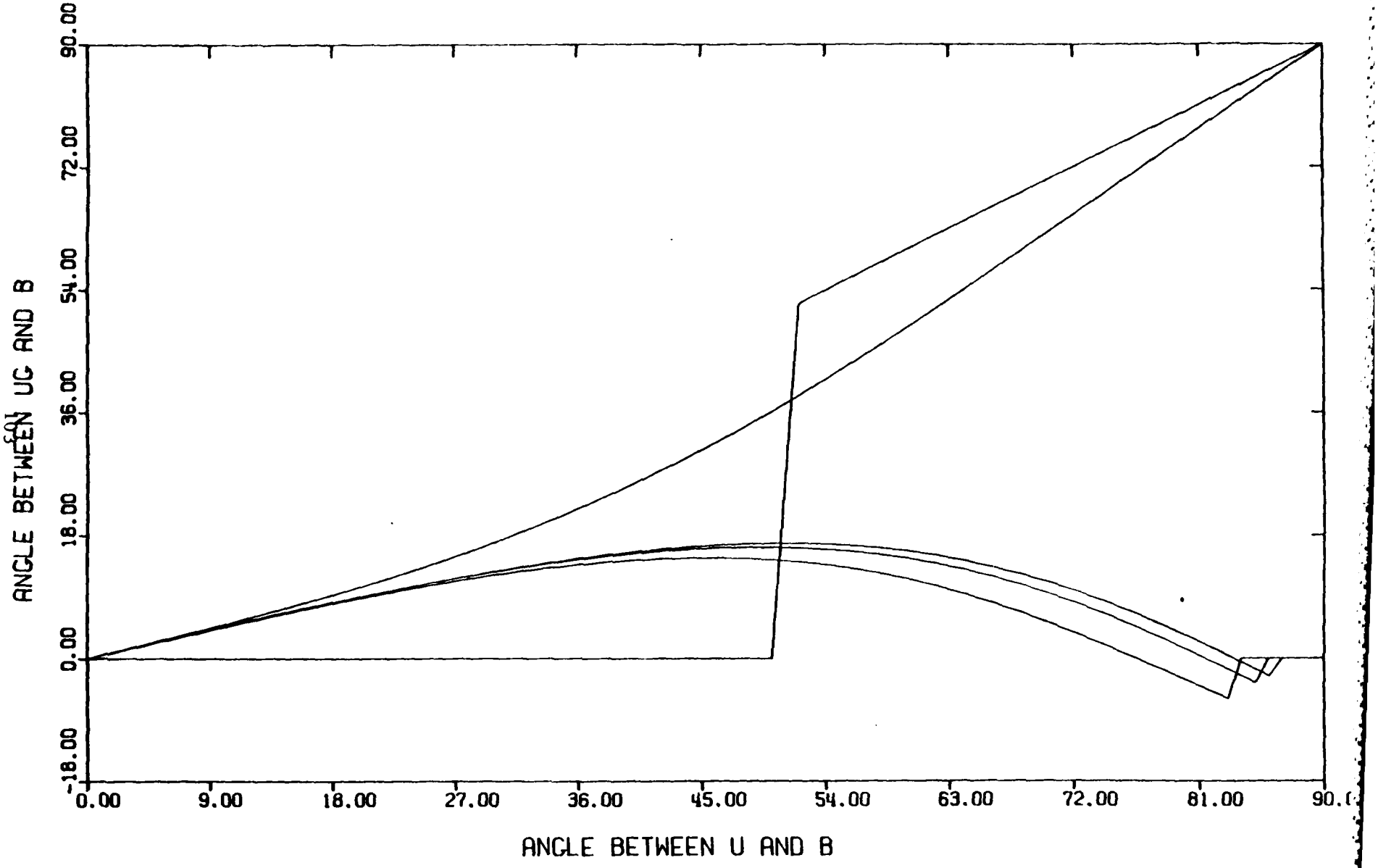
90.00
72.00
54.00
36.00
18.00
0.00
-18.00
ANGLE BETWEEN UC AND B
0.00
9.00
18.00
27.00
36.00
45.00
54.00
63.00
72.00
81.00
ANGLE BETWEEN U AND B

Figure 5.10

END

FILMED

4-86

DTIC